UNIVERSITEIT VAN PRETORIA
UNIVERSITY OF PRETORIA
YUNIBESITHI YA PRETORIA

Hydrogeochemistry of the groundwater in the Namaqualand region, South Africa: implications for surficial uranium mineralization

by

Sisanda Sesethu Makubalo

17397953

Submitted in partial fulfilment of the requirements for the degree

M.Sc. Hydrogeology

In the Faculty of Natural and Agricultural Sciences

University of Pretoria

Pretoria

Supervisor: Dr R.E. Diamond

Co-supervisor: Mr A.O. Kenan

February 2020

DECLARATION

I, Sisanda Sesethu Makubalo, declare that this dissertation titled "Hydrogeochemistry of the groundwater in the Namaqualand region, South Africa: implications for surficial uranium mineralization", which I hereby submit in partial fulfilment of the degree M.Sc. Hydrogeology at the University of Pretoria, is my own work and has not previously been submitted by me for a degree at this or any other tertiary institution.

SIGNATURE:

DATE:

ACKNOWLEDGEMENTS

Firstly, I would like to thank God who has given me the ability and strength to complete this study.

To my supervisor, Dr Roger Diamond and co-supervisor Mr Abdul Kenan, I wish to express my gratitude for your guidance, encouragement, honest opinions and, most importantly, for believing in me throughout this research. I am proud to be called your student.

It is difficult to overstate my gratitude to Neo Moabi, Jabulani Mathebula and Raymond Ngobeni for assistance with the groundwater sampling in the Namaqualand, and to Sis'Cwayita Mzamane for organizing the relevant literature for this study.

Thank you, to my Mom for your love and support throughout this research. Mandisa Mvusi, thank you for pushing and supporting me and being there whenever I needed a shoulder to cry on. To my friends and colleagues, thank you so much for caring and being there for me constantly.

To my mentor, Ms Refilwe Shelembe and my manager, Dr Taufeeq Dhansay, thank you for all the input and advice you have given me during my work on this project.

Lastly, I would like to acknowledge Council for Geoscience for funding the project, Mrs Zahn Nel for editing my dissertation, the Namaqualand farmers for giving me access to their farms and also to the South African Weather Services for providing me with the weather data I used in my research.

ABSTRACT

Since the discovery of the Yeelirrie deposit in Australia in 1972, exploration for surficial uranium deposits has been supported through hydrogeochemical studies of groundwater and the calculation of the carnotite solubility index (CSI). This study aims to evaluate groundwater quality and delineate potential areas where surficial uranium mineralization (i.e. carnotite) may take place in the Namaqualand region. Surficial uranium deposits are unconsolidated soils or sediments, usually of Tertiary to Recent age. The most common surficial uranium mineral is carnotite. The study area in Namaqualand is located in the arid to semi-arid Northern Cape Province of South Africa, which comprises a variety of metamorphic rocks of the Namaqua Metamorphic Province, overlain by Cenozoic sediments. A total of 85 water samples were collected from existing boreholes. Physicochemical properties (EC, TDS, pH, DO and Eh) were measured on site and samples were analysed for major ions and trace elements at the Council for Geoscience laboratory in Pretoria. The CSI was calculated using hydrochemical data, and interpolated using inverse distance weighting (IDW) and kriging to produce maps of potential carnotite mineralization. The groundwater of the area is alkaline, with elevated concentrations of EC, TDS, Na+, Cl-, F-and U. The predominant water types are Na-Cl, Na-HCO_3 and Mg-HCO_3. Most groundwater samples have uranium values that range from 1.2–5 120 ppb, which are above the World Health Organization drinking water quality guideline of 15 ppb. Analysis shows that, in the presence of carbonates, uranium mostly occurs in solution as $UO_2(CO_3)_2^{2-}$ and $UO_2(CO_3)_3^{4-}$. The CSI values ranged from -6.71 to -2.99 and those that ranged from 2.99 to -4 were in close proximity to known surficial uranium occurrences. The use of IDW and kriging interpolation methods revealed areas with potential for carnotite mineralization. The existence of suitable uranium source rocks, palaeochannels, climate and geomorphology makes the Namaqualand region prospective for calcrete-hosted uranium deposits. The CSI, used to delineate areas with a potential for surficial uranium mineralization in the Northern Cape, can be extrapolated to other areas with similar geological environments and climatic conditions. More sampling of groundwater is recommended to conduct a medical geology study to ascertain the impacts of uranium and other elements on the people, animals and plants of the area.

TABLE OF CONTENTS

LIST OF FIGURES

LIST OF TABLES

1 INTRODUCTION

1.1 Background and context of the study

This study forms part of a project under the Minerals and Energy theme (ST-2011-1118) at the Council for Geoscience (CGS). The project attempts to establish the distribution of surficial uranium mineralization in the Namaqualand area, based on the chemistry of groundwater samples taken within and around selected palaeochannels, in view of delineating the uranium potential areas for possible future exploration. The study area selected was based on prospectivity mapping for surficial uranium deposits that had been conducted by the CGS in the 2016/17 financial year (Kenan *et al*., 2017).

1.2 Uranium mineralogy and geochemistry

Uranium is a silvery white radioactive metal in the actinide series of the periodic table with symbol U and atomic number 92. Natural uranium essentially consists of two isotopes: ^{238}U with an abundance of 99.3% and ^{235}U with an abundance of 0.7% both of which slowly decay to ^{206}Pb and ^{207}Pb. Uranium exists in five oxidation states namely, U^{2+}, U^{3+}, U^{4+} (tetravalent), U^{5+}, and U^{6+} (hexavalent) (Burns and Finch, 1999; Khoury, 2015). However, only the U^{4+} and U^{6+} states are stable enough to be of practical importance. In natural waters and other environments U^{4+}, as (UO^{2+}) may be present with a low oxidation potential. Under reducing conditions U^{6+} as $(UO_2)^{2+}$ is the most stable oxidation state (Krupka and Serne, 2002). Most uranium minerals fall into two categories: Uranium as U^{4+} is a reduced species whereas oxidized species contain uranium as U(VI). Many uranium deposits are dominated by reduced uranium minerals (Burns and Finch, 1999). Uranium in the U^{6+} oxidation state is soluble in aqueous systems and the solubility is controlled by oxidation- reduction potential, pH and dissolved carbonate (Murphy and Shock, 1999).

Uranium is found in the earth's crust (0.003 ppm), almost everywhere in rocks and soils and in rivers and oceans. Traces of uranium are even found in food and human tissue. Organic material in the pore spaces of rocks creates a reducing environment. Within this reducing environment, the oxidizing uranium-bearing water passing through the rock precipitates uranium in the rock (Boyle, 1982). The U^{4+} state is the main state found in primary (endogene) minerals of uranium, namely uraninite (Figure 1B), coffinite, brannerite and davidite (Table 1). The most common minerals containing entirely the U^{6+} state are secondary (supergene) minerals (Table 1), namely autunite (Figure 1C), carnotite (Figure 1D), gummite, saléeite, torbernite (Figure 1A), uranocircite, uranophane and zeunerite (Boyle, 1982; Khoury, 2015). If U^{235} is ingested or inhaled, its radioactivity poses a high risk of lung and bone cancer (Toens and Partners, 1998). Highly elevated uranium in groundwater is the result of the dissolution of

uranium-bearing minerals that have been in contact with groundwater for long periods of time. Uranium is also chemically toxic at high concentrations of 15 ppb in groundwater and can cause damage to internal organs, particularly the kidneys. Animal studies suggest that uranium may affect reproduction, the developing foetus, and increase the risk of leukaemia and soft tissue cancers (Toens and Partners, 1998).

Table 1. Uranium ore minerals (Burns and Finch, 1999; Khoury, 2015).

Uranium minerals	
Reduced uranium minerals	
Name	**Chemical formula**
uraninite	UO_2
brannerite	$(U,Ca,Y,Ce)(Ti,Fe)_2O_6$
coffinite	$U(SiO_4)_{1-x}(OH)_{4x}$
Secondary uranium minerals	
Name	**Chemical formula**
autunite	$Ca(UO_2)_2(PO_4)_2$. 8-12 H_2O
carnotite	$K_2(UO_2)_2(VO_4)_2$. 1–3 H_2O
gummite	gum like amorphous mixture of various uranium minerals
saléeite	$Mg(UO_2)_2(PO_4)_2$. 10 H_2O
strelkinite	$Na_2(UO_2)_2(V_2O_8)$. $6H_2O$
torbernite	$Cu(UO_2)_2(PO_4)_2$. 12 H_2O
tyuyamunite	$Ca(UO_2)_2(VO_4)_2$. 5-8 H_2O
uranocircite	$Ba(UO_2)_2(PO_4)_2$. 8-10 H_2O
uranophane	$Ca(UO_2)_2(HSiO_4)_2$. 5 H_2O
zeunerite	$Cu(UO_2)_2(AsO_4)_2$. 8-10 H_2O

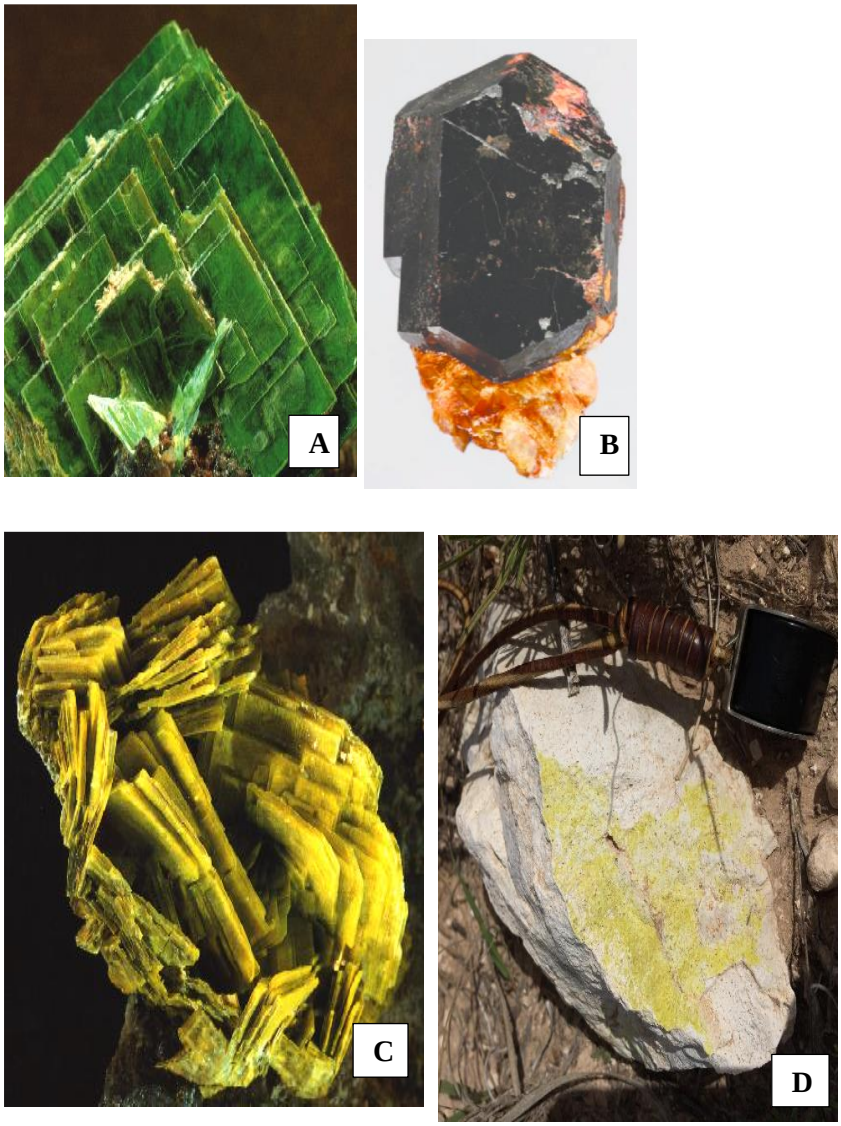

Figure 1: Types of uranium ore minerals: A. torbernite, B. uraninite, C. autunite and D. carnotite (IAEA, 2013).

1.2.1 History of uranium ore deposits

Uranium was first discovered in 1789 by Martin Klaproth, a German chemist in the Czech Republic, as the mineral pitchblende from the Joachimsal silver mines (Lehmann, 2008). Uranium was first isolated in 1841 by Eugene Péligot and its radioactivity was identified by a French scientist, Henri Becquerel, in 1896. From 1898 to the 1920s, Marie Curie and her husband Pierre Curie discovered two uranium daughter products, polonium and radium through various experiments in their laboratory. Radium was used for therapeutic purposes and as a source of X-rays in the field of medicine during World War I (Cole, 1998). In 1939, Hann and Stransman discovered that one isotope of uranium, ^{235}U, was fissionable, triggering a process known as a "chain reaction", which released an immense amount of

energy that led to the development of nuclear weapons for World War II (Bennet and Thomson, 1989). The energy released by fission was later used to heat water, create steam, and turn turbines to generate electricity. Nowadays this is still one of the most significant uses of uranium.

Uranium is found throughout the world, but quantities sufficient to be mined economically are limited to a few known regions. Canada has the highest-grade uranium, while Australia has the most known uranium reserves. Kazakhstan, South Africa, Niger, Namibia, and Brazil also have significant deposits.

1.2.2 General description of all the deposits

Uranium ore deposits are formed under a variety of geological conditions in metamorphic, igneous, hydrothermal, sedimentary and superficial environments. The average uranium content of the earth's continental crust is ~2.8 wt ppm U (granite 3–5 ppm, sedimentary rocks 2–3 ppm) while seawater contains uranium at a concentration of 0.003 ppm. Uranium deposits are classified into two types, namely primary uranium ore deposits and secondary uranium ore deposits. Primary ore deposits (endogene) of uranium concentrate in granitic or alkali volcanic rocks, hydrothermal veins, marine black shales and Precambrian age placer deposits (Lidman *et al*., 2012). Secondary ore deposits (supergene) are formed later when uranium is dissolved in oxidizing aqueous solutions in the U^{6+} valence state, and may be redistributed from primary source rocks into porous sedimentary rocks and structures by groundwater (Boyle, 1982).

Globally, there are 15 principal types of uranium deposit classified according to their approximate economic significance, namely intrusive, granite-related, polymetallic iron oxide breccia complex or iron oxide-copper-gold, metasomatite, metamorphite, Proterozoic unconformity, collapsed breccia pipe, sandstone, palaeoquartz-pebble conglomerate, surficial, lignite-coal, phosphorite and black shale (Bruneton *et al.*, 2014). However, approximately 75% of the world's uranium reserves are derived from five principal types of uranium deposit, namely intrusive, polymetallic iron oxide breccia complex, metasomatite, Proterozoic unconformity and sandstone (Figure 2) (Cuney, 2009; IAEA, 2013). These deposits are assigned on the basis of their geological setting (subtype) such as host rock, alteration, ore mineralization, and age of the ore deposit. The deposits are discussed in detail by the International Atomic Energy Agency (IAEA, 2013). For the purposes of this study, only South African deposits will be discussed, with particular emphasis on the Namaqualand surficial deposits (cf. 1.2.3.5).

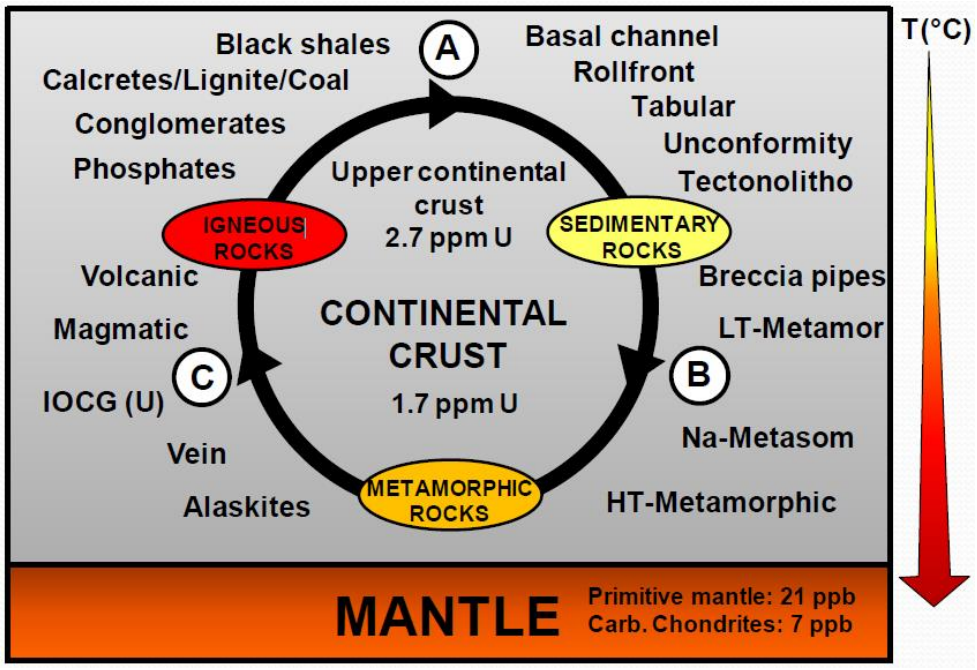

Figure 2: Types of uranium deposit variations over time: A. alteration, erosion, transport, deposition, B. diagenesis, metamorphism, and C. partial melting and crystal fractionation (Cuney, 2009).

1.2.3 South African uranium deposits

There are about seven uranium deposit types in South Africa (as defined by IAEA, 2013). Uranium occurs in quartz-pebble conglomerates of the Witwatersrand Basin, in sandstones of the Karoo Uranium Province, in lignite-coal of the Springbok Flats Basin, in intrusive rocks, such as the carbonatites of, for example, the Phalaborwa Igneous Complex, in surficial Namaqualand deposits and in vein-type and phosphate carbonate deposits (Figure 3) (Cole, 1998). The major part of the uranium resource inventory in South Africa is hosted by quartz-pebble conglomerates and derived tailings, with significant amounts of resources in sandstones and coal-hosted deposits. In 2014, the IAEA reported that Witwatersrand uranium production amounted to 540 t U of a global uranium production of 41 000 t per year (IAEA, 2014). The other deposit types account for a relatively small fraction of the national uranium resource inventory. Virtually all of South Africa's historical uranium production has been from quartz-pebble conglomerate deposits, with a small proportion being from the Phalaborwa copper-bearing carbonatites. All current production is derived from quartz-pebble conglomerate deposits (Kenan and Chirenje, 2016).

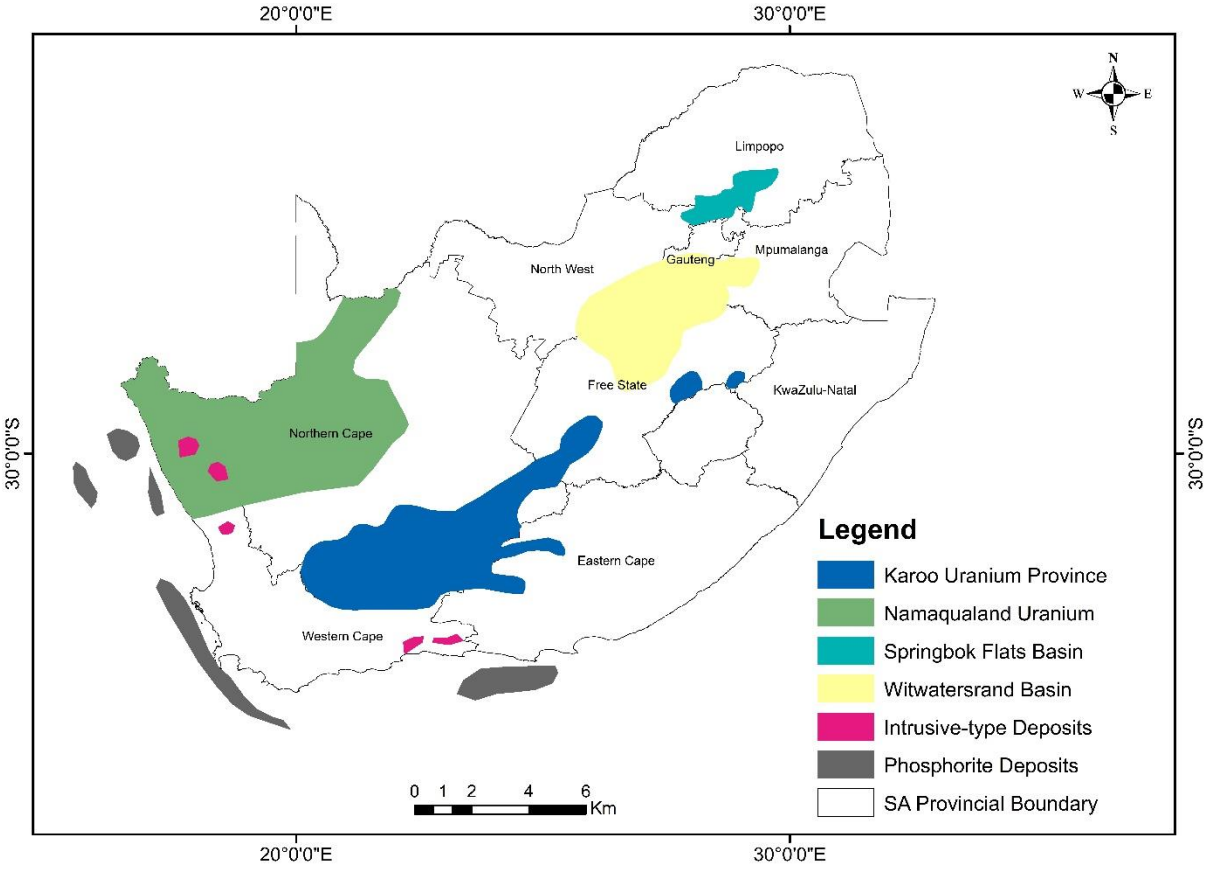

Figure 3: Distribution of the major uranium deposits in South Africa (modified from Cole, 1998).

1.2.3.1 Witwatersrand Basin

The uraniferous quartz-pebble conglomerates of the Witwatersrand Basin, occurring within the Central Rand Group of Gauteng Province, are by far the most important uranium host rocks in South Africa. These deposits also contain gold as a significant commodity. The quartz-pebble conglomerates were deposited in a braided river environment on alluvial fans or fan deltas that centripetally entered the Witwatersrand Basin (Pretorius, 1976).

1.2.3.2 Karoo Uranium Province

The sandstone type deposits of the Karoo Supergoup occur in peneconcordant tabular orebodies. This metallogenic province, described by Cole *et al*. (1991), extends from the northeastern part of the Western Cape across the southern part of the Northern Cape and into the Free State, as far as Bloemfontein. Uranium is hosted within the Elliot and Molteno Formation sandstones. Although feasibility studies were conducted, the uranium has never been exploited, (Van der Merwe, 1986).

1.2.3.3 Springbok Flats Basin

Uranium is concentrated in coal and in the carbonaceous shales of the Permian Ecca Group and can be correlated with the Volksrust Formation in the main Karoo Basin (Christie, 1989). Uranium potential

was detected at depths of between 20 and 650 m, with most occurrences being clustered between 100 and 200 m below the surface.

1.2.3.4 Intrusives

Uranium was extracted in the Phalaborwa Complex in 1971 as a by-product of copper. However, uranium production from this complex is low compared to Witwatersrand uranium production. Uranium occurs in uranothorianite with late-stage foskorite and carbonatite which form the core of Loolekop pyroxenite body at the centre of Phalaborwa Complex. The *in situ* grade of uranium is 30 ppm U (Cole, 1998). Granite gneiss of the Namaqualand Metamorphic Complex generally shows anomalous uranium concentrations averaging between 5 and 25 ppm U (Stettler and Cole, 1984). The principal uranium-bearing mineral is uraniferous thorianite ($ThSiO_4$). The Concordia granite, which is widely distributed in central Namaqualand, has a higher average uranium concentration of 35 to 70 ppm U than the other granites in the area (Jacob *et al.*, 1986). Uranium is also found in the granites of the George pluton, with concentrations lower than 100 ppm U.

1.2.3.5 Namaqualand surficial uranium deposits

This study focusses on the spatial distribution of surficial uranium mineralization in Namaqualand based on the groundwater chemistry from numerous boreholes. Surficial uranium deposits are unconsolidated soils or sediments usually of Tertiary to Recent age (Boyle, 1982; Toens and Hambleton-Jones, 1984). Uraniferous surficial deposits form in various environments, depending on the source of the ore-forming elements, the morphology and the climate (Toens and Hambleton-Jones, 1984). These are environments where deeply weathered, uranium-rich granites occur in a semi-arid to arid climate (Misra *et al.*, 2011). Globally, surficial uranium-rich deposits are not uncommon, and are typically formed in calcrete developed by evaporation and calcite precipitation in fluviatile to playa systems, in arid to semi-arid climatic conditions. The most common surficial uranium mineral is carnotite and, to lesser extent, tyuyamunite. Carnotite $K_2(UO_2)2V_20_8.3H_20$, is a potassium uranyl-vanadate which commonly occurs as a secondary accessory mineral in uranium ore deposits (Figure 4) and results from the alteration of uraninite (UO_2) or other uranium- or vanadium-bearing minerals. Tyuyamunite $Ca(UO_2)2V2O_8.(5\text{-}8)H_2O$ is a hydrated calcium uranyl-vanadate which is closely related to carnotite. Mineralization of carnotite is commonly cemented by secondary minerals, such as calcite, gypsum, dolomite, ferric oxides and halite.

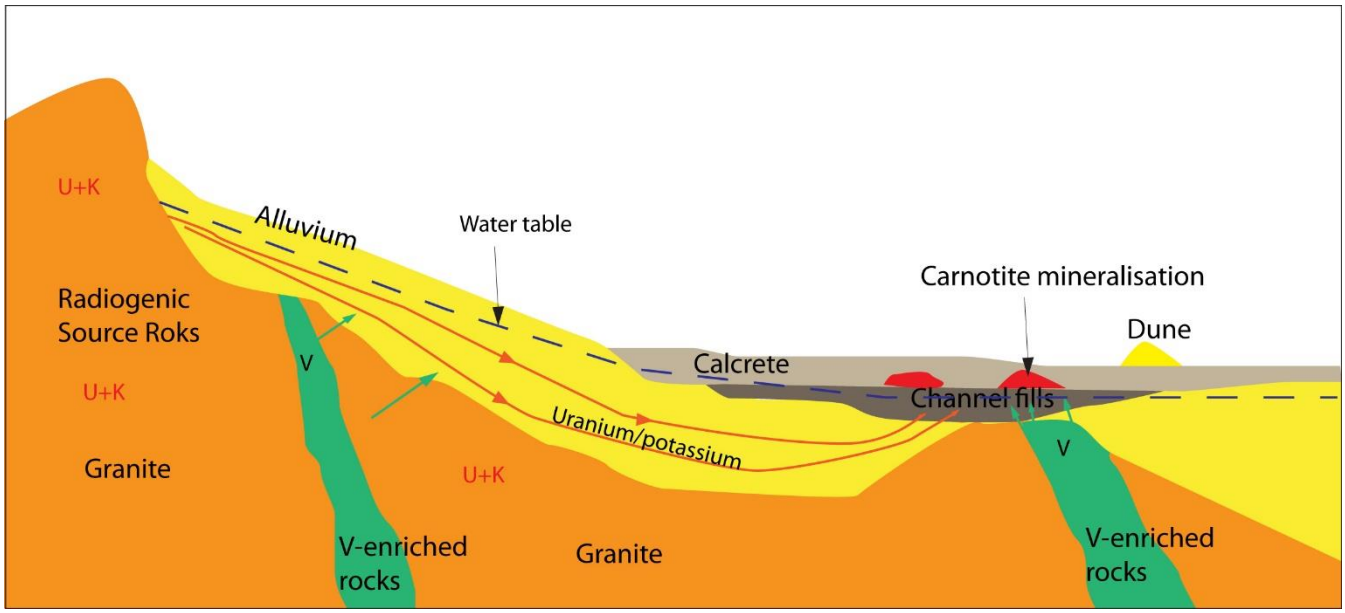

Figure 4: Diagram depicting carnotite formation and mineralization (Hou *et al.*, 2007).

The surficial deposits in the Namaqualand region were discovered in the mid-1970s as a result of major exploration of surficial uranium deposits in South Africa and Namibia (Kenan and Chirenje, 2016). The most significant uranium discovery, to date, is the Henkries deposit (also known as the Namakwa uranium deposit) which has been investigated since the mid-1970s. Tertiary to Recent surficial sediments are found on the Bushmanland Plateau of the Namaqua Metamorphic Province, with some occurring below the escarpment and on the coastal plain (Hambleton-Jones *et al.*, 1986). The sediments filling palaeodrainage channels are mainly confined to the river courses with the main ones being the Koa and Sout. Towards the Orange River, the sediments attain thicknesses in excess of 300 m. In the Koa River Valley, the sediments tend to be upward fining, having boulders and gravels near the base and well-sorted aeolian sand higher in the sequence, some of which was probably reworked by fluvial action (Hambleton-Jones *et al.*, 1986).

According to Hambleton-Jones *et al*. (1986), surficial uranium deposits in Namaqualand may be subdivided into three types, namely fluvial, lacustrine and pedogenic (Figure 5). However, within the study area, only fluvial and lacustrine deposits are found. Lacustrine and fluvial deposits predominate in the region south of the Orange River between Upington and the west coast. These deposits represent the potentially important uranium deposits in the Namaqualand region (Hambleton-Jones *et al.*, 1986).

1.2.3.5.1 Fluvial deposits

Fluvial deposits occur in sediments of valley fills and floodplains, with most forming in oxidizing environments, dominated by calcite, the cementing material (Hambleton-Jones *et al*., 1986). The fluvial deposits (Figure 6) contain a small portion of the uranium deposits, of the surficial uranium resources

in South Africa. The largest is the Brulkolk deposit, which is located 70 km southwest of Kakamas (Carlisle, 1980). The Brulkolk deposit comprises numerous layers of weakly uraniferous sand and gravel over a distance of up to 3 km, a width of 400 m, with a thickness of between 0.1 and 2 m. These sediments lie on granite-gneisses of the Namaqualand Metamorphic Complex and are covered by at least 0.75 m aeolian sand and/or alluvium. The principal uranium mineral in these deposits is carnotite, accompanied by calcrete or gypsum cement (Carlisle, 1980). The main source of uranium which underlies the fluviatile deposits are the granite-gneisses of the Namaqualand Metamorphic Complex. The uraniferous pedogenic calcrete of Pleistocene age and older is the source rock of uranium for more recent deposits found on the farm McTaggarts Camp 453, 20 km southwest of Upington (Treasure, 1977). Uranium was transported in neutral to oxidizing solutions (uranyl carbonate complex) and was precipitated with calcium carbonate in areas of high evaporation (Cole, 1998).

1.2.3.5.2 Lacustrine deposits

According to Cole (1998), lacustrine deposits (Figure 6) in the Namaqualand region occur in pans where the internal drainage comprises only an inlet, or pans characterized by drainage comprising both inlets and outlets. Pan sediments in the Namaqualand region consist of salt, gypsiferous clay, massive gypsum, clay, sand and diatomaceous earth. Low uranium grades of 100 ppm or less are found in the lacustrine deposits (Levin, 1980). This value is lower than the maximum uranium grade (340 ppm) in fluvial deposits. The main uranium mineral is carnotite derived from uranium found within nearby granite-gneisses and older pedogenic calcretes. Carnotite was concentrated evaporatively with carbonate and or gypsum (Carlisle, 1980). The most important examples of the lacustrine deposits are Kannikwa, 15 km east of Pofadder, Henkries, 80 km north-northeast of Springbok and Rus-en-Vrede, 170 km north-northeast of Upington. Kannikwa has an average thickness of 0.2 m and a grade of less than 170 ppm U. Rus-en-Vrede is about 1 m thick with an average grade of 100 ppm (Levin, 1978). The largest deposit, at Henkries, has an average thickness of 5.8 m and a grade of 570 ppm (Richards, 1975).

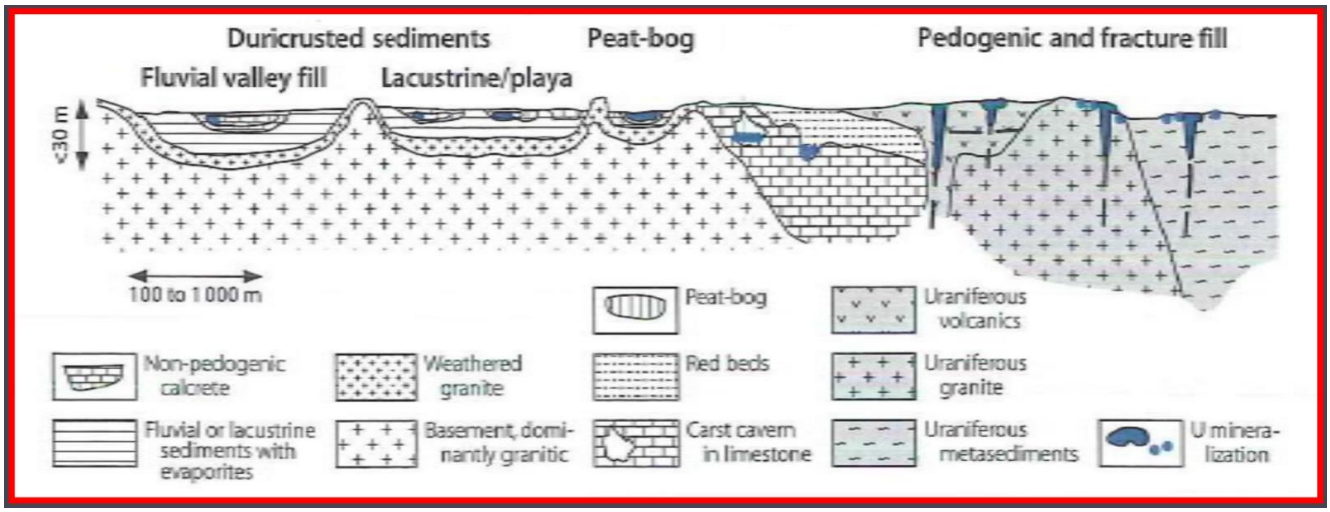

Figure 5: Surficial uranium deposits (Hambleton-Jones, 1986).

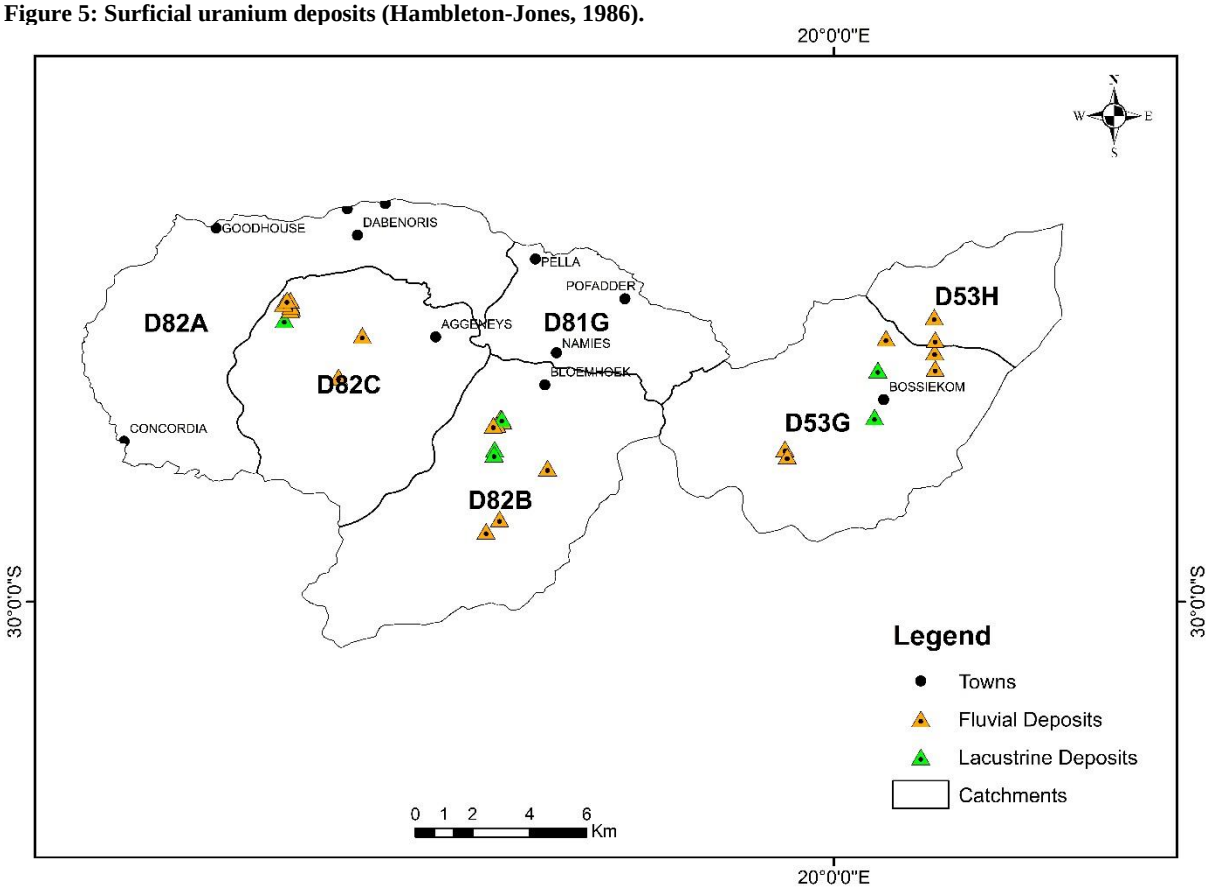

Figure 6: Locations of the various types of surficial uranium deposit in the study area (SAMINDABA, 2018).

1.2.3.6 Phosphorite deposits

Consolidated and unconsolidated phosphorus-bearing sediments, containing low concentrations of uranium, are situated on the continental shelf off the west and south coasts of South Africa between Cape Recife and the Namibian border. The uranium concentration ranges from 10–431 ppm U. The phosphorite deposits are associated with the Dwyka Group where it underlies or forms the lateral margins of pans northwest of Upington (Levin, 1978). The uranium is hosted in the apatite crystals within nodules of calcareous mudrock, with concentrations of up to 950 ppm U (Levin, 1980). At Zandkops Drift, uranium is associated with niobium and rare earths in an alkaline carbonatite complex.

1.2.3.7 Vein-type deposits

The vein-type deposits comprise the rare-earth element thorium, but also contain low concentrations of uranium. The deposits consist of monazite-apatite-rich veins hosted by granite gneiss of the Namaqualand Metamorphic Complex (Andreoli *et al.*, 1994). The monazite contains between 519 and 680 ppm U.

2 PROBLEM STATEMENT AND SCOPE OF THE PROJECT

Most near-surface mineral deposits in South Africa have been discovered, and the challenge is to find new, more deeply buried resources. The advantage of groundwater as a tool for geochemical exploration in search of new mineral deposits, such as porphyry copper, volcanogenic massive sulphides, sandstone-hosted uranium and surficial uranium has been recently demonstrated in several hydrogeochemical studies, where several boreholes were sampled and analysed for water chemistry (Leybourne and Cameron, 2006). Research in India, Canada, the USA, Chile and Namibia has shown that it is possible to find chemical traces in groundwater samples in known areas of mineralization. Water is the "universal solvent" and all natural substances will dissolve in the water to some measurable extent, given proper time and circumstances (Miller, 1979). Groundwater circulates at great depths underneath the earth's surface; therefore each area will have a certain water chemistry signature depending on the geology, environment and history. Hydrogeochemical analysis is considered to be a cost-effective tool for discovering new mineral deposits. It is against this backdrop that the present study was established to conduct hydrogeochemical mapping in Namaqualand in view of delineating potential surficial uranium deposits.

To date, no carnotite distribution map of the Namaqualand region has been produced. Moreover, very limited research has been conducted on the geochemistry of the groundwater in the palaeochannels, or on its effect on uranium distribution and its environmental impact. This study will therefore be important for the future delineation of new uranium resources of the Republic of South Africa.

2.1 Research aims and objectives

The project aims to delineate areas that have potential for carnotite mineralization, based on hydrogeochemistry. In addition, an evaluation of water quality is conducted by identifying boreholes registering uranium concentrations above the South African water quality guidelines.

The specific objectives of the project are:

- to study the chemistry of groundwater within the existing boreholes situated on palaeochannels in the Namaqualand region
- to study the geochemistry and spatial distribution of uranium in the groundwater

- to investigate carnotite distribution using the CSI formula:

$$CSI = \log \frac{[K][U][V]}{1.13 \times 10^4 [HCO3^-]^2}$$ in view of producing a carnotite potential map

- to identify high-risk areas that may cause harm to humans as a result of the uranium content in the groundwater.

2.2 Site selection

The selection of the study area was based on the areas delineated by prospectivity mapping for surficial uranium deposits that had been carried out by the CGS. Areas that had been delineated as potential surficial uranium deposits were selected for groundwater sampling (Kenan *et al*., 2017). The boreholes are located within palaeochannels. Only functioning boreholes were sampled to obtain an accurate representation of the borehole water sampled.

3 FIELD SITE

3.1 Introduction

The study area is situated in the Namaqualand area of the Northern Cape Province, South Africa (Figure 7). Namaqualand is divided by the lower course of the Orange River into two portions — Little Namaqualand to the south (South Africa) and Great Namaqualand to the north (Namibia). The area is host to a variety of metamorphic rocks of the Bushmanland Plateau. Bushmanland is an arid area inland from Namaqualand where groundwater is the only source of water for most communities residing there (DWAF, 2003). Communities in the larger towns (e.g. Upington, Kleinzee and Nababeeb) have access to pumped water from the Orange River.

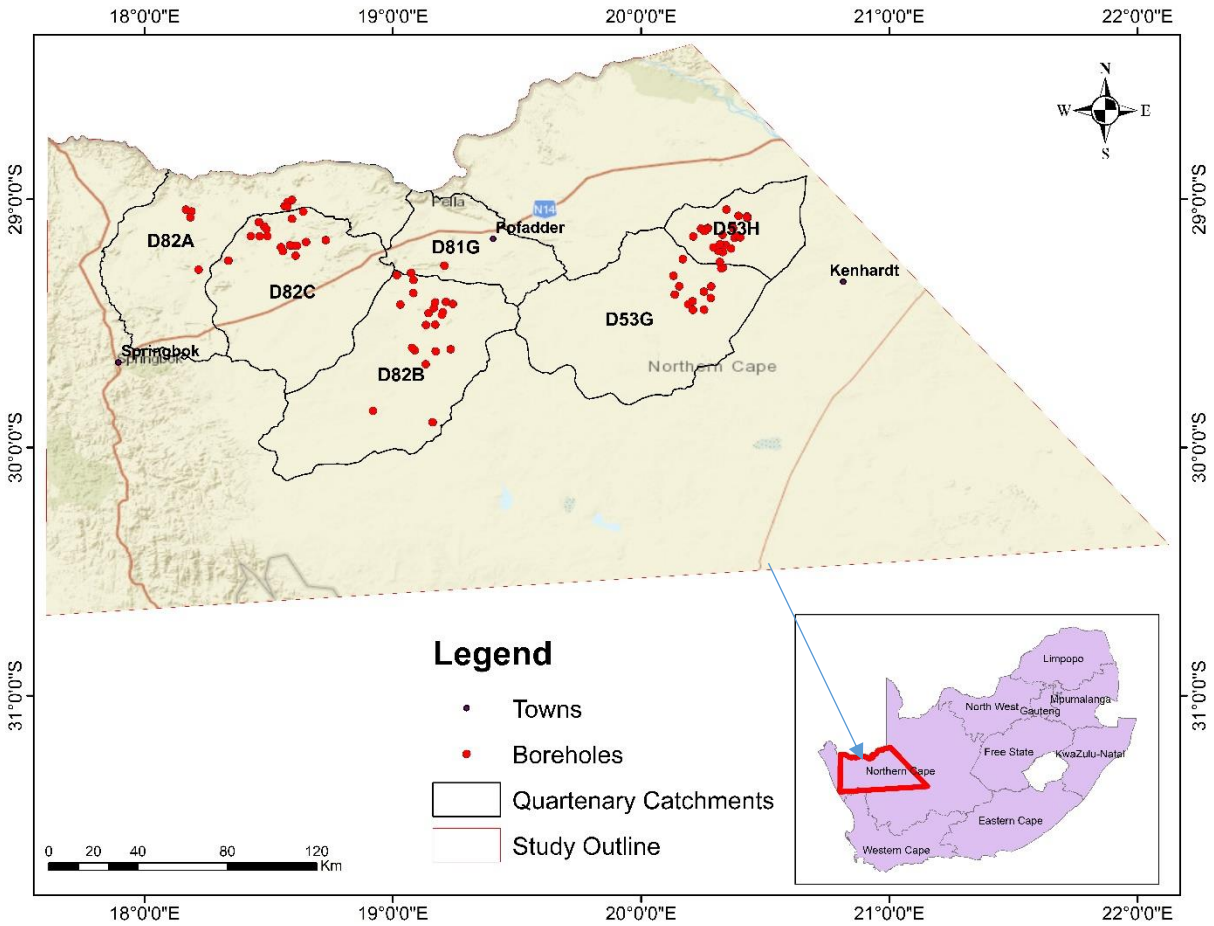

Figure 7: Locality map of the study area.

3.2 Site location

Locally, the sampled boreholes are distributed in the Lower Orange River water management area around the N14, from the north of Springbok, south of Aggeneys and Pofadder (Bushmanland) and Kenhardt (Figure 8). Eighty-five (85) groundwater samples were collected in July 2017. All the boreholes sampled are situated in or close to palaeochannels and past occurrences of surficial uranium deposits.The samples fall into six Quaternary catchment areas: D82A, D82C, D82B, D81G, D53G and D53H. Various methods of pumping groundwater from the aquifers were used, for example electricity-powered pumps, solar-powered pumps, wind-powered pumps (windmills) and diesel-powered pumps (Figure 9).

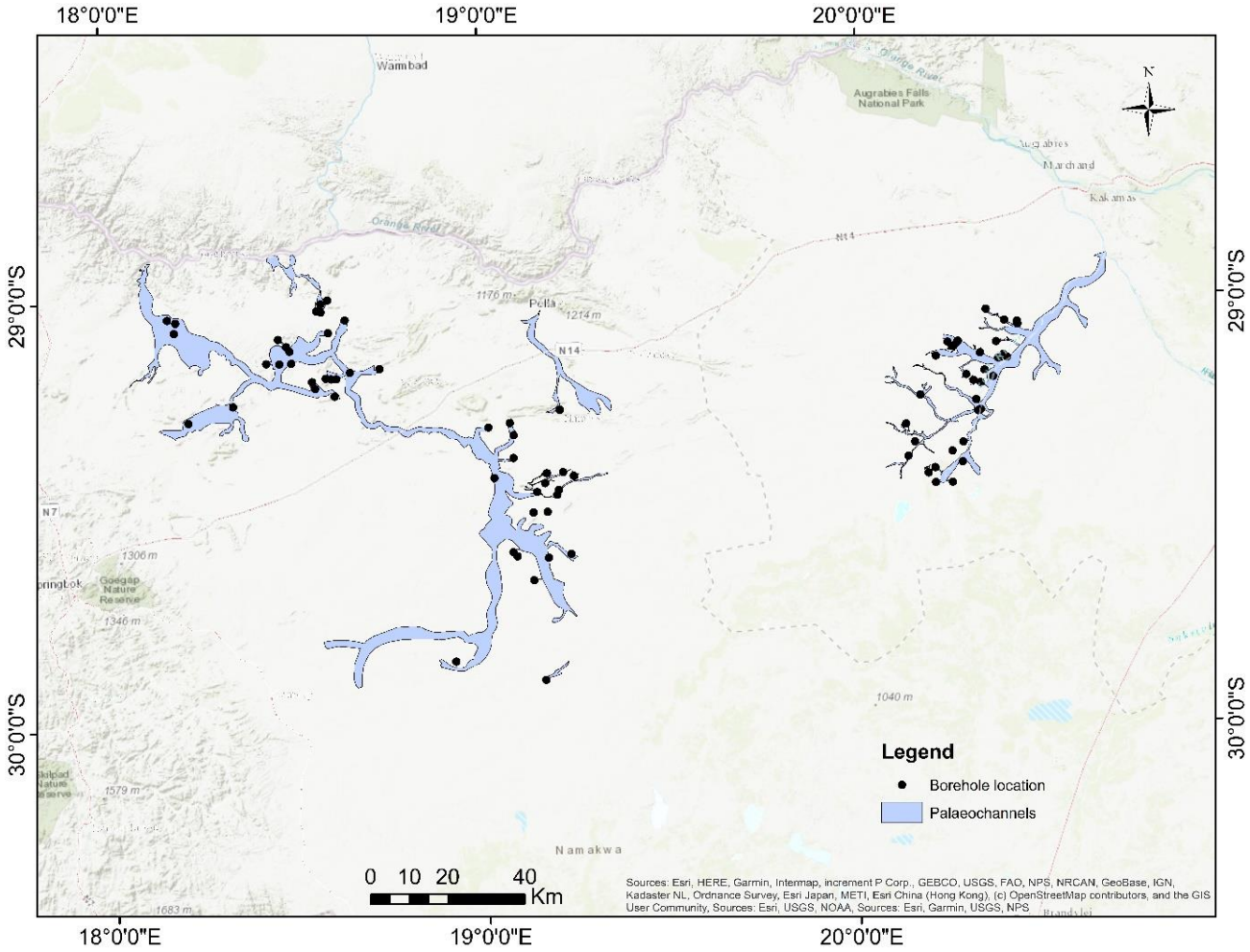

Figure 8: Distribution of groundwater sampling locations and palaeochannels.

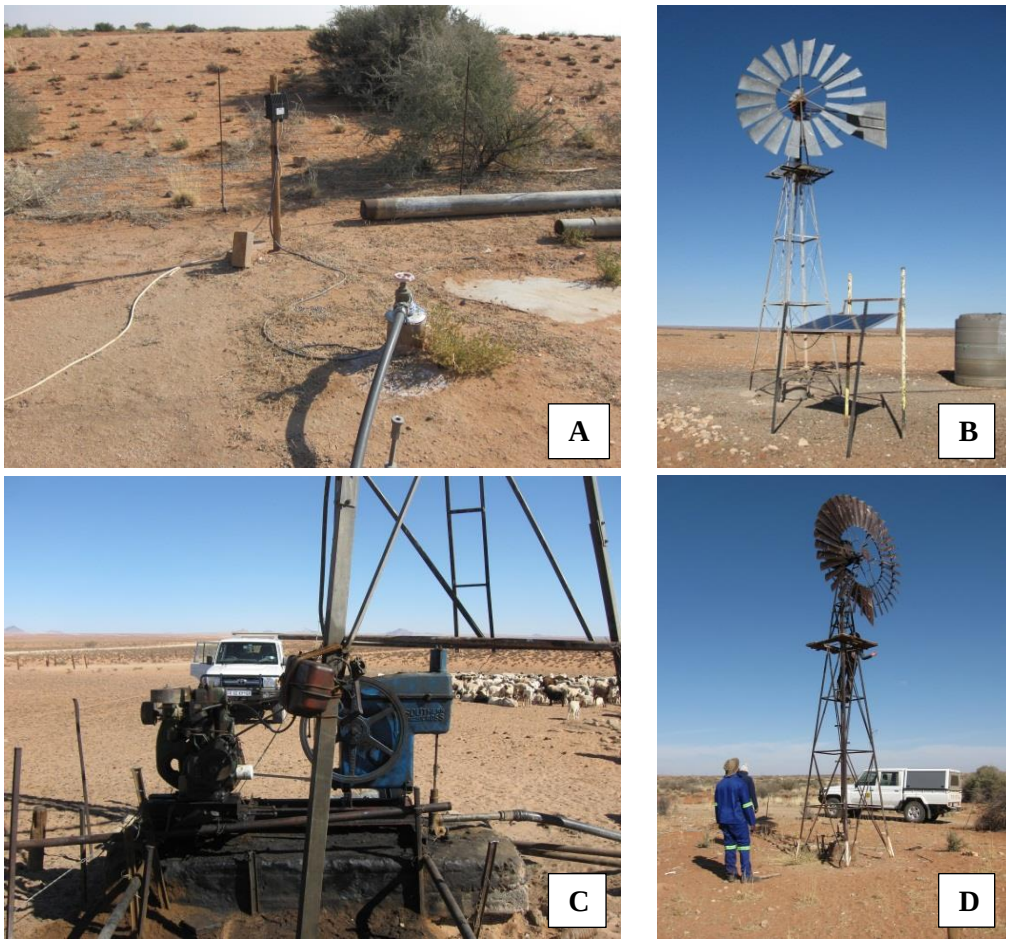

Figure 9: Field photos of groundwater sampling points (boreholes): A. typical electricity-powered pump, B. solar-powered pump, C. diesel-powered pump, D. windmill pump system.

3.3 Climate

The study area is located in an arid, hot region of South Africa, as characterized by the Koeppen classification (Olivier and Van Heerden, 1999). Climatic conditions of the area depend on the altitude and distance from the sea (Leshomo, 2011). Cold and dry severe frost occurs between April and August, with only certain parts of the coastal plain remaining frost free. Namaqualand often has prolonged droughts that are terminated abruptly by heavy floods (Olivier and Van Heerden, 1999). The climate graduates in a west–east direction from desert to poor steppe.

3.3.1 Precipitation

Namaqualand is a typical semi-arid area with the mountainous areas receiving higher rainfall than the arid lowlands due to orographic effects (Olivier and Van Heerden, 1999). Rainfall in Namaqualand is characterized by two pronounced geographical rainfall gradients (Desmet and Cowling, 1998). The first is a gradual latitudinal aridity gradient with the overall precipitation decreasing as one moves northwards into the southern Namib Desert. Perpendicular to this gradient is a longitudinal seasonality gradient from 100% winter rainfall along the coast to 100% summer rainfall in the interior (Desmet, 2007). Mean annual precipitation (MAP) increases from the coastal lowlands (west) to the escarpment zone (east) (Adams *et al*., 2004). Peak rainfall ranges from 50–400 mm per annum and occurs over the Kamiesberg Mountains (1.706 m) as a result of the orographic effect. In catchment D82A, rainfall ranges from 35–313 mm (Figure 10). Higher rainfall occurs in Namaqualand in the winter months from May and September, due to the cold, westerly fronts from the Atlantic coast. Heavy dewfall and advective coastal fog increase the amount of precipitation during the winter and summer months (Davis *et al*, 2016). Fog along the coastal region is generated by the cold Benguela current of the Atlantic Ocean.

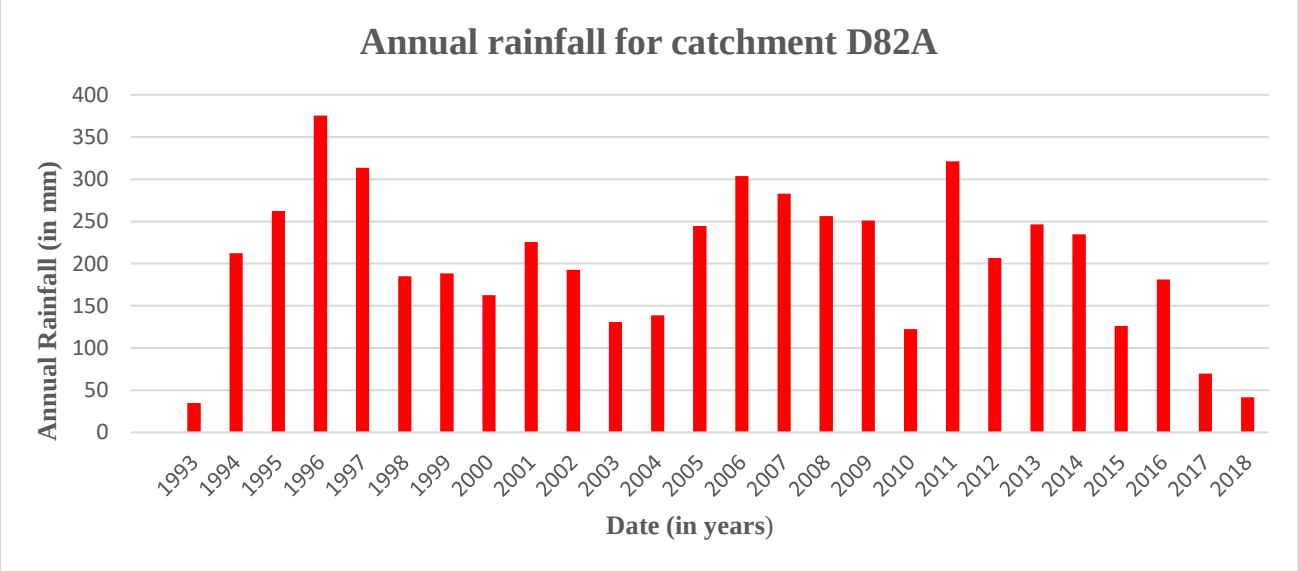

Figure 10: Annual rainfall from 1993–2018 for catchment D82A (South African Weather Services, 2017).

3.3.2 Temperature

Large variations between maximum and minimum, daily and seasonal temperatures characterize the region. Daily mean temperatures throughout the year range from 13–26 °C. Inland areas experience higher mean annual temperatures, while the escarpment and high-lying areas have a cooler temperature (Davis *et al*., 2016).

3.3.3 Evapotranspiration

Potential evaporation in Namaqualand is high due to the dry climate, and often occurs more prominently in the summer months than during the winter months. The potential evaporation of the area reportedly decreases from west to east and can exceed 2 000 mm (Table 2). There is more potential annual evapotranspiration (MAE) than the MAP in all the Quaternary catchments within the study area (Table 2). This results in the formation of evaporitic salts at the surface and in the subsurface (Nakwafila, 2015). Campbell *et al.* (1992) reported that evaporation in unconsolidated soils (alluvium) is observed at depths of 91 cm. Evapotranspiration in densely vegetated areas with shallow water levels is much higher than in areas of sparse vegetation and deep water levels (Van der Sommen and Geirnaert, 1988).

Table 2: Climatological data (MAE and MAP) for the various Quaternary subcatchments within the study area (Midgeley *et al.*, 1994).

Subcatchments	Area(km^2)	MAE (mm)	MAP (mm)	MAE/MAP
D53G	4747	2300	99	23
D53H	1589	2300	131	18
D81G	2007	2650	102	26
D82A	1917	2650	77	35
D82B	4877	2650	80	33
D82C	3996	2650	83	32

3.4 Vegetation

The biome of the area is the Nama–Karoo (Rutherford *et al.*, 1986). False Succulent Karoo occurs along the western boundary in a zone varying in width in a north–south direction from 15–80 km and in a patch south of Pofadder. Vegetation in Namaqualand is characterized by a combination of grasses and low shrubs which make up the Nama–Karoo biome (Adams *et al*., 2004). These shrubs are dominated by leaf succulents or deciduous-leafed woody perennial shrubs or subshrubs (Desmet, 2007). The Namaqualand flora comprise 3 500 species comprising 135 families and 724 genera (Driver *et al*., 2003). The recently revised South African vegetation map presents a more detailed overview of the vegetation of the region (Mucina *et al*., 2005).

3.5 Physiography

The landscape of the area consists of two regions, separated by the north–south-trending marginal escarpment. To the west, the topography is rugged and outcrops of basement gneisses in the form of tors and bornhardts form a significant portion of the terrain. Gently sloping sandy pediments coalesce to form the valley floors (McCarthy *et al.*, 1985).

3.6 Geomorphology

Namaqualand is characterized by three geomorphological regions, namely the coastal plain, an escarpment zone, and the Bushmanland Plateau (Adams *et al*., 2004). These features resulted from a number of geomorphic cycles (Partridge and Maud, 1987). The coastal lowlands are covered by recent sands and underlain by crystalline bedrock. The escarpment zone is defined by exposed domes, weathered material which extends to depths of about 0.5 m, fractured rocks, alluvium-filled valleys and palaeovalleys (Dollar, 1998). The Bushmanland Plateau is characterized by gently sloping pediments which amalgamate to form the valley floors (McCarthy *et al.*, 1985).

3.7 Soils

Namaqualand features a great diversity of soil types (Ellis and Lambrechts, 1986), which can broadly be grouped into three major categories (Desmet, 2007).

The first soil is a grey, yellow or red medium-grained sand with a low clay content. This soil type is mostly underlain by silica or calcium-rich hardpans. The second type is a variably grained sandy to loamy soil derived from *in situ* weathering of the underlying parent material found in the Kamiesberg and Richtersveld escarpment. The largest part of the area is characterized by a 30 cm shallow layer of sand overlying a mature calcrete hardpan and accumulations of sand and semi-mobile dunes which can be 2 m or deeper have gathered in the Koa River Valley (Desmet, 2007).

3.8 Land use

Namaqualand is an arid region which forms part of the western escarpment of South Africa (Desmet, 2007). Thousands of years ago, people of Namaqualand survived as hunters and gatherers and it is as recent as 2000 years ago that hunting and gathering were overtaken by livestock farming (Webley, 2007). In the 1800s the arrival of the Europeans introduced land ploughing for plant grains (Jowell and Folb, 2004). The majority of the land in 2001 was occupied by 80 000 inhabitants. Namaqualand is well known for livestock farming (sheep and goats), crops (mainly grapes) and mining. There are limited numbers of farmers in the 30 000 km^2 region, with only 25 farmers occupying more than10 000 km^2 of the land (Desmet, 2007). The Orange River Valley, especially around Upington, Keimoes and Kakamas, is intensively cultivated with grapes. High-grade copper was exploited in Springbok by the native people before the arrival of European explorers in the 1850s (Carrick and Kruger, 2007). Indeed, a wide variety of minerals, such as salt, molybdenum, vanadium, uranium, zinc, lead and copper have been mined in the Namaqualand (Agenbacht, 2007a). Surficial uranium deposits are found on the

Bushmanland Plateau with a few below the escarpment and on the coastal plains. Several deposits have been prospected in the past at Geelvloer, Brulkolk and Henkries (Figure 11) (Hambleton-Jones *et al.*, 1986).

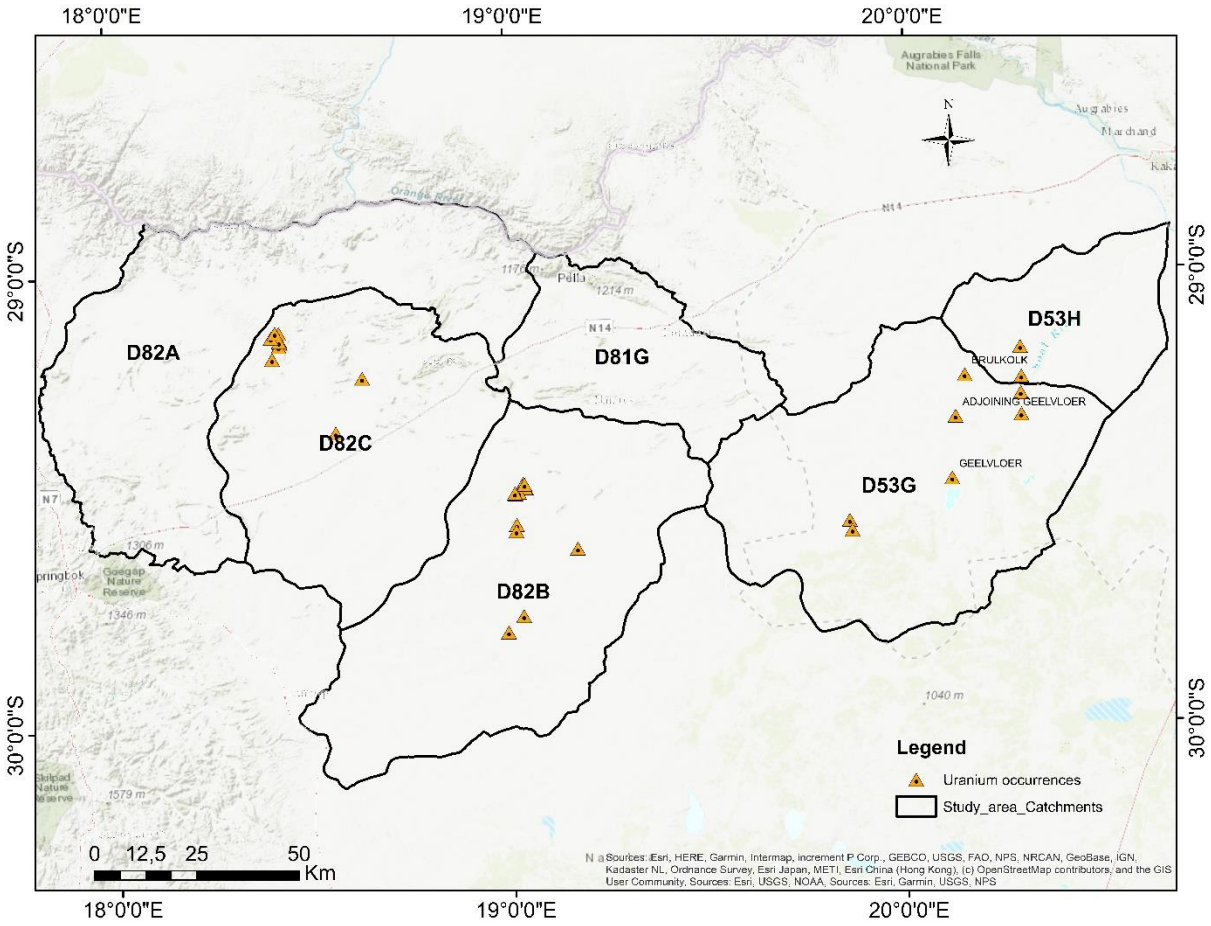

Figure 11: Prospected uranium deposits in the study area (CGS mineral database, 2018).

3.9 Regional geology

The Namaqualand surficial uranium deposits mostly occur in Tertiary to Recent (Cenozoic) surficial material overlying the basement rocks of the Bushmanland Plateau (named the Bushmanland Terrane by Cornell *et al.*, 2006) of the Namaqua Metamorphic Province (NMP). The Namaqualand geology can be subdivided into three geological provinces, namely the Namaqua Metamorphic Province, the Gariep Complex and the Phanerozoic cratonic cover (Tankard *et al.*, 1982; Visser, 1989). The NMP forms part of the 1300–1100 Ma Namaqua-Natal Province (NNP) (Cornell *et al*., 2006; Macey *et al*., 2017), which is one of several orogenic belts understood to have been involved in the assembly of the Rodinia Supercontinent (Dalziel *et al.*, 2000). This orogenic belt is known as the Namaqua-Natal Metamorphic Belt and comprises deformed and metamorphosed rocks, affected by structural, metamorphic and/or

thermal processes (Blignault *et al.,* 1983). The NNP outcrops over an area of 100 000 km^2 in the Northern Cape and over 200 000 km^2 in KwaZulu-Natal (Cornell *et al*., 2006).

The NMP comprises Proterozoic meta-volcanosedimentary successions which are intruded by various granitoids and which are largely covered by Cenozoic deposits and, to the southeast, by younger Mesozoic sediments and intrusive sheets of the Karoo Supergroup (Blignault *et al.,* 1983). In the west and extreme north, rocks of the NMP and its correlatives are bordered by formations of the late Proterozoic Gariep Supergroup and, in the east, adjoin the Kaapvaal Craton, with a marked structural discordance in both cases (Raith *et al.,* 2003). The Province is characterized by an intricate pattern of folding and faulting (Slabbert *et al.,* 1999).

Hartnady *et al. (*1985) subdivided the geology of the area into subprovinces, naming them the Bushmanland, Richtersveld, Gordonia and Kheis tectonic subprovinces. Cornell *et al.* (2009), in turn, subdivided the subprovinces (from west to east) into terranes, based on marked changes in the lithostratigraphy across structural discontinuities.

The Richtersveld Subprovince consists of volcanosedimentary rocks (gneisses, andesitic lavas, schists and quartzites) of the Richtersveld Subprovince (Robb *et al.,* 1999; Cornell *et al.,* 2006). These rocks underwent a D_1 deformation event that produced open isoclinal folds (Blignault *et al.,* 1983; Colliston and Schoch, 1996). The rocks of the Bushmanland Subprovince comprise para- and orthogneisses amphibolites, psammo-pelitic schists, quartzites, calc-silicate rocks and granitoids (Joubert, 1986; Nakwafila, 2015).

The study area is covered by variable thicknesses of Quaternary sediments. These sediments in general, overlie rocks of the Richtersveld and Bushmanland Subprovinces and Karoo sediments. The Karoo Supergroup in the study area consists of sandstones, shales and mudrocks of the Ecca Group and the Dwyka Group diamictites, with Jurassic dolerite intrusions (sills and dykes). The Quaternary catchments in the study area are characterized by alluvium, calcrete, pan sediments, calcareous and gypsiferous soil, red and grey aeolian sand and superficial cover. Calcrete is confined mainly to topographic highs of the Bushmanland Plateau adjacent to the Koa River Valley and, further east, occurs as scattered nodules and irregular layers within various superficial sediments such as unconsolidated wind-blown sand, various types of soil, rubble and unconsolidated gravel and scree derived from weathered Karoo diamictite and basement rocks (Figure 12). Joubert (1971), Jack (1980), Theart (1980) and Albat (1984) carried out detailed mapping of the Namaqualand rocks on a 1:100 000 scale.

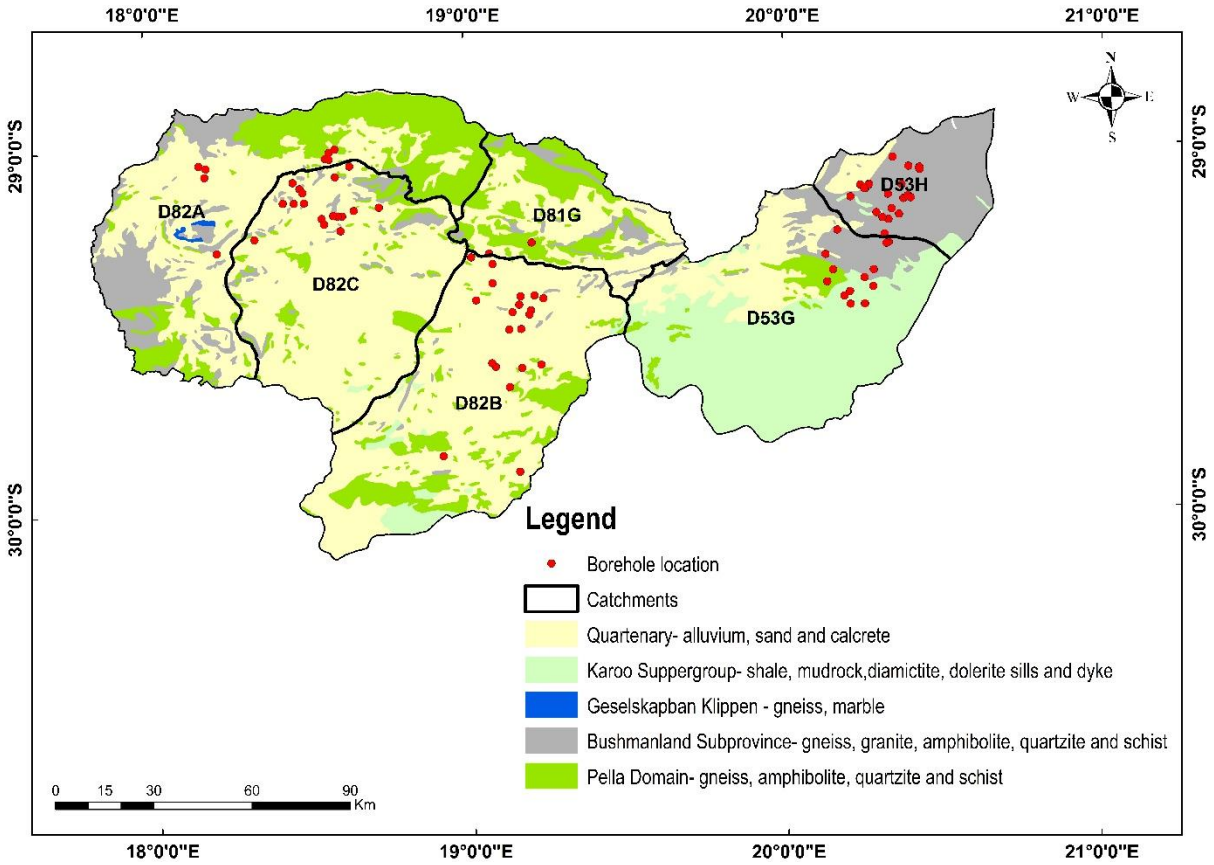

Figure 12: Surface geology of the study area, with Quaternary catchments shown (modified from Macey *et al.*, 2018).

3.10 Drainage history

The Koa Palaeovalley is associated with mineralization of surficial uranium and important alluvial diamonds, consolidated in calcretes and pedocretes, respectively (Agenbacht, 2007a; Almond and Pether, 2009). Two ridges (Houmoed Highlands and Kouberg Highlands) act as watershed boundaries which run parallel to the Koa, resulting in the drainage being directed towards the Buffels River in the southwest and south and towards the upper reaches of the Hartbees River in the southeast (Agenbacht, 2007b).

The Sout River has outlets which are characteristic of a fluvial system, but the pans have typical pan characteristics. Many surficial uranium deposits, such as the Brulkolk and Geelvloer, occur in the Sout River drainage channel. These deposits were only prospected.

3.11 Hydrology

Rivers in Namaqualand are largely ephemeral, owing to the low rainfall in the arid to semi-arid region, with the Gariep River to the north being the only perennial river (Nakwafila, 2015). Peak rainfall in arid regions tend to cause peak flood discharge despite the low annual rainfall (Tooth, 2000). During the Tertiary period, the main drainage pathways of the ephemeral rivers in central Namaqualand were reformed several times owing to the different stages of tectonic and eustatic events which led to the creation of numerous palaeochannels (De Wit, 1993). The main ephemeral rivers in the area are the Bul, the Orange, the Brak, the Kaboe and the Sout River (Figure 13).

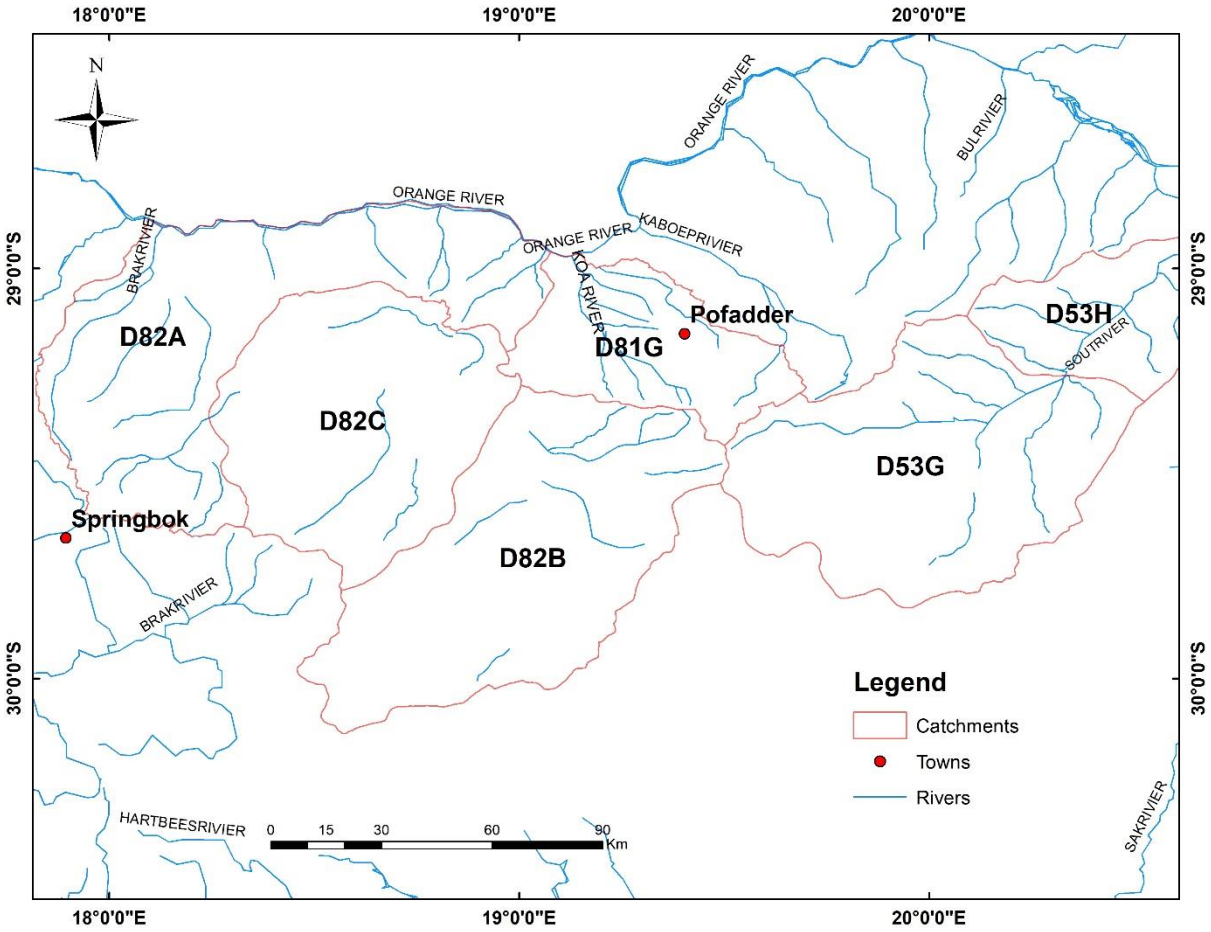

Figure 13: Distribution of rivers in the study area.

3.12 Hydrogeology

In Namaqualand, groundwater occurs in three different aquifer systems, namely (1) fractured bedrock, (2) the weathered zone or regolith and (3) sandy/alluvial aquifers. However, hydraulically, the fractured bedrock and weathered zone aquifers in the region are closely linked to form the so-called basement aquifers (Adams *et al*., 2004). The underlying geology of the igneous and metamorphic rocks (e.g. the granites and gneisses) and their deformation history or structural evolution control and influence the geometries of the aquifer systems in Namaqualand (Conrad and Adams, 2003; Pietersen *et al*., 2009).

3.12.1 Basement aquifers

Basement aquifers are linear systems associated with fault-controlled valleys (Pietersen *et al*., 2009). Basement aquifers are prominent in the mountainous escarpment zone, and the weathered zone aquifers are used as targets for groundwater resources. The weathered zone aquifers act as reservoirs that recharge the fractured bedrock aquifers (Adams *et al*., 2004). The clays act as a hydraulic barrier in the

areas where there are extensive clays between the two aquifers (the weathered zone aquifer and the fractured bedrock aquifer), thereby reducing the linkages within the aquifer system (Titus *et al.*, 2003).

3.12.2 Sand/alluvial aquifers

Namaqualand basement aquifers are overlain by alluvial aquifers associated with ephemeral rivers, palaeochannels and coastal plains (Adams *et al*., 2004; Titus *et al.,* 2009). Alluvial aquifers associated with ephemeral river systems are reportedly shallower than those associated with the coastal plain (Pietersen *et al*., 2009). In Namaqualand, boreholes and large-diameter wells are usually drilled in river courses and alluvium-filled valleys, with most of these overlying granitic bedrock.

4 METHODOLOGY

4.1 Fieldwork and water sampling

Field data collection was conducted in Namaqualand in six Quaternary catchment basins. In order to achieve a good spatial distribution, boreholes that were easy to access were selected for sampling, using the borehole information from the National Groundwater Archives (NGA) in the Department of Water and Sanitation (DWS) database. The borehole data were captured in the early 1980s. The selected boreholes were located in the areas delineated by prospectivity modelling for surficial uranium deposits that had been conducted by Kenan *et al*. (2017). The selected boreholes are found in palaeochannels and, in some cases, are located in close proximity to known surficial uranium occurrences. Groundwater samples were taken from 85 boreholes at a spacing of 5 km or greater within each Quaternary catchment. Samples were collected directly from fully functional boreholes in July and October 2017, during winter and spring, respectively. Geographic coordinates of all the collected samples were captured using a standard hand-held global positioning system receiver. The samples were collected based on the comprehensive guide for groundwater sampling methods by Weaver *et al.* (2007).

4.1.1 Sampling procedures

Care was taken during sample collection to minimise potential cross-contamination between sampling points. These measures included using a new pair of disposable gloves, syringe, and filter for the collection of each distinct water sample. All the sample bottles and lids were thoroughly rinsed with distilled water and then with the borehole water to be sampled. Samples were taken from the groundwater in functioning boreholes, whereas in cases where the water in the boreholes was stagnant, these boreholes were purged for at least 3–5 minutes before sampling to obtain a representative groundwater sample. The process of purging boreholes is described by Weaver *et al.* (2007). A 5 L bucket was used to collect groundwater from the borehole. The sampling bucket and syringes for the filtered samples were rinsed with the water to be sampled with.

4.1.2 Physicochemical properties

Field measurements of dissolved oxygen (DO), electrical conductivity (EC), pH, oxidation reduction potential (Eh), salinity, total dissolved solids (TDS) and temperature (T) were measured *in situ* using field meters for each borehole. A pH meter, SevenEasy, Mettler-Toledo GmbH and a probe were used to measure the pH of the water samples from the Namaqualand area. Prior to the measurement, the pH meter was calibrated using three buffers with pH 4, pH 7 and pH 10. Sufficient amounts of the sample, enough to immerse the probe, were placed in a 50 mL glass beaker. The probe was rinsed with deionized water and a small amount of the sample. Then the probe was immersed in the sample, and the pH was

taken once the reading had stabilised. EC is a measure of the total dissolved ionic species in an aqueous phase and can be measured using a meter and a probe. A Jenway 4010 conductivity meter was calibrated before sample analysis, using 0.1 M KCl standard solution. A sufficient amount of the sample, to immerse the probe, was placed in a 50 mL glass beaker. The probe was rinsed with deionized water and a small amount of the sample. Then, the probe was immersed in the sample and the EC reading was taken after it had stabilised.

4.1.3 Sampling for cation and anion analyses

A 100 mL high-density polyethylene (HDPE) liquid sample bottle with a ratchet cap was used. Cation samples were filtered in the field to <0.45 µm and acidified immediately using 3 mL of nitric acid (HNO_3) with a pH of 2 as per the CGS laboratory specifications to keep the metals dissolved and to prevent precipitation. Samples collected for anion analyses were also filtered on site to <0.45 µm but were not acidified. The above sampling procedure was carried out, as outlined by Weaver *et al.* (2007). The collected samples were then stored in an insulated cooler box and dispatched to the laboratory for analysis.

4.1.4 Sampling for alkalinity analyses

A 100 mL HDPE liquid sample bottle with a ratchet cap was used. The bottles were filled to the top to prevent the formation of bubbles that may contain oxygen, and hence introduce unwanted oxygen into the water samples. Original samples were kept unfiltered and un-acidified, in order to keep the alkalinity as constant as possible as filtering could cause possible de-gassing. The samples were then stored in an insulated cooler box and dispatched to the laboratory for analysis.

4.2 Laboratory analysis

4.2.1 Cations

The analysis of water samples for cations was performed using inductively coupled plasma mass spectrometry (ICP-MS) at the CGS laboratory in Silverton, Pretoria. A Perkin Elmer ELAN® DRC II ICP-MS system, equipped with a Meinhard nebulizer and a cyclonic quartz ICP-MS spray chamber, was used for the analysis. Cation analysis was performed using two separate methods: TM-CHE032 (majors) was used for the following major elements: Na, Mg, Al, K, Ca and Fe. TM-CHE033 (traces) was used for the following trace elements: Li, Be, B,, V, Cr, Mn, Co, Ni, Cu, Zn, Ga, As, Se, Rb, Sr, Mo, Ag, Cd, Te, Ba, Tl, Pb, Bi and U.

4.2.1.1 Calibration and internal standards

Calibration curves for the major elements were constructed using four calibration standards and a process blank. The four calibration standards for the major element analyses were prepared from certified stock solutions at concentrations of 100, 1000, 2500 and 5000 µg/L each for Na, Mg, Al, K, Ca and Fe. The four calibration standards for the trace elements were prepared from certified stock solutions at concentrations of 102, 510, 1025 and 2050 µg/L for Na, Mg, Al and K; 200, 1000, 2500 and 5000 µg/L for Ca; 20, 100, 250, and 500 µg/L for B, Fe, Zn, As and Se; 2, 10, 25 and 50 µg/L for the remainder of the trace elements. GR grade reagents and ultrapure water were used for all dilutions. In and Ir were added online as internal standards using a Y connector at concentrations of 100 and 150 µg/L respectively. The online addition dilution factor for the internal standard was approximately four times by volume. Where trace elements data were duplicated using the major element method, reported data were selected according to the most suitable calibration range for the sample values

4.2.1.2 Sample preparation

All the water samples were filtered through a 0.45 µm hydrophilic membrane filter and acidified in the field. In the laboratory, samples were then diluted 50 times for the major element analyses and 10 times for the trace element analyses with 2% GR grade HNO_3 /ultrapure water to keep the analytes in solution and to reduce the TDS. In-line standard addition was done for the samples in the same way as for the standards during the analyses.

4.2.1.3 Quality assurance

The quality of the analyses was maintained by repeat analysis of blanks, calibration standards, selected samples and independent quality control standards during each analytical run. The instrument was re-calibrated every 25 samples. Prior to analysis, the instrument was set up according to the manufacturer's specifications. Additional elements were used for the detector cross-calibration, while several custom solutions were prepared for more accurate tuning of the mass spectrometer. The applicable detection limits are listed in Table 3.The CGS laboratory regularly takes part in the SABS water check laboratory proficiency testing scheme (group 1) (Code B149). A typical Z-score of between +0.63 and +1.83 was obtained during the period (2015/ 2017) that samples for this project was analysed (SABS, 2017).

Table 3: Detection limits of the analytical methods.

Major elements	µg/L	Trace elements	µg/L	Anions	mg/L
Na	32.81	**Li**	0.22	**F**	0.06
Mg	5.61	**Be**	0.08	**Cl**	0.1
Al	12.49	**B**	2.1	**NO_2**	0.008
K	48.05	**Al**	78.6	**Cr(VI)**	0.0008
Ca	90.02	**V**	0.01	**NO_3**	0.01
Fe	67.69	**Cr**	0.6	**PO_4**	0.02
		Mn	0.5	**SO_4**	0.41
		Fe	23.9		
		Co	0.01		
		Ni	0.04		
		Cu	0.2		
		Zn	3.6		
		Ga	0.02		
		As	0.06		
		Se	0.9		
		Rb	0.07		
		Sr	0.03		
		Mo	0.01		
		Ag	0.4		
		Cd	0.03		
		Te	0.04		
		Ba	0.31		
		Tl	0.06		
		Pb	0.06		
		Bi	0.01		
		U	0.002		

4.2.2 Anions

Determination of common anions necessary for the characterization of water and/or an assessment of the need for a specific treatment. A discrete analyser (Thermo Gallery Plus) provides a single instrumental technique that can be used for the analysis of different anion species in a single analytical run. Seven anion species (F^-, Cl^-, NO_2^-, Cr(VI), NO_3^-, PO_4^{3-} and SO_4^{2-}) were analysed using a discrete analyser at the CGS laboratory in Silverton, Pretoria (method TM-CHE010). All water samples were filtered through a 0.45 µm hydrophilic membrane filter in the field. The samples were pre-diluted in the laboratory using ultrapure water (18.2 mega Ohm), where required. The instrument was set up to automatically dilute samples to fall within the calibration range and to flag samples where this could not be achieved.

4.2.2.1 Calibration

Individual calibration standards were set for each analyte at concentrations of 100 mg/L for SO_4^{2-} and Cl^-, 20 mg/L for NO_3^-, 10 mg/L for PO_4^{3-} and F^-, 0.488 mg/L for Cr(VI) and 5 mg/L for TON (total organic nitrogen). The NO_2^-, value was calculated by subtracting NO_3^- from the measured TON. The instrument was set up to automatically dilute the initial calibration standard to achieve a calibration curve of several points for each element.

4.2.2.2 Quality assurance

Quality control standards were analysed after every tenth sample to verify the quality of the results. A quality control standard, at 10% the concentration of the calibration standard, was used to monitor accuracy during every analytical run. The applicable detection limits are listed in Table 3. The CGS laboratory regularly takes part in the SABS water check laboratory proficiency testing scheme (Code B149) (group 3). A typical Z-score of between +0.42 and +1.64 was obtained during the period (2015/ 2017) that samples for this project was analysed (SABS, 2016).

4.2.3 Alkalinity

Alkalinity measurements were obtained using potentiometric titration by means of a Metrohm 905 titrando equipped with Tiamo version 2.5 software. The instrument consists of a Metrohmn 854 iconnect pH electrode and a Metrohmn EC electrode. The instrument pH electrode was verified using buffer solutions of pH 4.0, 7.0 and 9.2 respectively. EC was verified using a 1413 EC standard. A primary standard of sodium carbonate ($NaCO_3$) was oven dried at 250 °C for 4 hours. For the standardization process, 0.3 g of the primary standard was weighed and transferred into a 1000 mL volumetric flask to prepare 300 mg/L of the primary standard to standardize 1.0 molar (M) hydrochloric acid (HCl). For quality control (QC), 2.12 g of carbonate sample was weighed to prepare a 20 mg/L QC sample, transferred into a litre volumetric flask and filled completely with deionized water to make a QC sample. A 100 mL aliquot of the QC sample was ran for every tenth sample to account for 10% replicate. The samples (100 mL) were titrated with a standardized 1.0004 M HCl to an endpoint pH of 4.5 where the titrant volume is recorded and used to determine the concentration of the each sample according to the CGS SOP: 1111: Determination of Total alkalinity in water and wastewater by potentiometry (Determination of alkalinity in water) as adopted from the standard methods for the examination of water and wastewater (Eaton *et al.*, 1998).

4.3 Uranium Geochemistry

Geochemical modelling was done using software code PHREEQC (Parkhurst and Appelo 1999). A computer program PHREEQC geochemical code (Parkhurst and Appelo 2013) has been used to determine the solubility of U and major mineral species and its interaction between groundwater systems of the study area. The saturation index (SI) of groundwater samples with respect to mineral precipitation is expressed by SI = log (IAP/Ksp) where IAP is ion activity of the solution; Ksp is equilibrium constant of the reaction considered at temperature (T) (Lee and Strickland 1988). The ability of chemical species to remain in solution is calculated from the SI of the minerals that could precipitate as a result of ionic activities of the necessary chemical species. If the water is exactly saturated with the dissolved mineral, SI equals to zero. Positive values of SI indicate saturation, and negative values indicate undersaturation (Appelo and Postma 1996). The groundwater geochemical data were used for modelling to obtain possible uranium species that may be present in the study area. The dissolutions of carnotite and tyuyamunite as written in the PHREEQC database:

$KUO_2VO_4 + 4H^+ = K^+ + UO_2^{+2} + VO_2^+ + 2H_2O$ (1)

$Ca(UO_2)_2V_2O_8 + 8H^+ = Ca^{2+} + 2UO_2^{+2} + 2VO_2^+ + 4H_2O$ (2)

From these equations, the saturation indices (SI) reflecting the degree of saturation of the groundwater with respect to carnotite and tyuyamunite is written as:

$SI_{carnotite} = a[K^+]a[UO_2^{2+}]a[VO_2^+]/a[H^+]^4K_{carnotite}$

$SI_{tyuyamunite} = a[Ca^{2+}]a[UO_2^{2+}]^2a[VO_2^+]^2/a[H^+]^8K_{tyuyamunite}$

Where a = activity, $K_{carnotite}$ and $K_{tyuyamunite}$ = the equilibrium constant for reactions (1) and (2).

4.4 Risk analysis on areas associated with uranium content in the groundwater of the study area

Risk is defined as the chance of something happening that will have an impact either on environment, health or other factors of interest. Risk is measured as the product of the probability of the risk happening and the impact of that risk, therefore: risk = probability x impact.

The identification of high risk areas that may be a threat to human health due to uranium contents in the groundwater is done by using the above formula of probability multiplied by the impact. The probability expressed here is the likelihood of uranium concentration in the groundwater within the study area,

while the impact is represented by the population density that may be affected by the consumption of groundwater with high uranium contents. A map of uranium concentrations was created by gridding the surface of uranium contents in the groundwater using the inverse distance weighting (IDW). The impact map was created using the population density in the study area. These two maps were then combined by multiplication to produce the risk map.

4.5 Carnotite solubility index

The CSI was calculated using the following equation (Hambleton-Jones and Smit, 1986):

$$CSI = \log \frac{[K][U][V]}{1.13 \times 10^{4}\,[HCO3^{-}]^{2}}$$

where:

CSI = carnotite solubility index

[K] = total potassium concentration (expressed as ppm or mg/L of the metal in solution)

[U] = total uranium concentration (expressed as ppb or µg/L of the metal in solution)

[V] = total vanadium concentration (expressed as ppb or µg/L of the metal in solution)

[HCO_3^-]= bicarbonate concentration in aqueous solution (expressed as ppm or mg/L).

It is important to note that the CSI is determined using the actual concentrations of the active species in solution i.e. K, U, V, HCO_3^- and pH.

The formula that was used to calculate the CSI was taken from the global study of surficial uranium deposits by Hambleton-Jones and Smit (1986), shown below:

It is important to note that the above formula was been derived using actual concentrations of potassium, uranium, vanadium, bicarbonates and, crucially, pH values. The original formula, from which the above formula was derived, is shown below:

$$CSI = \frac{10^{pH-9.02}[EK.EU.EV]}{1 + 10^{4.5-pH} + 10^{-5.69+pH}(BC)^{2} + 10^{-17.00+2pH}(BC)3}$$

where:

CSI = carnotite solubility index

EK = total potassium concentration (expressed as ppm or mg/L of the metal in solution)

EU = total uranium concentration (expressed as ppb or µg/L of the metal in solution)

EV = total vanadium concentration (expressed as ppb or µg/L of the metal in solution)

BC = bicarbonate concentration in aqueous solution (expressed as ppm or mg/L).

Under perfect conditions, it is anticipated when the CSI is equal to zero that the solution is in equilibrium with carnotite. However, Hambleton-Jones and Smit (1986) pointed out that, even under ideal conditions, the CSI does not reach zero. In areas of carnotite mineralization, the values of CSI are usually as low as -3. These low CSI values may be ascribed to the fact that the equation is based on theoretical chemical equilibria for ideal solutions. Hambleton-Jones and Smit (1986) further stipulated that the expected low CSI values in the areas that are favourable in terms of carnotite mineralization are attributable to the fact that the precipitation of carnotite in nature does not take place in ideal solutions, but rather in solutions that contain other compounds in various concentrations. In addition, the precipitation of carnotite is influenced by the oxidation potential of the groundwater and the presence of clays and hydrated iron oxides where nucleation and adsorption onto the surfaces can take place. Therefore it is advisable to use a low value of CSI as the threshold between anomalous and background values (Hambleton-Jones and Smit, 1986). Other factors that may influence the low values of CSI include the possible dissociation of bicarbonates from carbonates before laboratory analysis is conducted, which may cause an increase in pH values and the adsorption of uranium and vanadium ions onto the interior walls of plastic sample bottles (Hambleton-Jones and Smit, 1986). Calculation of the CSI has also been applied in Australia by Mann and Deutscher (1978), who made similar assumptions as Hambleton-Jones and Smit, 1986. Mineral equilibrium calculations, based on known mineralogy and groundwater chemistry (also known as CSI) have been used to understand geochemical controls on uranium precipitation in the calcrete palaeochannel deposits of Namibia (Bowell *et al.*, 2009).

Hambleton-Jones and Smit, 1986 made the following assumptions:

when CSI $\geq$-3 the solution is oversaturated with carnotite and it will precipitate;

when CSI < -3 the solution is undersaturated with carnotite and the latter will dissolve.

5 RESULTS

5.1 Groundwater quality

5.1.1 Field parameters

The quality of the groundwater was evaluated against the South African water quality guidelines (SAWQG) and the World Health Organization (WHO) standards. The temperature of the water samples ranged from 7.3 to 27.6 °C with a mean temperature of 18.0 °C. The water in the study area is neutral to alkaline, with pH values ranging from 7.13–8.91 (See Appendix 1). The water samples fall within the safe range of SAWQG for pH of 6–9. EC of the groundwater samples ranges from 22 (borehole SSM031) to 1443 mS/m (borehole SSM035), with an average of 350 mS/m. About 75% of the groundwater samples exceeded the maximum permissible limit of 150 mS/m for EC (Figure 14). The TDS value ranges from 315–9980 mg/L, with an average of 2452 mg/L. Only 2% of the water samples have a TDS value <500 mg/L (Figure 15). Based on the SAWQD target range, a TDS classification of 84% means that the water in the boreholes is brackish (TDS >1000 mg/L). Of the boreholes, 16% registered a TDS value (<1000 mg/L) indicating fresh water. Salinity in the groundwater samples varies from as low as 0.22 to 8.28 g/L. The study area has salt pans, which are a sign of an elevated salinity content (Figure 16). The redox potential is positive in all the boreholes, with a minimum value in borehole SSM08 (0.06 V) and a maximum value in borehole SSM055 (0.28 V).

Total alkalinity ranges from 61–903 mg/L, with an average of 360 mg/L, exceeding the maximum permissible limit of 50–100 mg/L set by the SAWQG. The results of the field parameters are shown in Appendix 1.

Figures 14, 15, 17 and 18 have been drawn using the ArcGIS Spatial Analyst tool in view of verifying the variability of EC, TDS, Na^+ and Cl^- in the groundwater of each catchment.

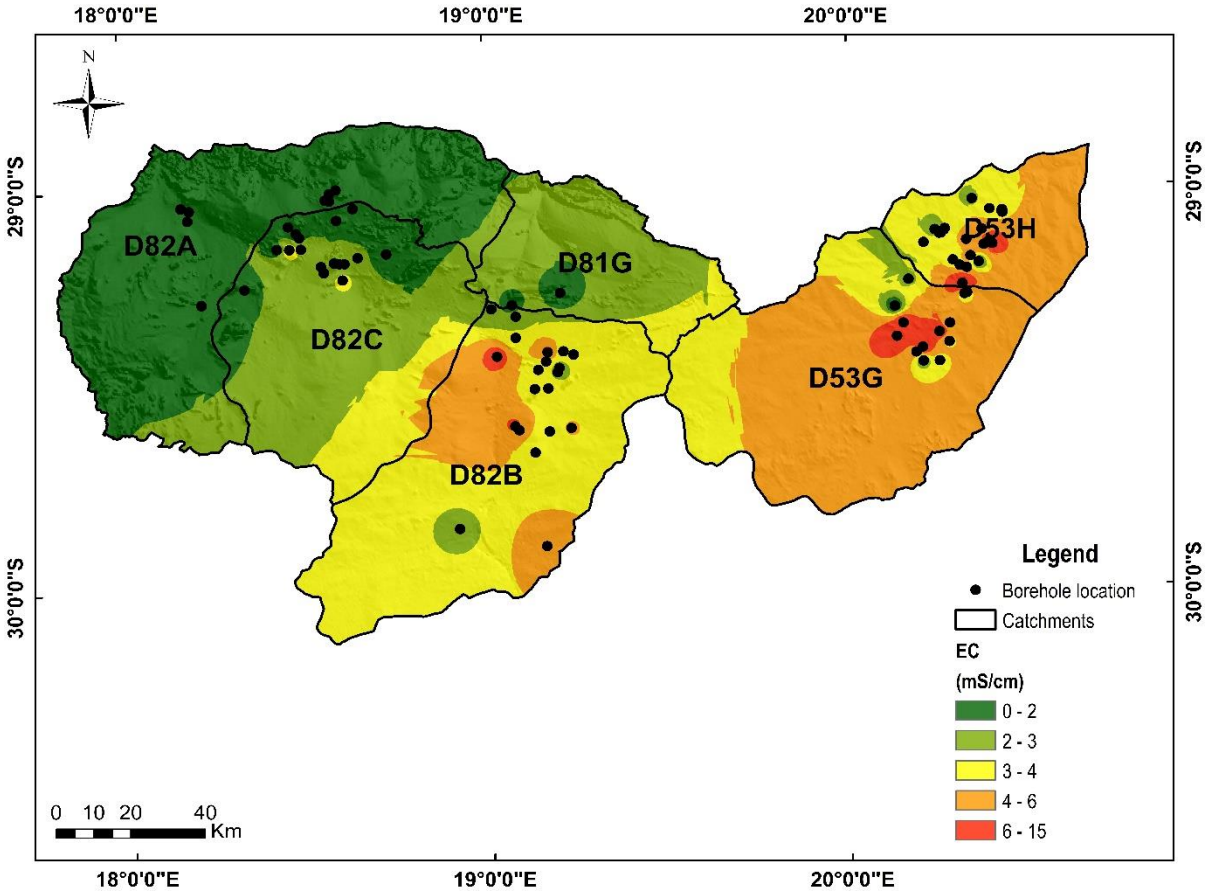

Figure 14: Spatial distribution of EC in the borehole water of the study area.

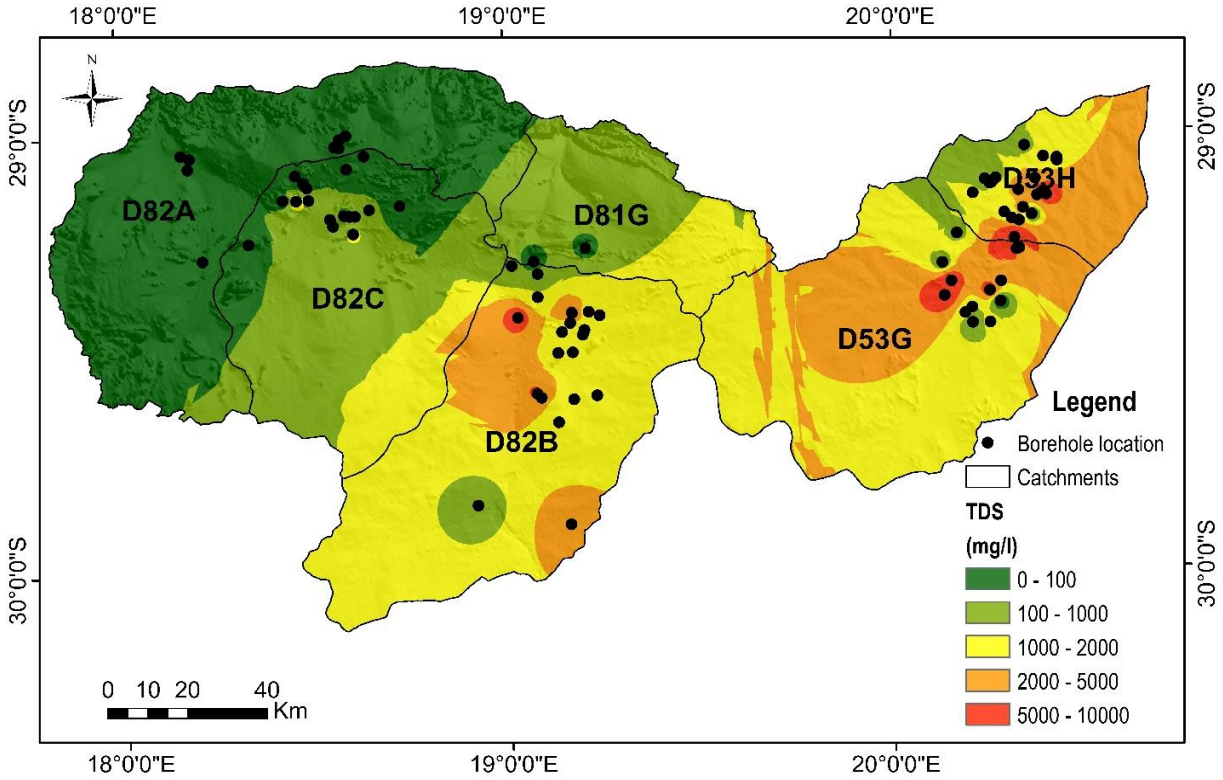

Figure 15: Spatial distribution of TDS in the borehole water of the study area.

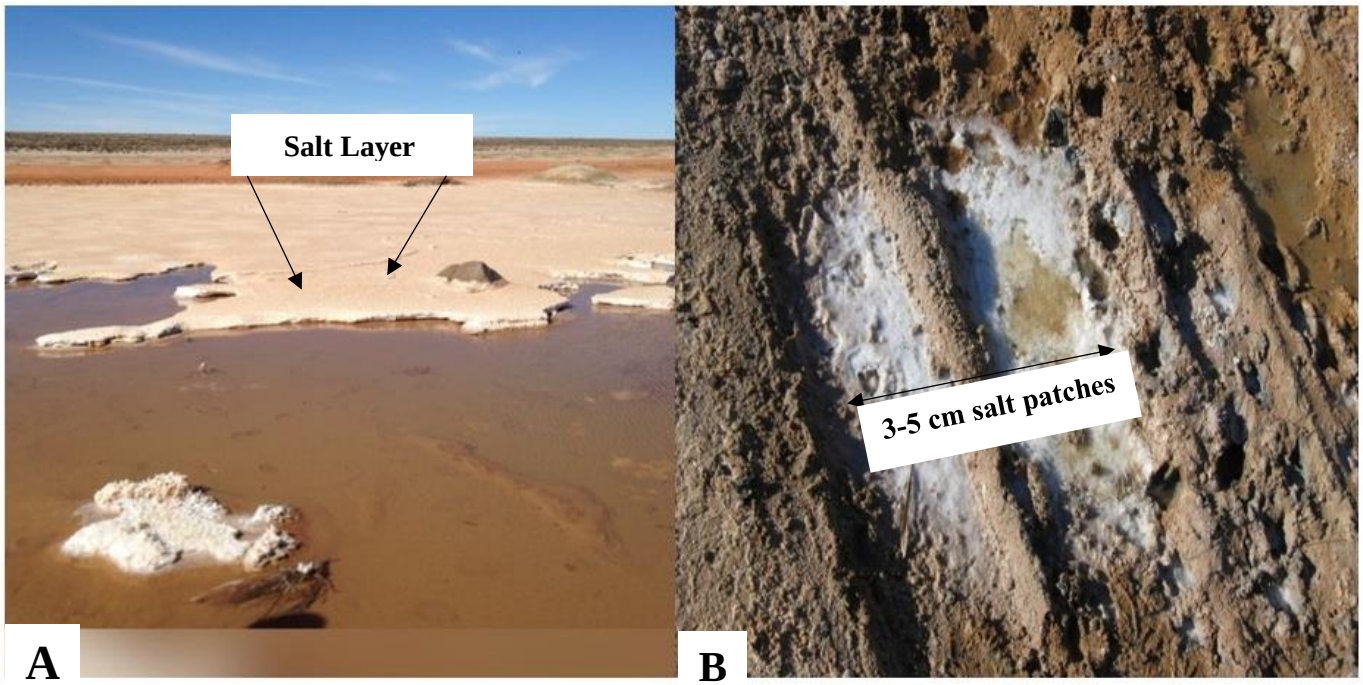

Figure 16: A. Thick salt layer found at Bosluis Pan in Gamoep, B. 3– 5 cm salt patches found on the gravel road at Bitterputs se Pan.

5.1.2 Major ion chemistry

The distribution of major ions in the groundwater is as follows: $Na^+ > Ca^{2+} > Mg^{2+} > K^+$ and $Cl^- > SO_4^{2-} > HCO_3^- > NO_3^-$ (Table 4). The concentration of Na^+ shows a large variation from 84.38–12802 mg/L, averaging 908 mg/L. About 79% of the samples have Na^+ values greater than the permissible limit of 200 mg/L for drinking water (Figure 17). The concentration of Ca^{2+} in the study area ranges from 49–926 mg/L, with an average of 258 mg/L. As per the SAWQG target water range, 91% of the samples from this study exceed the permissible limit of 75 mg/L of Ca^{2+}. The concentration of Mg^{2+} ranges from 14.01–329 mg/L, with an average value of 70.9 mg/L. The K^+ concentration ranges from 2.3–19.7 mg/L, with an average of 20.13 mg/L. The distribution of anion concentrations ranges from 114–5100 mg/L Cl^- (Figure 18), 86.35–3802 mg/L SO_4^{2-}, 61–903 mg/L HCO_3^-, and <0.01–299 mg/L > NO_3.

Sample SM032 has the highest values of Na^+ (12802 mg/L) and Cl^- (5100 mg/L) which exceed the highest TDS value (10000 mg/L). The field instrument was not able to measure the high salinity and TDS of the sample. Perhaps there was an error in the laboratory measurement of the concentrations of Na^+ and Cl^-. In the analysis of the data, sample SM032 was removed.

Table 4. Summary statics of the groundwater parameters, with their SAWQG water target ranges.

Parameter	Min	Max	Mean	Standard deviation	SAWQG (DWAF, 1996) target water ranges
T (°C)	7	28	18	5	-
pH	7	9	8	0.40	6 - 9
EC (mS/m)	22	1443	350	15	0 -7
TDS (mg/L)	315	10000	2500	1700	0 - 450
Sal (g/L)	0.22	8	15	84	-
Ca^{2+} (mg/L)	49	930	258	171	0 - 32
Mg^{2+} (mg/L)	14	330	71	53	0 - 30
Na^+ (mg/L)	85	3670	1000	1500	0 - 100
K^+ (mg/L)	3	3250	60	350	0 - 50
F^- (mg/L)	0.04	6	3	1	0 - 1.1
Cl^- (mg/L)	115	5100	1500	2000	0 - 100
HCO_3^- (mg/L)	0.00	1000	360	200	-
SO_4^{2-}(mg/L)	11	3800	615	510	0 - 200
NO_3^-(mg/L)	0.01	300	51	52	0 - 6

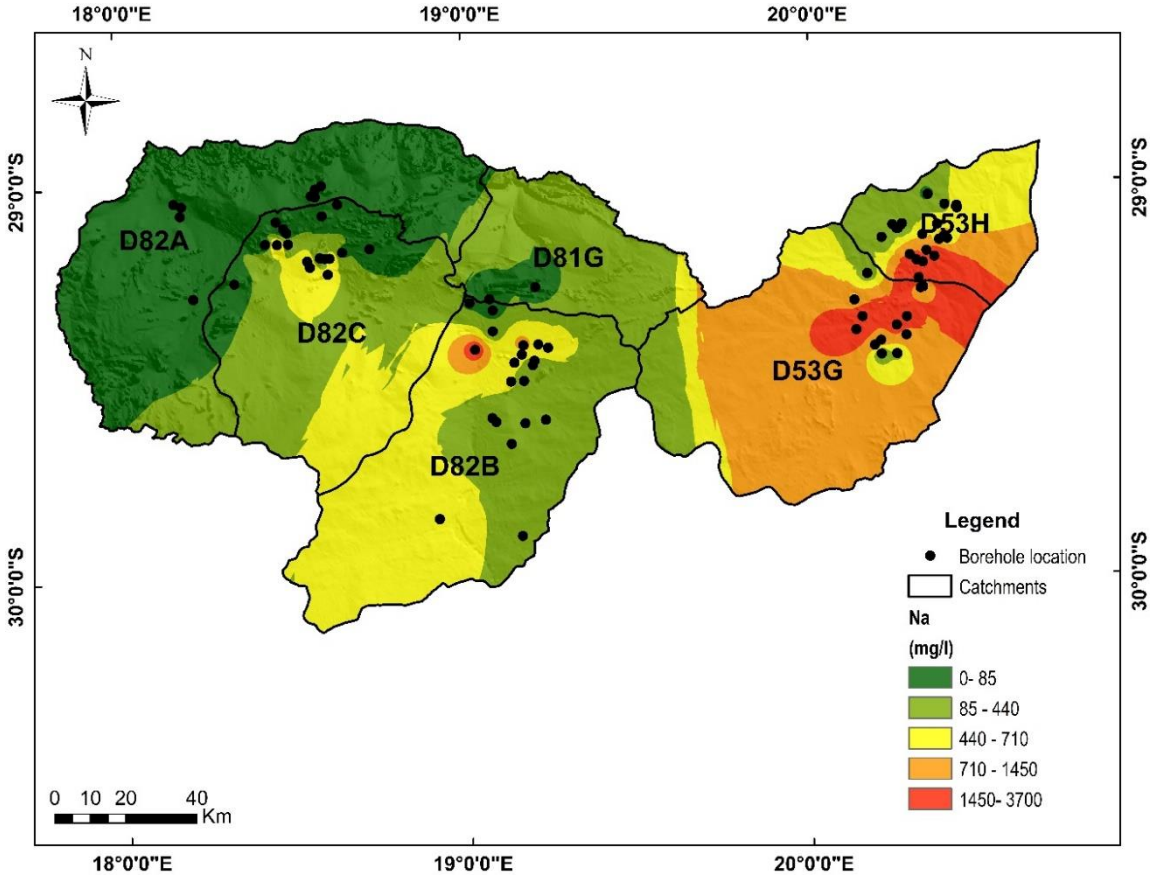

Figure 17: Spatial distribution of sodium (Na) in the borehole water of the study area.

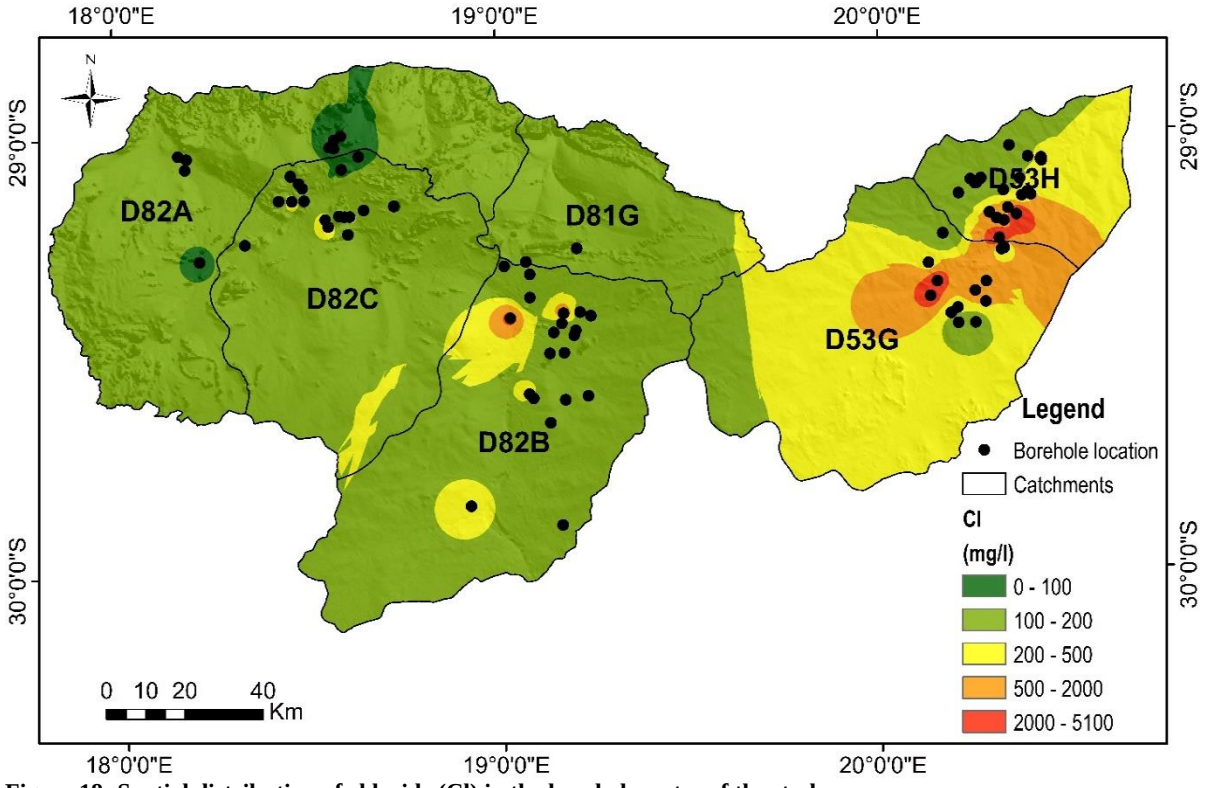

Figure 18: Spatial distribution of chloride (Cl) in the borehole water of the study area.

The stacked bar graph plots in Figures 19, 20, 21, 22, 23, and 24 show the distribution of cations (Ca^{2+}, K^{+}, Mg^{2+}, Na^{+}) and anions (SO_4^{2-}, Cl^{-},NO_3^{-} HCO_3^{-}) in catchments D82A, D82B, D82C, D53G, D53H and DG18. The concentration of ions in each groundwater sample is represented in milligrams per litre. The plots were produced to assess and describe the water composition of the samples and the contaminants. The groundwater within the catchments is abundant in Na^{+}, Cl^{-}, HCO_3^{-}, SO_4^{2-} and Ca^{2+}, with lower abundances of Mg^{2+}, NO_3^{-} and K^{+}.

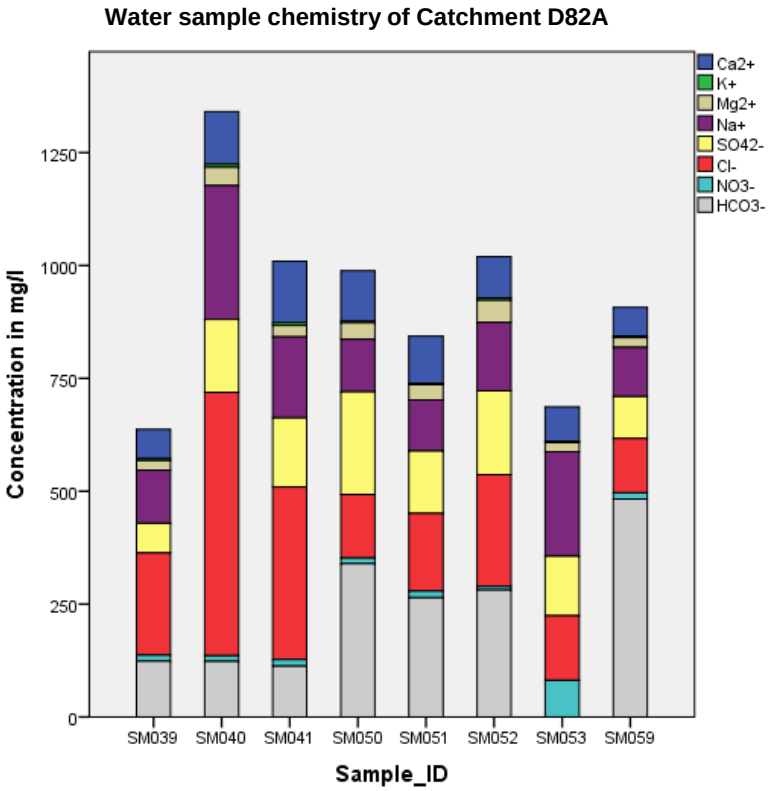

Figure 19: Stacked bar graph of the groundwater chemistry results in catchment D82A.

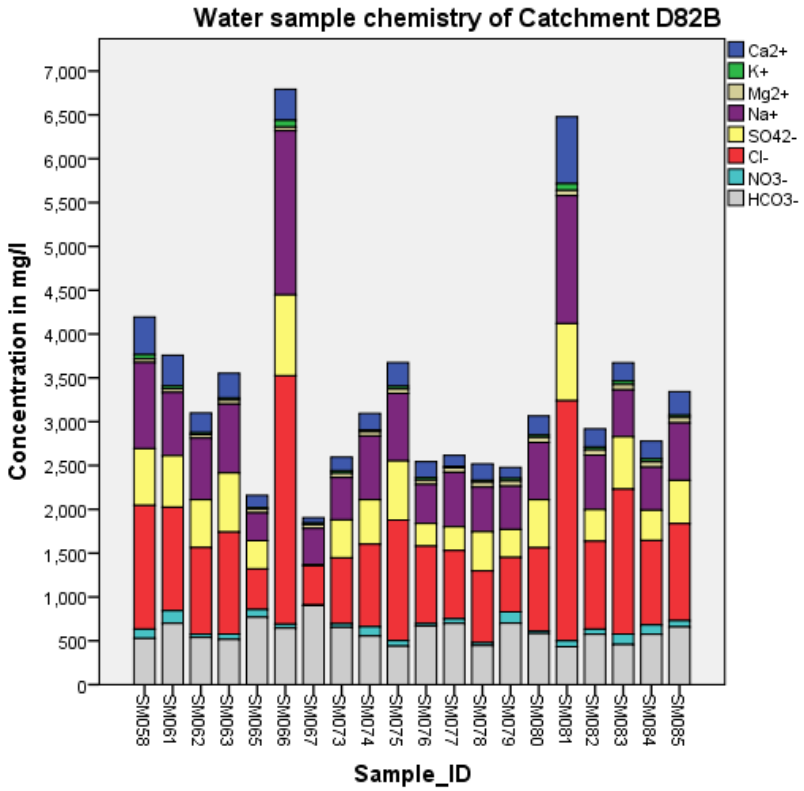

Figure 20: Stacked bar graph of the groundwater chemistry results in catchment D82B.

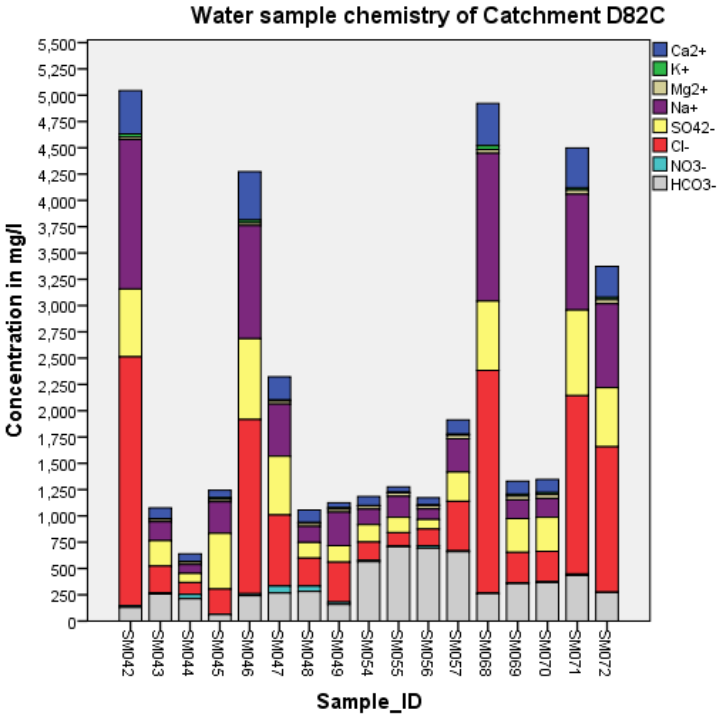

Figure 21: Stacked bar graph of the groundwater chemistry results in catchment D82C.

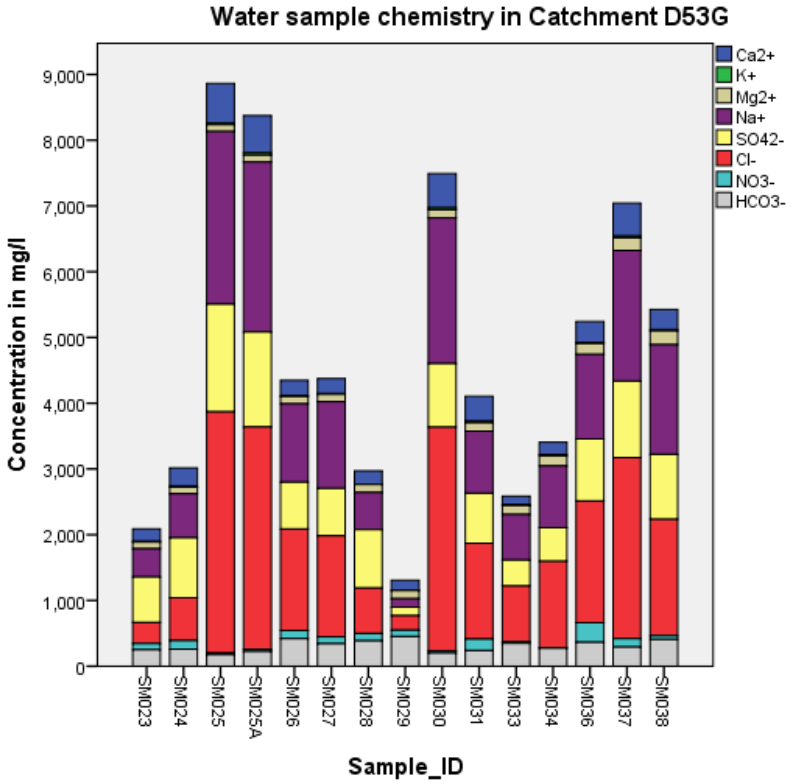

Figure 22: Stacked bar graph of the groundwater chemistry results in catchment D53G.

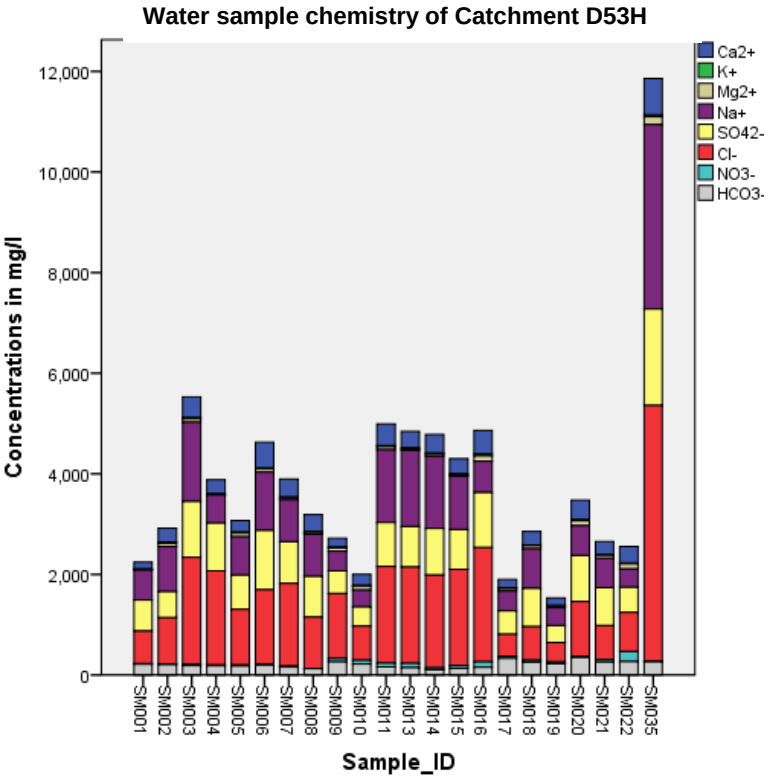

Figure 23: Stacked bar graph of the groundwater chemistry results in catchment D53H.

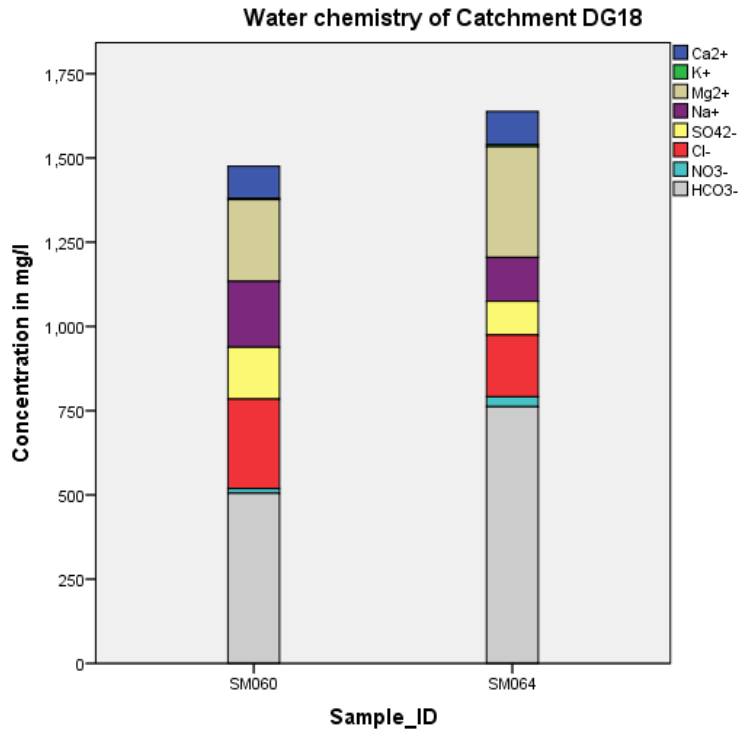

Figure 24: Stacked bar graph of the groundwater chemistry results in catchment DG18.

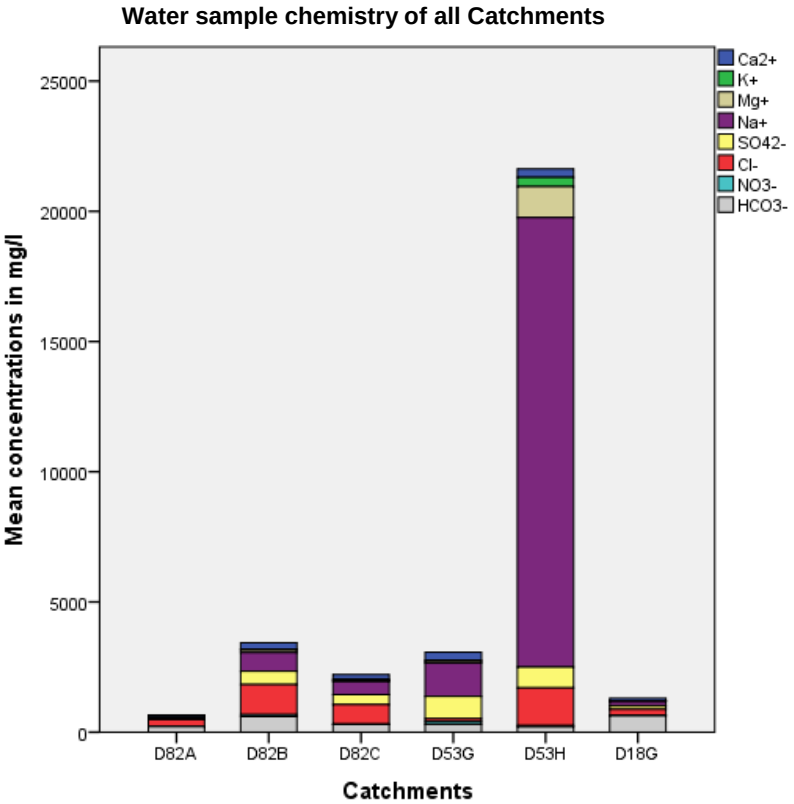

Figure 25: Stacked bar graph showing the mean concentrations of the major ions in each catchment.

The mean concentration of the major ions in Figure 25 shows a large variation, with most catchments dominated by Na^+ and Cl^-, except catchment DG18 which contains mostly elevated values of HCO_3^-. Catchment D53H (SM035) has the highest concentration of Na^+ which is located on the biotite and quartz-feldspar gneisses of the Bushmanland Subprovince.

5.1.3 Trace elements

With regard to trace elements, (Figure 26 and 27), arsenic and strontium were shown to register elevated concentrations. Most trace elements, such as copper, aluminium, beryllium, manganese, cobalt, lead, vanadium and chromium, were barely detectable in the groundwater. Only sample SM050 registered an elevated vanadium concentration of 55400 ppb. Arsenic concentrations ranged from 18–74 ppb and strontium values ranged from 6.3–10900 ppb. Fluoride concentrations ranged from 0.04–5.87 mg/L. Most samples reached the fluoride SAWQG target range of 0.0–1.0 mg/L. Table 5 lists the minimum and maximum trace element concentrations in each catchment.

Table 5. Minimum and maximum trace element concentrations in each catchment.

Element (ppb)	Catchment D82A	Catchment D82B	Catchment D82C	Catchment D53G	Catchment D53H	Catchment DG18
Uranium	5-69	30-182	2-5120	7-300	41-340	49-81
Strontium	435-1400	1100-10900	6.3-5600	1300-8970	1800-12100	600-800
Arsenic	19-23	23-65	18-55	21-63	22-74	21-22

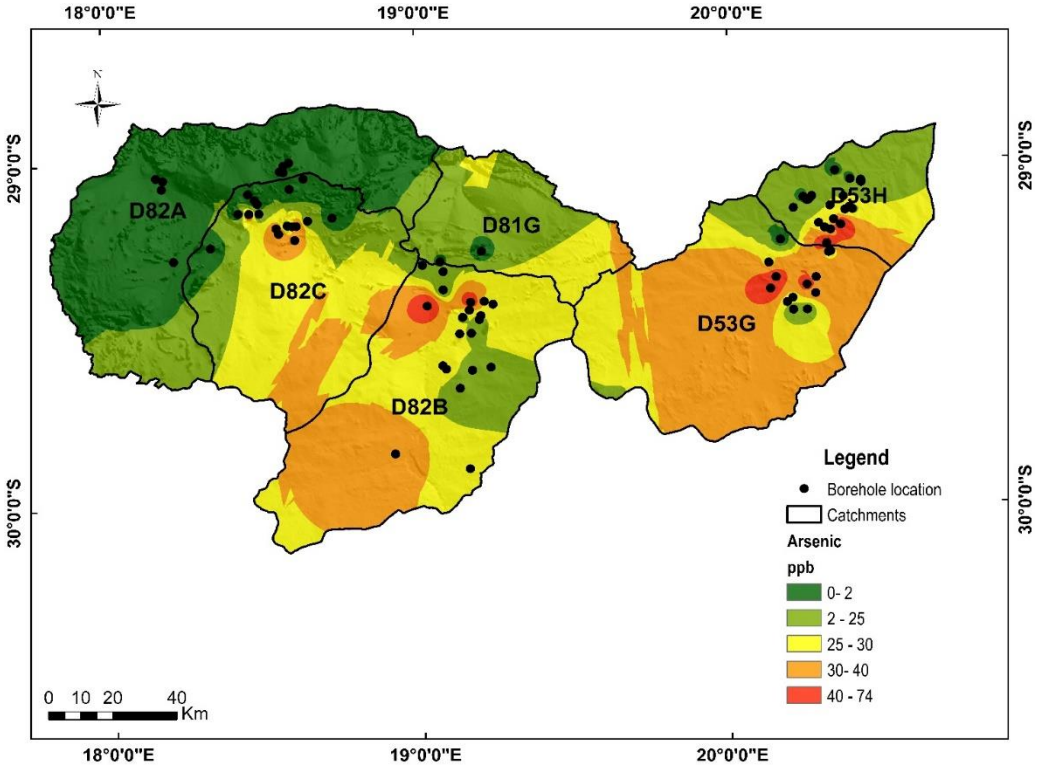

Figure 26: Map of the arsenic concentrations in the borehole water of the catchments.

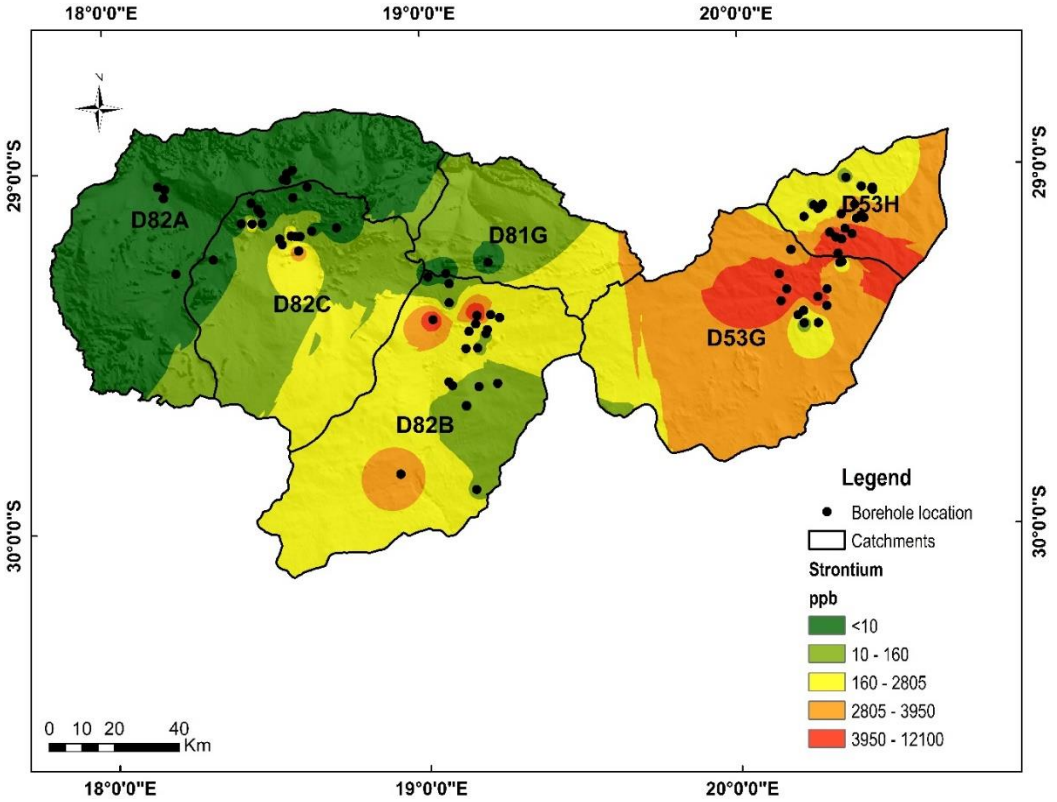

Figure 27: Map of the strontium concentrations in the borehole water of the catchments.

6 DISCUSSION

Groundwater chemistry largely depends on the lithology and hydrological properties of the geological unit, the chemical composition of recharged water, various chemical processes occurring within the geological unit, and the amount of time the water has remained in contact with the unit. The data for this study are presented and analysed based on stacked bar charts, spatial distribution maps, variability graphs, interpolation maps, a Piper diagram, a box plot, scatter plots and a Schoeller diagram. To verify the suitability of the collected groundwater samples for drinking and irrigation purposes, they were compared with the recommended standard values.

6.1 Hydrochemistry

Groundwater pH in the study area is neutral to alkaline and is within the safe limit as prescribed by the WHO, 2011). These pH values are in agreement with those obtained by Leshomo (2011) for the granite-related groundwater from this area which ranged between 7.0 and 7.9. Although there are no specific health effects associated with pH, deleterious effects result when changes in the pH of the groundwater result in high dissolved concentrations of metals.

The groundwater has high EC and TDS values in the majority of the area with high concentrations of Na^+, Cl^-, SO_4^{2-} and NO_3^-. The high levels of EC and TDS in the groundwater samples are mainly the result of elevated concentrations of Na^+ and Cl^- and, to a lesser extent, SO_4^{2-}. There are higher values of EC in the Koa River drainage system and this is regarded as a discharge area (Levin, 1983). The high values of salinity in the study area may be caused by the high evaporation and low gradients of Namaqualand.

The high TDS levels in the groundwater directly indicate the presence of high concentrations of soluble salts and cause the water to be unsuitable for drinking (Hem, 1985). Furthermore, the physical properties and fertility of the soil are affected by surplus TDS in the groundwater (Chaudhary and Satheeshkumar, 2018). This high amount of TDS causes severe permeability problems and affects the growth of plants.

The concentrations of Na^+ ranged from 85 to 12900 mg/L, with an average of 910 mg/L. No health-based guideline value is proposed for Na^+; however based on a taste threshold, the sodium concentration in water is advised not to exceed 100 mg/L (DWAF, 1996) and most samples exceed the permissible limit. Na^+ is found in the decomposition of the mineral plagioclase in granites and granitic gneisses of the study area. Besides the sodium released from granites and granitic gneisses of the area, a large salt

contribution is also expected from anthropogenic activities (spatial agricultural activities), coastal rainfall and fog in the arid environment (Nell *et al.*, 2014). An increase in Na^+ in groundwater is also assumed to result from the cation exchange of Ca and Mg ions in the mineral-water interaction.

High values of Na^+ are unsuitable for water use due to the adsorption of Na^+ onto the soil cation exchange sites, dispersion of soil aggregates, and reduction of soil permeability (Gholami and Srikantaswamy, 2009). The sodium adsorption ratio (SAR) is the concentration of sodium relative to calcium and magnesium. SAR indicates the suitability of water for use in agricultural irrigation. Application of irrigation water with high SAR to soil over several years can shift the calcium and magnesium in the soil due to the sodium in the water (Kumar *et al.*, 2009). This causes a decrease in the ability of the soil to form stable aggregates, a loss of soil structure and tilth and a decrease in infiltration and the permeability of the soil to water, leading to problems with crop production.

High SO_4^{2-}concentrations in the analysed samples are probably attributable to the oxidation of sulphide minerals in the igneous rocks and concentration through evaporation within the study area.

The carbonate and bicarbonate concentration in the groundwater is derived from carbonate weathering and the dissolution of carbonic acid in the aquifers. The value of HCO_3^- is observed from 61–903 mg/L, which is the dominant ion in some of the groundwater (catchment DG18). The higher concentration of HCO_3^- in the water suggests a dominance of mineral dissolution.

The concentration of As in the study area reaches up 74 ppb, which is higher than the WHO guideline value of 10 ppb. As can be released through natural processes such as the weathering of rocks and sediments, hydrothermal ore deposits, volcanic eruption and geothermal activities (Nriagu *et al.*, 2007). Also, the discharge in the use of As for compounds in industrial and agricultural activities such as glass manufacturing and the steel melting process contributes as a threat to the groundwater. The overall pH values of the groundwaters are near neutral to slightly alkaline (7.13–8.91). Under these conditions As^{5+} is the most prevalent species (Abiye and Bhattacharya, 2019). Arsenic in metamorphic rocks occurs in high concentrations which can be toxic and carcinogenic in groundwater (Jordana and Batista, 2004). Based on the spatial maps (Figure 26 and 27), elevated concentrations of arsenic and strontium occur within catchments D53G, D53H, D82C and D82B.

NO_3^- occurs in high levels in the groundwater of the study area, and is derived from a variety of processes and sources, and understanding these processes is helpful in groundwater quality studies. Sources of nitrate pollution in the groundwater are from agricultural fertilizer application, animal habitats, sewerage systems and areas of manure storage (Wick *et al.*, 2012). Elevated NO_3^- levels pose a threat once converted to nitrite, and may cause the illness methemoglobinemia. Methemoglobinemia

is a condition in which the body is deprived of oxygen, causing a blue-grey discoloration of the skin. A person suffering from this condition may also experience an elevated resting heart rate, weakness, nausea and, in some cases, the illness may lead to death. The people most likely to suffer from methemoglobinaemia are infants because they may be fed a baby formula prepared with water high in nitrate (Comly, 1945; Johnson *et al.*, 1987; Rail, 1989). Methemoglobinemia should be suspected in all patients with a sudden onset of cyanosis that does not improve with the administration of oxygen or after ingestion or administration of a potential oxidative agent. Blood with elevated methemoglobin has been described as chocolate, brownish-blue, or dark red in colour (Cortazzo *et al.*, 2014).

6.2 Water types

A Piper diagram (Figure 28) was constructed to illustrate the water composition within the study area and to highlight the processes occurring in the groundwater. Over space and time, groundwater chemistry is influenced by hydrogeochemical processes within the groundwater. Based on the Piper plot, the predominant water types in the study area are Na-Cl, Na-HCO_3 and Mg-HCO_3, followed by the water type Na-SO_4, which is represented by three samples. From the Piper diagram, it is evident that Na^+, Cl^- and HCO_3^- are the most dominant ions in the groundwater of the study area.

6.2.1 Na-Cl water type

Sixty-one per cent (61%) (52 samples) of the sampled water in the study area is the Na-Cl (Table 6) water type and these boreholes are mostly distributed in Quaternary sediments in contact zones with granites, gneisses and quartzite. The Na-Cl water type is characterized by high values of TDS (up to 10000 mg/L) and mean EC values of 3.5 mS/cm, which represent brackish to saline water. High Cl^- does not exist in the rocks and the high values of Cl^- in the groundwater of the study area are from ocean aerosol that was brought by rain, dry deposition and westerly winter cold fronts. This means that most of the high Na+ in the groundwater is also from the sea. High values of Cl^- can impart a salty taste to the groundwater and cause corrosion in the water pipes (WHO, 2011). High concentrations of Na^+ and Cl^- cause poor-quality groundwater within the study area, and the high values of EC and TDS are mainly due to the high levels of Na^+ and Cl^-. After long-term use, high values of EC can cause gastrointestinal irritation in humans (Ramesh and Elango, 2012).

The elevated concentrations of Na^+ and Cl^- in the sampled water occur mainly in catchments D53H, D53G, D82B and D82C. Catchments D53H and D53G are located in the Sout River (Figure 13) palaeochannel which shows a continuous groundwater flow from one catchment to the other and, hence, a similar concentration of these ions in the sampled groundwater. The Sout River palaeochannel runs from the southwest in catchment D53H to the northeast in catchment D53G.

Table 6. Different groundwater types in catchment D82A (yellow), D82B (green), D82C (blue), D53G (Red),D53H (brown) and DG18 (navy) in the study area.

Sample_ID	Catchment_ID	Water type	Sample_ID	Catchment_ID	Water type
SM039	D82A	Na-Cl	SM001	D53H	Na-Cl
SM040	D82A	Na-Cl	SM002	D53H	Na-Cl
SM041	D82A	Na-Cl	SM003	D53H	Na-Cl
SM050	D82A	Na-HCO_3	SM004	D53H	Na-SO_4
SM051	D82A	Na-HCO_3	SM005	D53H	Na-Cl
SM052	D82A	Na-HCO_3	SM006	D53H	Na-Cl
SM053	D82A	Na-Cl	SM007	D53H	Na-Cl
SM059	D82A	Na-HCO_3	SM008	D53H	Na-Cl
SM042	D82C	Na-Cl	SM009	D53H	Na-Cl
SM043	D82C	Na-Cl	SM010	D53H	Na-Cl
SM044	D82C	Na-HCO_3	SM011	D53H	Na-Cl
SM045	D82C	Na-SO_4	SM013	D53H	Na-Cl
SM046	D82C	Na-Cl	SM014	D53H	Na-Cl
SM047	D82C	Na-Cl	SM015	D53H	Na-Cl
SM048	D82C	Na-Cl	SM016	D53H	Na-Cl
SM049	D82C	Na-Cl	SM017	D53H	Na-Cl
SM054	D82C	Na-HCO_3	SM018	D53H	Na-Cl
SM055	D82C	Na-HCO_3	SM019	D53H	Na-Cl
SM056	D82C	Na-HCO_3	SM020	D53H	Na-Cl
SM057	D82C	Na-Cl	SM021	D53H	Na-Cl
SM068	D82C	Na-HCO_3	SM022	D53H	Na-Cl
SM069	D82C	Na-Cl	SM032	D53H	Na-Cl
SM070	D82C	Na-HCO_3	SM035	D53H	Na-Cl
SM071	D82C	Na-Cl	SM023	D53G	Na-SO_4
SM072	D82C	Na-Cl	SM024	D53G	Na-Cl
SM058	D82B	Na-Cl	SM025	D53G	Na-Cl
SM061	D82B	Na-Cl	SM025A	D53G	Na-Cl
SM062	D82B	Na-Cl	SM026	D53G	Na-Cl
SM063	D82B	Na-Cl	SM027	D53G	Na-Cl
SM065	D82B	Na-HCO_3	SM028	D53G	Na-Cl
SM066	D82B	Na-Cl	SM029	D53G	Mg-HCO_3
SM067	D82B	Na-HCO_3	SM030	D53G	Na-Cl
SM073	D82B	Na-Cl	SM031	D53G	Na-Cl
SM074	D82B	Na-Cl	SM033	D53G	Na-Cl
SM075	D82B	Na-Cl	SM034	D53G	Na-Cl

Sample_ID	Catchment_ID	Water type	Sample_ID	Catchment_ID	Water type
SM076	D82B	Na-Cl	SM036	D53G	Na-Cl
SM077	D82B	Na-Cl	SM037	D53G	Na-Cl
SM078	D82B	Na-Cl	SM038	D53G	Na-Cl
SM079	D82B	Na-Cl	SM060	DG18	Mg-HCO_3
SM080	D82B	Na-Cl	SM064	DG18	Mg-HCO_3
SM081	D82B	Na-Cl			
SM082	D82B	Na-Cl			
SM083	D82B	Na-Cl			
SM084	D82B	Na-Cl			
SM085	D82B	Na-Cl			

6.2.2 Na-HCO_3 water type

The Na-HCO_3 water type is found in twelve boreholes in the study area, and may be the result of the hydrolysis of Na-silicates such as sodic plagioclase released from the granitic and gneissic rocks (Chae *et al*., 2006). This water type also has high levels of pH, which shows that the water is alkaline as well as indicating ion exchange.

6.2.3 Mg- HCO_3 water type

The Mg-HCO_3 water type is found in catchment DG18. This type is represented by two samples (SM060 and SM064). These boreholes are located on the Quartenary sediments (alluvium and calcrete) in the study area. Mg^{2+}, Ca^{2+} and HCO_3^- are probably derived from rock weathering. The similarity in water type of the groundwater samples in catchment DG18 suggests that similar geochemical processes may be controlling the water chemistry and that the water in the aquifer has the same origin.

6.2.4 Na-SO_4 water type

The Na-SO_4 water type is represented by three boreholes (SM004, SM023 and SM045) which are located on granites and granitic gneisses of the Bushmanland Subprovince. The Na and SO_4 is derived from the dissolution of sulphide minerals from the igneous rocks and from anthropogenic activities in the study area.

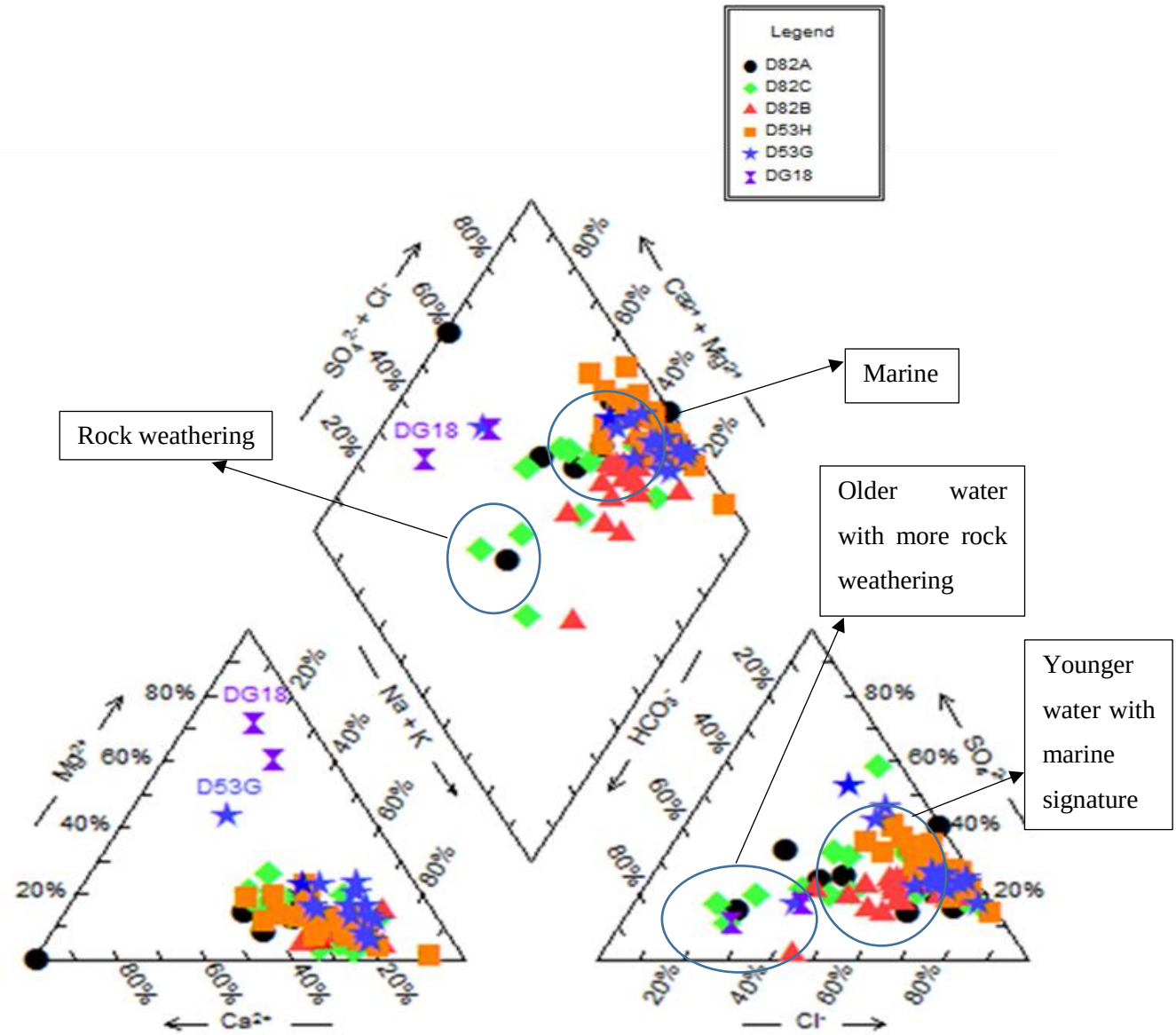

Figure 28: A Piper diagram showing the groundwater composition in catchments D82A, D82B, D82C, D53G, D53H and DG18.

In the cation triangle, most groundwater samples plot in the $Na^+ + K^+$ dominant area with only the samples in catchment DG18 plotted on the Mg^{2+} dominant type area. In terms of the geology, high Na^+ and K^+ are attributable to the igneous and metamorphic rocks within the study area which contain abundant potassium and plagioclase feldspars.

The other groundwater samples in the area plot in the no-dominant type area which may suggest different sources of groundwater resulting from the different lithologies of the area. Most groundwater samples in the anion triangle plot in the Cl^- apex, which suggests a seawater composition, with two samples from catchment D82C and D53G plotting on the SO_4^{2-} water type. The low rainfall, trend of

slope and topography of Namaqualand and long residence of water give lots of time for rock-water interaction which results in variation in the water chemistry.

In the diamond-shaped field, samples are distributed between 15 and 65% Ca^{2+}+ Mg^{2+}, 30–80% Na^{+}+ K^{+} and 20–80% SO_4^{2-} and Cl^{-}. The samples shifted on the far right of the diamond-shaped area (buffered by a triangle) have high Na^{+} and Cl^{-} which depicts a strong marine signature or presence of salt in the groundwater samples while the area with high Ca^{2+}+ Mg^{2+} and HCO_3^{-} represents rock weathering. The trend from high to low Cl^{-} implies that the groundwater shifts from a sea-dominated area to a rock-dominated area.

The fluoride concentration in the groundwater of the study area was found to be above the WHO guideline value of 1.5 mg/L for drinking water. The spatial distribution of fluoride ion concentrations in groundwater is illustrated in Figure 29. The fluoride is derived from the local geology which mainly comprises granites and granitic gneisses covered by alluvium, calcareous and gypsiferous soil. Sample SSM067 shows the highest concentration of F^{-}, and this borehole is located in the Stalhoek Complex leucocratic biotite gneiss and a quartz-feldspar gneiss. Furthermore, intensive evaporation processes in the Namaqualand cause high concentrations of fluoride. High fluoride concentrations in the groundwater are also related to the long residence time of groundwater owing to an enhanced water-rock interaction where the tritium level usually falls below 1.7 TU. This indicates a substantially long circulation time within the weathered granitic aquifer (Abiye *et al.*, 2018). Alkaline and high EC between 750 and 1750 µS/m create conditions favourable to the dissolution of fluoride (Abiye and Leshomo, 2013).

At least 0.6 mg/L of F^{-} concentration is acceptable for human consumption as it supports strong teeth and bones (Brindha and Elango, 2011). However, extended explosure to F^{-} can result in permanent and incurable effects such as dental and skeletal fluorosis. Moreover, such exposure can damage neurons and the brain, as well as the reproductive system, particularly as the level and period of exposure increases (Kut *et al.*, 2016; Abiye *et al.*, 2018).

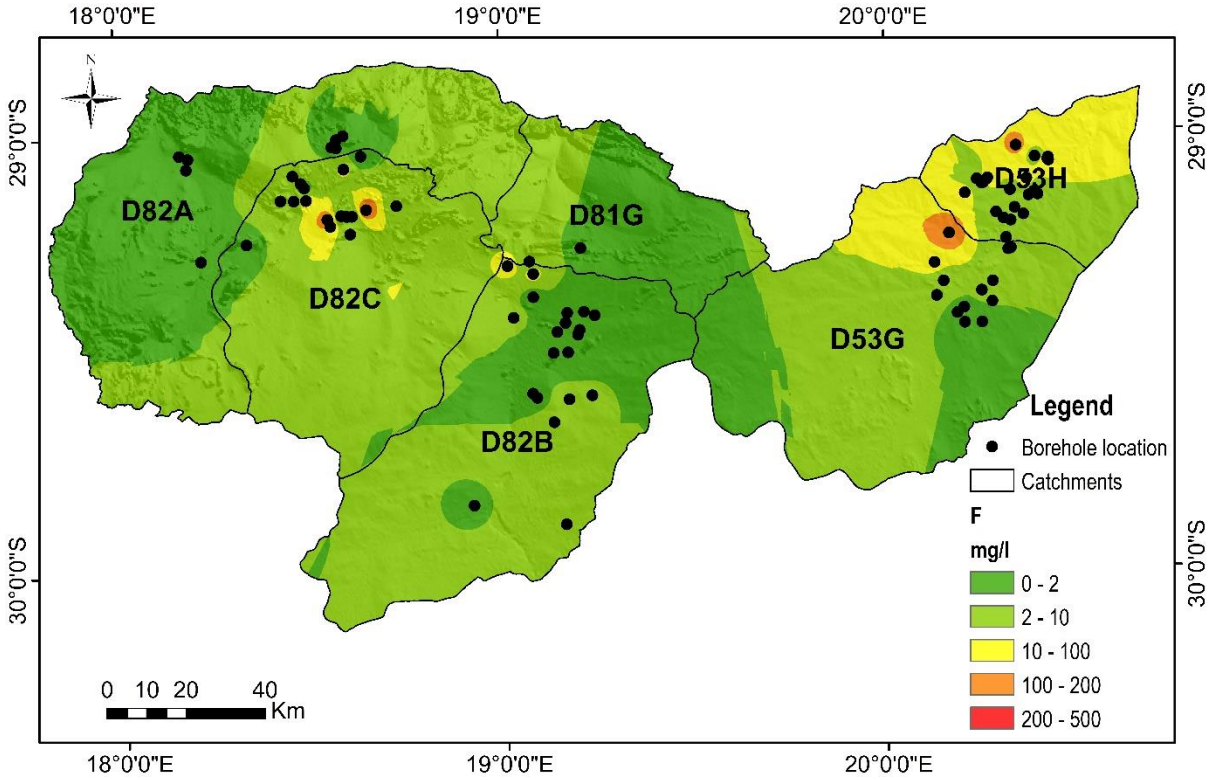

Figure 29: Spatial distribution of fluoride (F) in the borehole water of the study area.

The scatter plot in Figure 30 shows a strong correlation (Pearson's R^2= 97) between Na^+ and Cl^-. This correlation between these two major ions indicates that most salinity in the groundwater of the area is attributable to marine aerosol evaporation or mixing processes (Nencetti *et al.*, 2005; Rabemanana *et al.*, 2005; Portugal *et al.*, 2006).

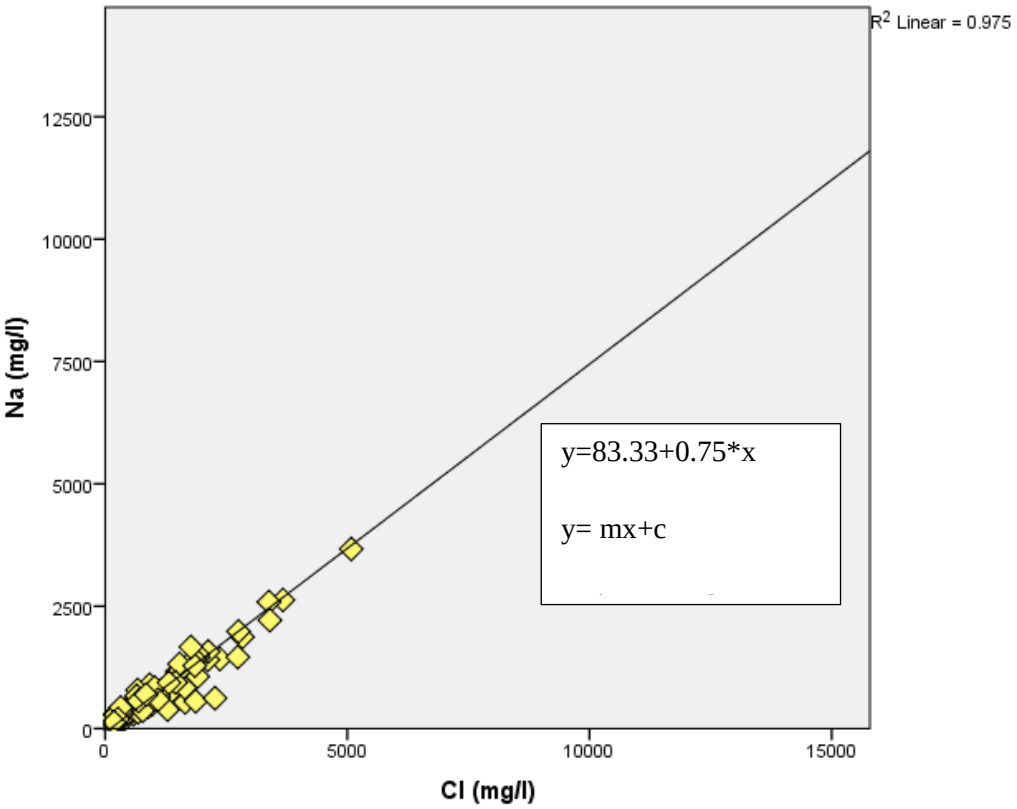

Figure 30: Scatter plot of Na vs Cl created using IBPM SPSS statistics software.

The plot of EC and Cl^- (Figure 31a) shows a good linear correlation. There is poor relationship seen between EC vs Mg^{2+}, or alkalinity (Figure 31b, c and d). This means Mg^{2+} and alkalinity are not major constituents of dissolved ions. Na^+ (Figure 31d) has a good correlation with EC.

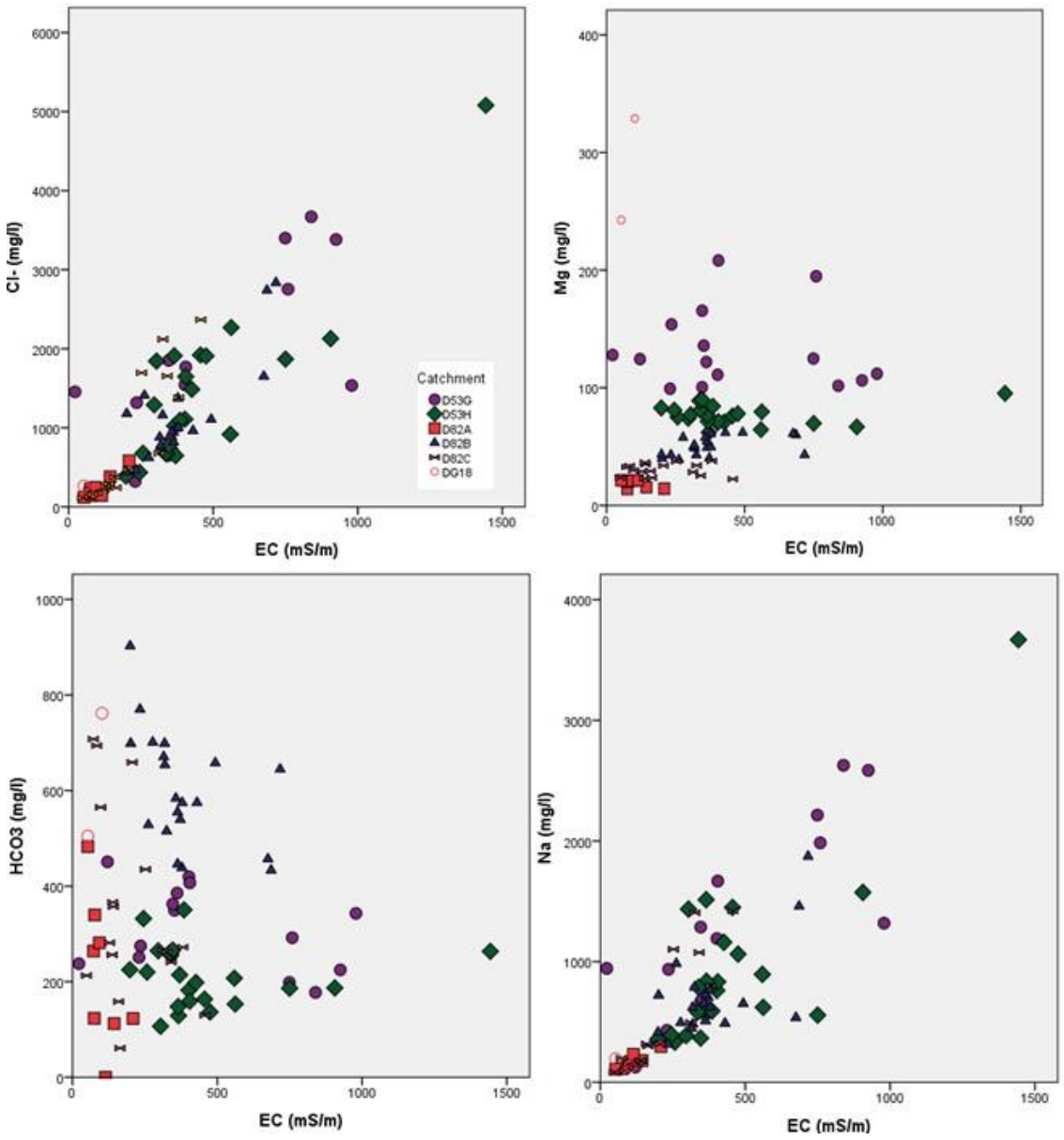

Figure 31: (a, b, c, d): Scatter plots of major ions (Cl-, Mg^{2+}, HCO_3- and Na^+) against EC.

The high correlation between Na^+ and SO_4^{2-} (Figure 32) gives an indication of the excess Na^+ that resulted from the dissolution of the sodium sulphate. Sample SSM032 shows the highest Na^+ value in all the groundwater samples which. The borehole from which the sample was taken is located in biotite gneiss of the Brulkolk Formation. This sample is an anomaly that was removed from the data to obtain a better representation of the relationship between sodium and sulphate.

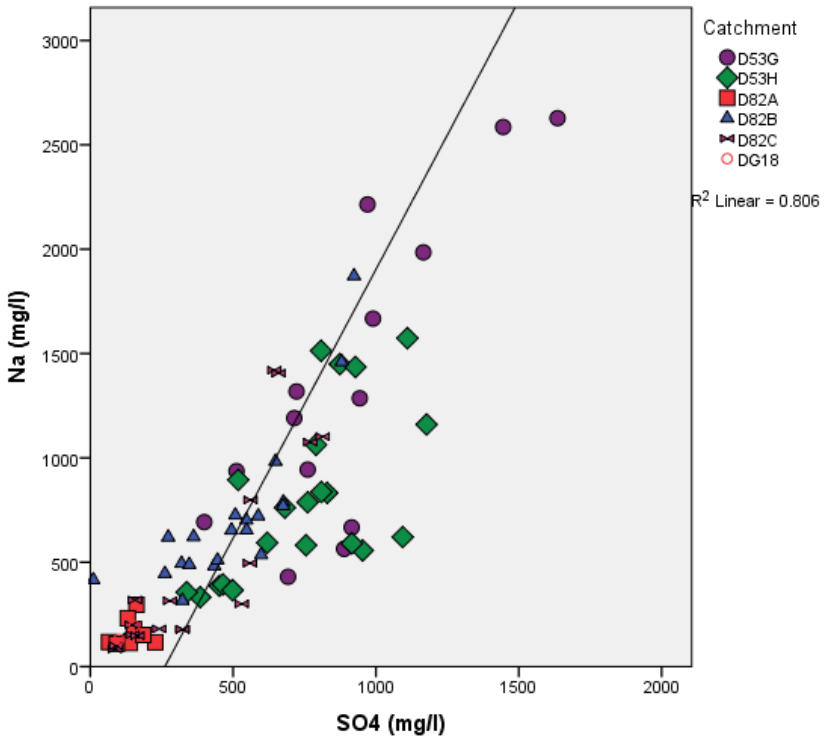

Figure 32: Scatter plot of correlation (Pearson's R2 = 0.81) between Na+ vs SO_4^{2-}

The Schoeller diagram (Figure 33) shows the water chemistry in catchments to have an order of decreasing concentration of Cl^-> Na^++K^+>SO_4^{2-}> Ca^{2+}> Mg^{2+}> HCO_3^-. The catchments have distinctive increasing concentrations of Mg^{2+} from catchments D82A, D82C, D82B, D53H, D53G and DG18. High values of Mg^{2+} are usually found in mafic and ultramafic rocks. The high values of Mg^{2+} in the borehole water may originate from olivine, garnet, amphibole and pyroxene.

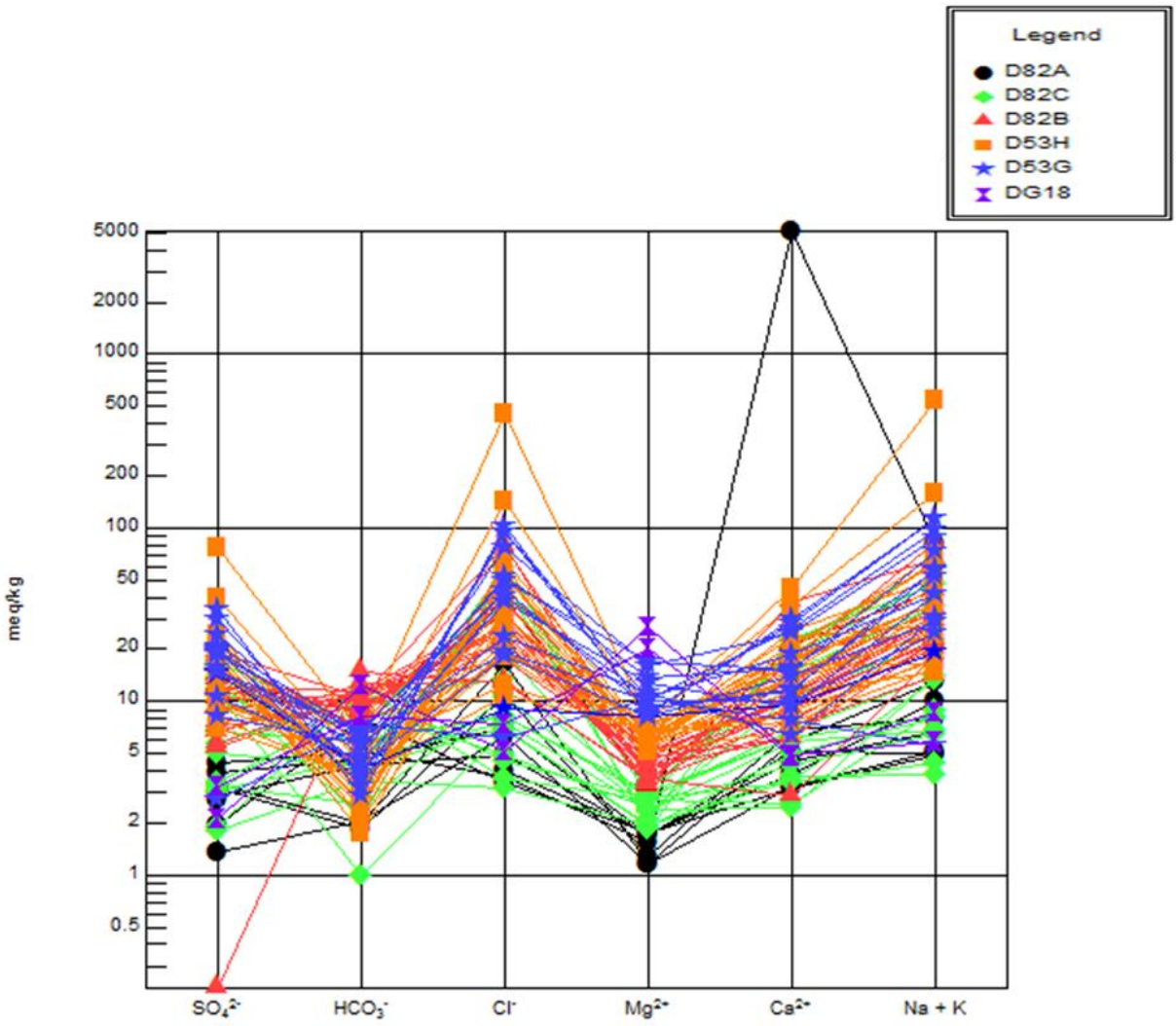

Figure 33: Schoeller diagram of the groundwater concentrations of main ionic constituents in the different catchments.

Most of the boreholes in catchment D82A are located in Quaternary sediments with calcrete, alluvium and sand covering most of the geology in the catchment, thus accounting for the low concentrations of magnesium in the borehole water. Catchment D82C comprises mostly calcrete, sand and alluvium and three boreholes with high Mg^{2+} values are situated in granites, gneisses and calc-silicate rocks. Boreholes in catchment D82B are in close proximity to the mafic rocks of the Keimoes Suite with lesser boreholes situated in Quaternary sediments. The sampled boreholes in catchment D53H are situated in Kameelputs biotite gneiss, amphibolite and schist. The concentration of Mg^{2+} ranges from 14–330 mg/L. Catchment D53G boreholes are located in diamictites of the Dwyka Group and amphibolites of the Grappies Group, with SM028 having the highest Mg^{2+} concentration (136 mg/L) of all the catchment boreholes. Boreholes in the DG18 catchment have the highest concentrations of Mg^{2+} of all the samples in the study area and are situated in schists.

6.3 Uranium

Uranium concentrations in the groundwater depends on uranium source rocks, the dissolution of the existing carnotite and tyuyamunite mineralisation, and the geomorphology of the area (Adithya *et al.*, 2016). The high uranium concentration is attributable to the uranium source rocks and sediments in the study area. The study area consists of granites, granitic gneisses and pegmatites that are enriched in natural uranium.

The arid to semi-arid climate, particularly the influence of evapotranspiration and the concentrations of carbonate, phosphate, vanadate, fluoride, sulphate, silicate, calcium, and potassium, plays an important role in U (IV) oxidation in the groundwater. The high values of uranium in the area may be attributable to the oxidizing nature of the groundwater.

The sampled groundwater has an alkaline pH, which plays an important role in the solubility of uranium. The samples show a positive redox potential (0.06– 0.28 V), which is an indication of the presence of oxygen which also increases uranium solubility. Oxygen in the groundwater is attributable to fractures and faults in the study area.

The good relationships between uranium with salinity and total dissolved salts (increase in uranium in the groundwater with increase in both salinity and total dissolved salts) may have been attributed to ion-exchange reaction dynamics. These ion-exchanges reactions are caused by competition of cations for available adsorption of the grain surface of minerals (Kumar *et al.*, 2011 and references therein). The soluble uranium species UO_2^{+2} (VI) are strongly adsorbed on minerals surfaces due to less competition in low ionic-strength of groundwater while in the case of high ionic-strength of groundwater these species are released into the groundwater due to high salinity and total dissolved salts.

Furthermore, there may be two main sources of uranium in the groundwater, one being the source rocks (gneisses and granites) in the study area, while the other source may be the dissolution of already formed carnotite and tyuyamunite in the groundwater. Based on the groundwater modelling results, there are a number of areas that have negative values of carnotite and tyuyamunite saturation indices. These negative values means the reaction that is favoured is the dissolution of carnotite and tyuyamunite once these minerals come in contact with the groundwater (Figure 34 and 35). These two sources of uranium may explain the bimodal trends for uranium against other elements/chemicals in the study area. For example, once carnotite and tyuyamunite dissolves into the groundwater, the resulting groundwater chemistry will probably have increasing amounts of uranium, vanadium, potassium, and calcium. On

the other hand, the uranium source rocks (gneisses and granites) are not spatially related to say the vanadium source rocks for example (see Figure 12, geology map). This will cause a poor correlation between uranium and vanadium.

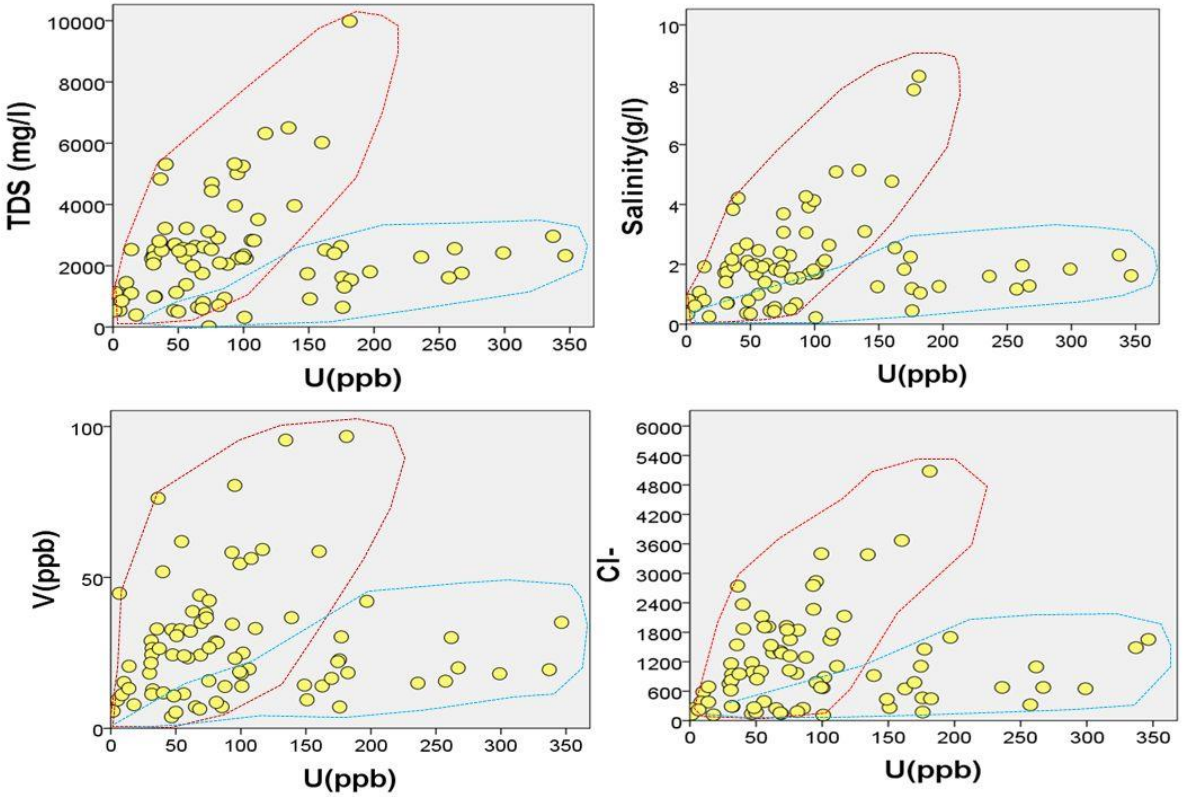

Figure 34: Graphs showing the relation between uranium and total dissolved salts, salinity, vanadium and chloride in the groundwater.

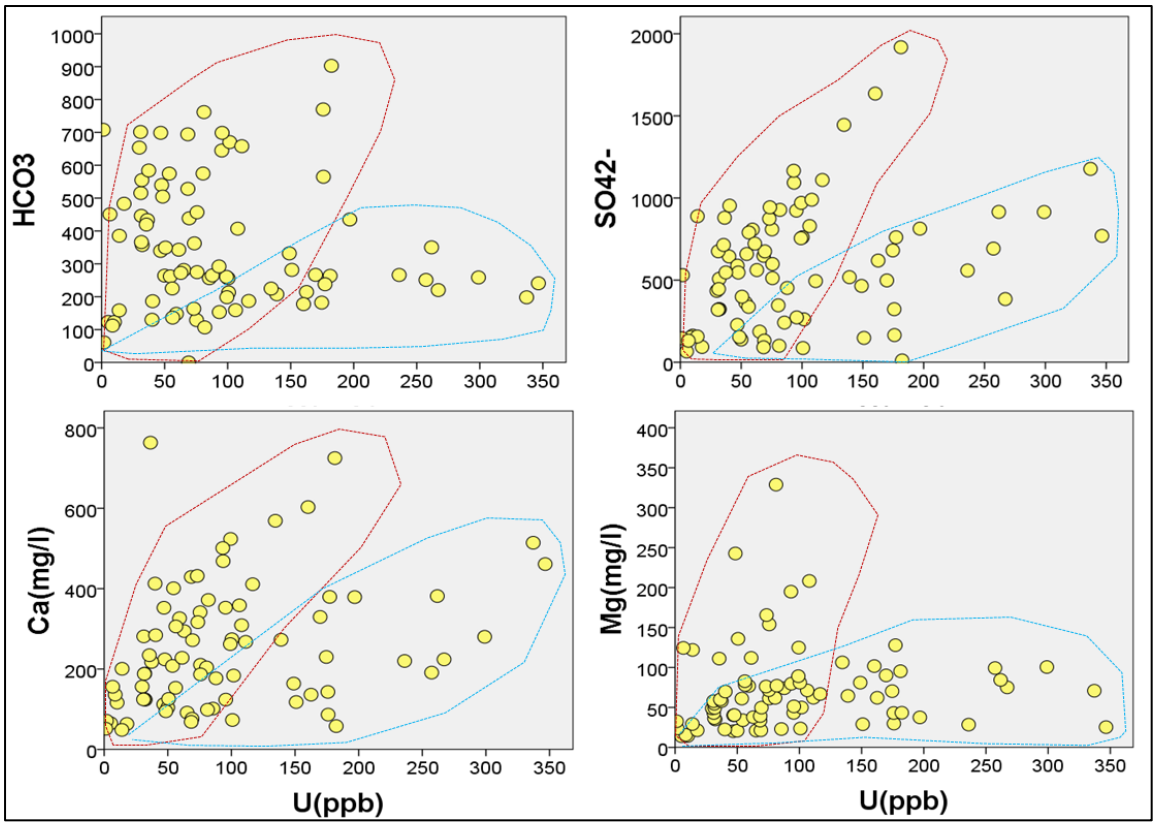

Figure 35: Graphs showing the relation between bicarbonates, sulphates, calcium and magnesium in the groundwater.

6.3.1 Uranium geochemistry and its spatial distribution

6.3.1.1 Uranium Mineral Saturation Indices

The SI of U minerals was attempted for all the groundwater samples and only 66 samples are saturated with U minerals (Table 7). A total of 6 uranium mineral species were isolated from the saturation index calculation of mineral phases. The main feature of these mineral species are the dominance of the mineral tyuyamunite [$Ca(UO_2)_2(VO_4)_2 .8H_2O$] and carnotite [$K_2(UO_2)_2(VO_4)_2 .3H_2O$] as the main uranium host. However other phases such as schoepite [$(UO_2)_8O_2(OH)_{12}.12(H_2O)$], dihydroxy(dioxo)uranium [$UO_2(OH)_2$], Abernathyite [$K(UO_2)(AsO_4).4(H_2O)$] and Paraschoepite [$UO_3.2(H_2O)$] are also present in minor amounts. From these, mineral species except in sample (SM001 and SM003) shows dissolution (negative SI). Sample SM001 and SM003 are supersaturated with tyuyamunite (4.5847) and carnotite (2.9528). Nearly all of the samples that are saturated with respect to carnotite are located in the palaeochannels. The tyuyamunite and carnotite are formed mostly within the Na-Cl water type with pH between 7.1 up to 7.7 (Table 7).

Table 7: Saturation indices of uranium mineral species of groundwater samples in the study area.

Mineral	Formula	Saturation Indices	pH	No. of Samples
Tyuyamunite	$Ca(UO_2)_2(VO_4)_2$ .5 $8H_2O$	4.5847- -0.2263	7.1-8.5	42
Carnotite	$K_2(UO_2)_2(VO_4)_2$.$3H_2O$	2.9528 - 0.7212	7.1-7.7	24
Schoepite	$(UO_2)_8O_2(OH)_{12}$.$12(H_2O)$	-0.3540	7.3	1
Dihydroxy(dioxo)uranium	$UO_2(OH)_2$	-0.9999	7.3	1
Abernathyite	$K(UO_2)(AsO_4)$.$4(H_2O)$	-2.5280	7.3	1
Paraschoepite	UO_3.$2(H_2O)$	-2.9754	7.3	1

The carnotite and tyuyamunite saturation indices shows a very good relationship with a positive correlation of about 94%. This means that the areas where there is carnotite undersaturation are the same areas where there is tyuyamunite undersaturation. Similarly, tyuyamunite saturation and carnotite saturation are also occurring in the same areas. The high values of carnotite and tyuyamunite saturation indices are restricted within the rocks of the Bushmanland Subprovince. These rocks include granites, gneisses, amphibolite and schists. The results of the modelling of groundwater using PHREEQC shows that the contribution of uranium in the groundwater is not restricted by only the source rocks (granites, gneisses) but also by the dissolution of the existing carnotite/tyuyamunite mineralisation into the groundwater. In most areas, tyuyamunite and carnotite saturation indices (Figure 48 Figure 49and 49) are negative and therefore favours the dissolution of these mineralisation into these undersaturated groundwaters.

The Eh-pH diagrams is plotted to understand the dominant species of uranium and vanadium in the groundwater within the study area. The pH and Eh of water affect U speciation and adsorption and precipitation rates. The groundwater samples (red diamonds) mostly plot in the $UO_2(CO_3)_2^{2-}$ field, with a few samples plotting in the $UO_2(CO_3)_3^{4-}$ field (Figure 36).

As shown in Figure 36, in the gently acidic to slightly alkaline pH conditions (pH 5.5–8), uranyl dicarbonate $UO_2(CO_3)_2^{2-}$ predominates and, in the more alkaline environments (above pH 8), the polycarbonate $UO_2(CO_3)_3^{4-}$ is the dominant uranium species. The redox potential (Eh) in the $UO_2(CO_3)_2^{2-}$ stability field extends from just above 0 to about 0.9, while the Eh of the $UO_2(CO_3)_3^{4-}$ stability field ranges from -0.5 to +0.8. The mobility of uranium in water, in oxidizing conditions, is enhanced by these carbonate complexes. The groundwater in the study area contains a high content of dissolved carbonates.

As shown in Figure 37, in the acidic to slightly alkaline pH conditions (pH 4–8.5), $H_2VO_4^-$ dominates and, in the more alkaline environments (above pH 8), HVO_4^{2-} is the dominant vanadium species dissolved in water. The redox potential (Eh) in the $H_2VO_4^-$ stability field extends from just above -0.2 to about +1, while the Eh of the HVO_4^{2-} stability field ranges from -0.4 to +0.8.

Uranium is transported in the oxidized six-valent state (carnotite), as the uranyl, UO_2^{2+}, or $UO_2(OH)^+$ ion, depending on pH. Uranium solubility in the study area is influenced by the presence of carbonates CO_3^{2-} which form the dicarbonate ($UO_2(CO_3)_2^{2-}$) and tricarbonate ($UO_2(CO_3)_3^{4-}$) complexes (Blake *et al.*, 1956 and Garrels and Christ, 1965). Neutral to alkaline pH conditions and oxidizing Eh produce the H_2VO^{4-} pentavalent vanadium species that may occur in equilibrium with uranyl species. The vanadium is in a pentavalent state whereas uranium is in a hexavalent state. The dissolved V^{5+} and U^{6+} state favours carnotite solution (Bharti *et al.*, 2015).

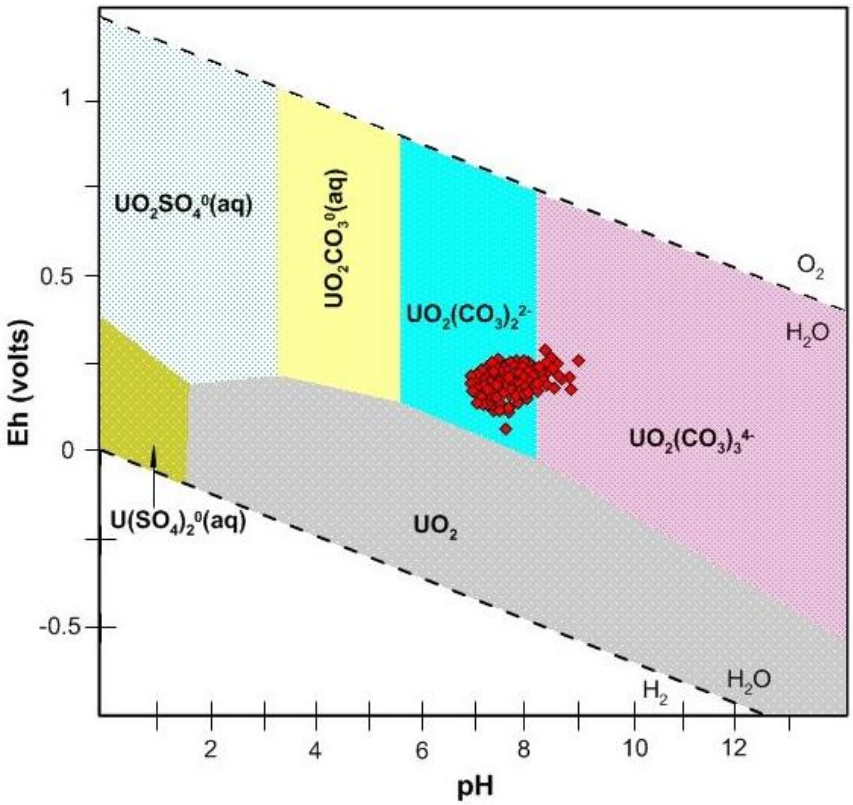

Figure 36: Eh-pH plots of representative groundwater samples showing the valence states of uranium in the groundwater samples represented by red diamonds for the samples within the study area.

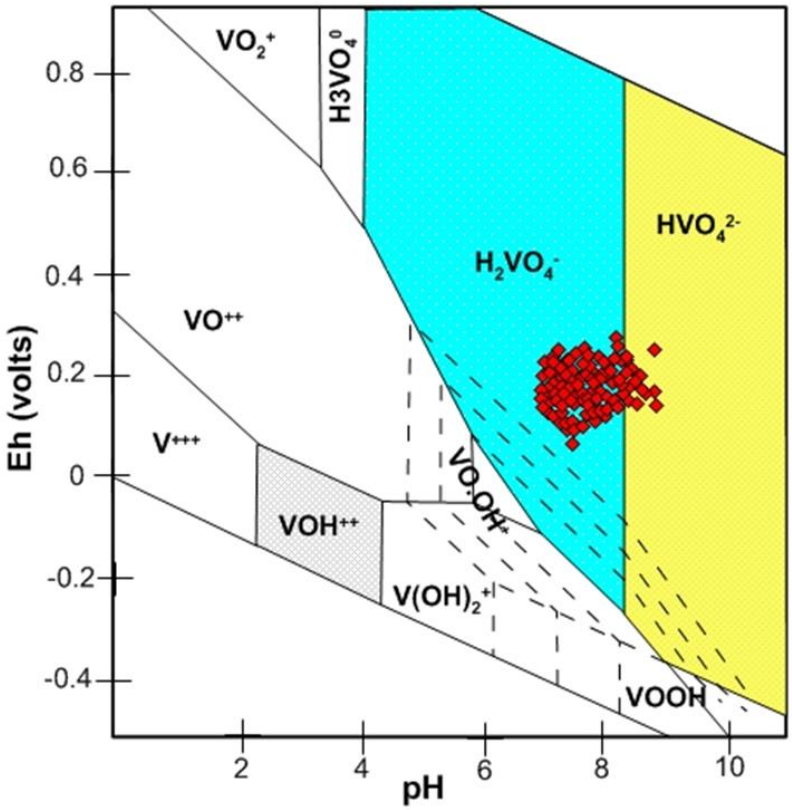

Figure 37: Eh-pH plots of representative groundwater samples showing the valence states of the vanadium in groundwater samples and red diamond for samples within the study area.

The spatial distribution of uranium varies widely within the study area, with some sample localities displaying high concentrations and others with low concentrations. Based on the spatial distribution of uranium, catchments D82C, D53H and D53G showed higher concentrations of uranium than other catchments. These catchments are located in Quaternary and Tertiary sediments which are in close proximity to the granitic and gneissic rocks in the study area. The majority of the boreholes (about 90% of all the boreholes sampled) have uranium concentrations above the threshold value of 15 ppb (Figure 42). Uranium concentrations in the groundwater samples range from 1.2–5120 ppb, with a mean value of 155 ppb. Sample SSM057 has the highest value of 5120 ppb uranium and is situated in a palaeochannel bounded by biotite gneiss. High uranium concentrations are a threat to the communities living in the vicinity.

6.3.2 Uranium impact in the groundwater for human health on human health

The risk map produced is based on a simple 3x3 matrix, with categorisation of probability and impacts into low, medium and high Figure 38.

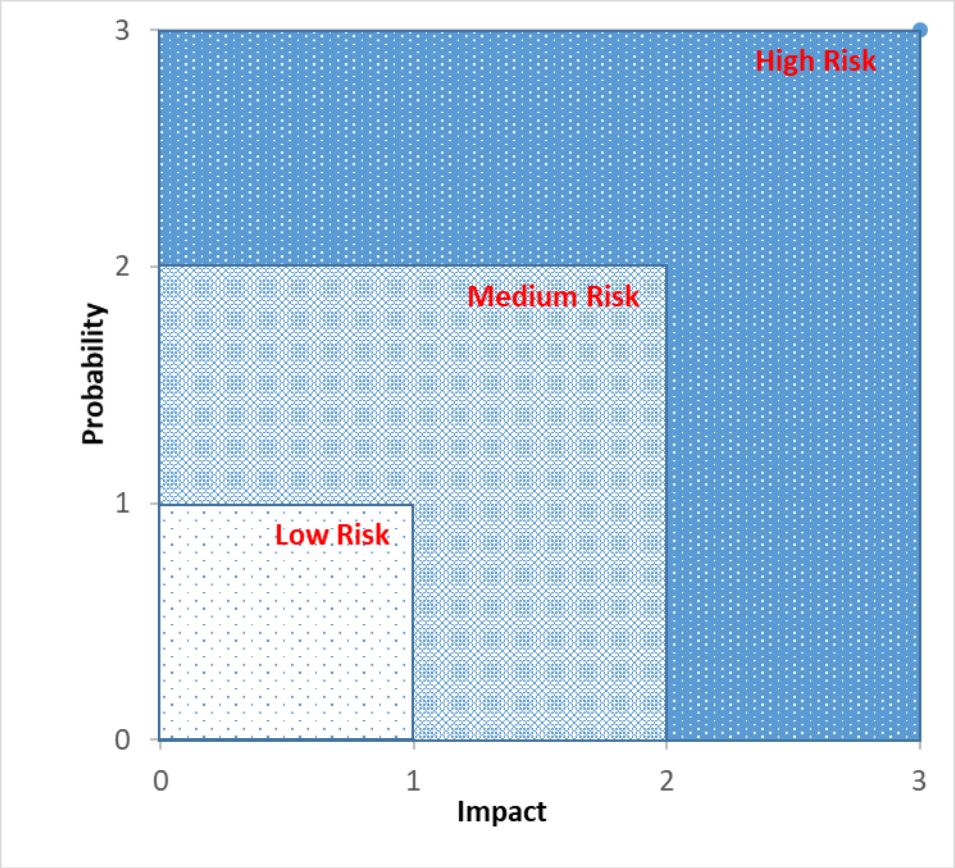

Figure 38: The 3 x 3 risk matrix used for risk map in the study area. The low, medium and high are denoted by 1, 2 and 3 respectively.

The uranium concentration was classified into 3 groups according to: group I – Low (0-15 ppb), II – Medium (15-350 ppb) and III (350- 5120 ppb) – High. The population density was also classified into 3 groups per square kilometre: group I – 0-10, II – 10-100 and III – >100.

The probability map of uranium concentration (Figure 39) is medium to high in most parts of the study area with only a small portion of the area (to the far west) with low uranium contents. A large part of the study area has a population density of about 0-10 people per square kilometre (Figure 40). In the areas of Aggeneys, Pella, Concordia and Pofadder, the population density is more than 100 people per square kilometre, which also coincide with areas of high uranium contamination in the groundwater (Figure 41).

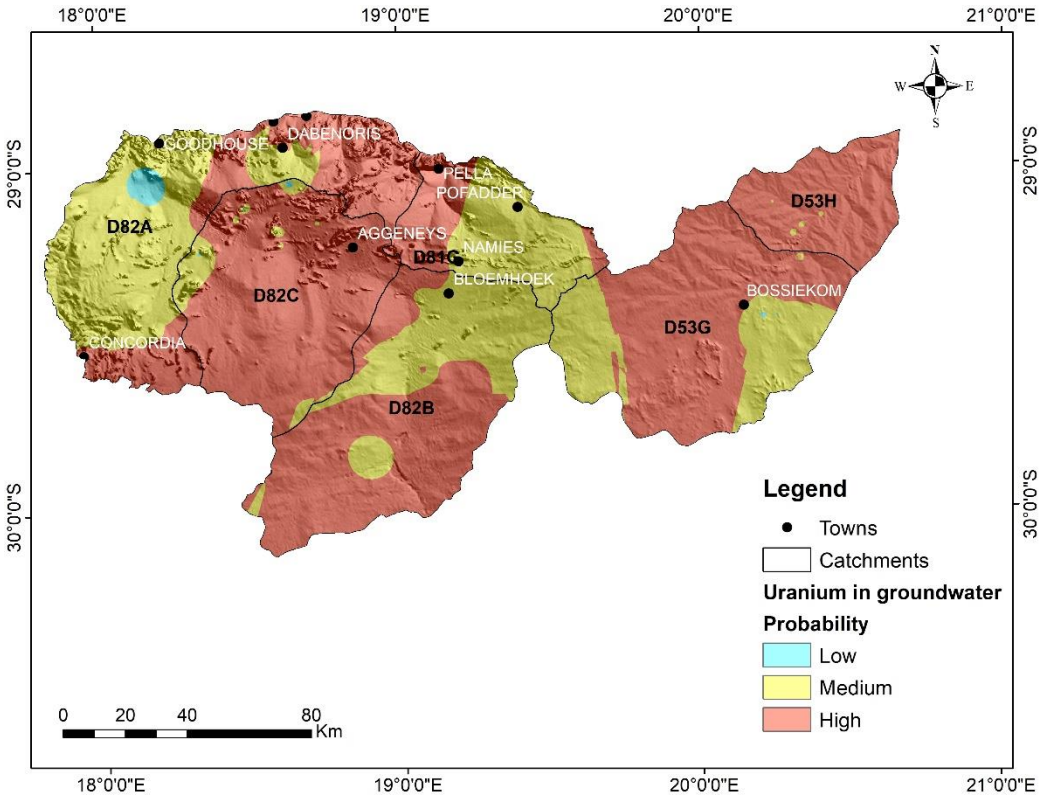

Figure 39: Probability of uranium in the groundwater samples of the study area.

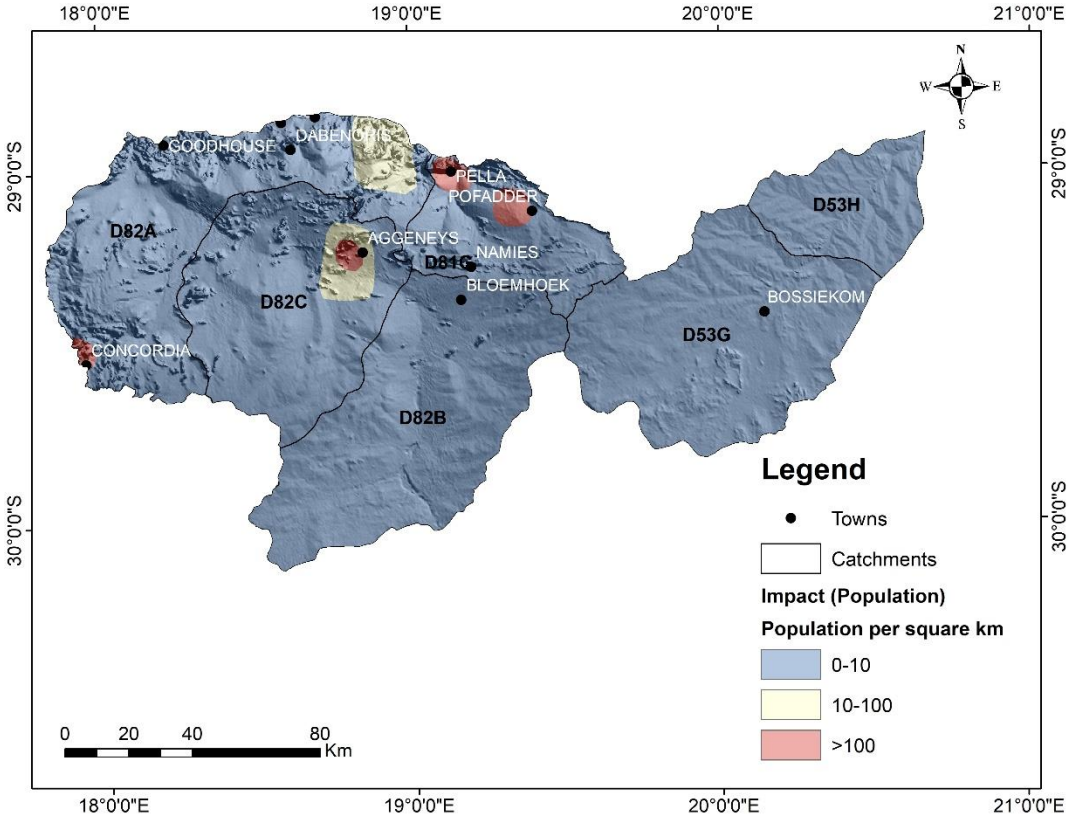

Figure 40: Population density per square kilometre in the study area.

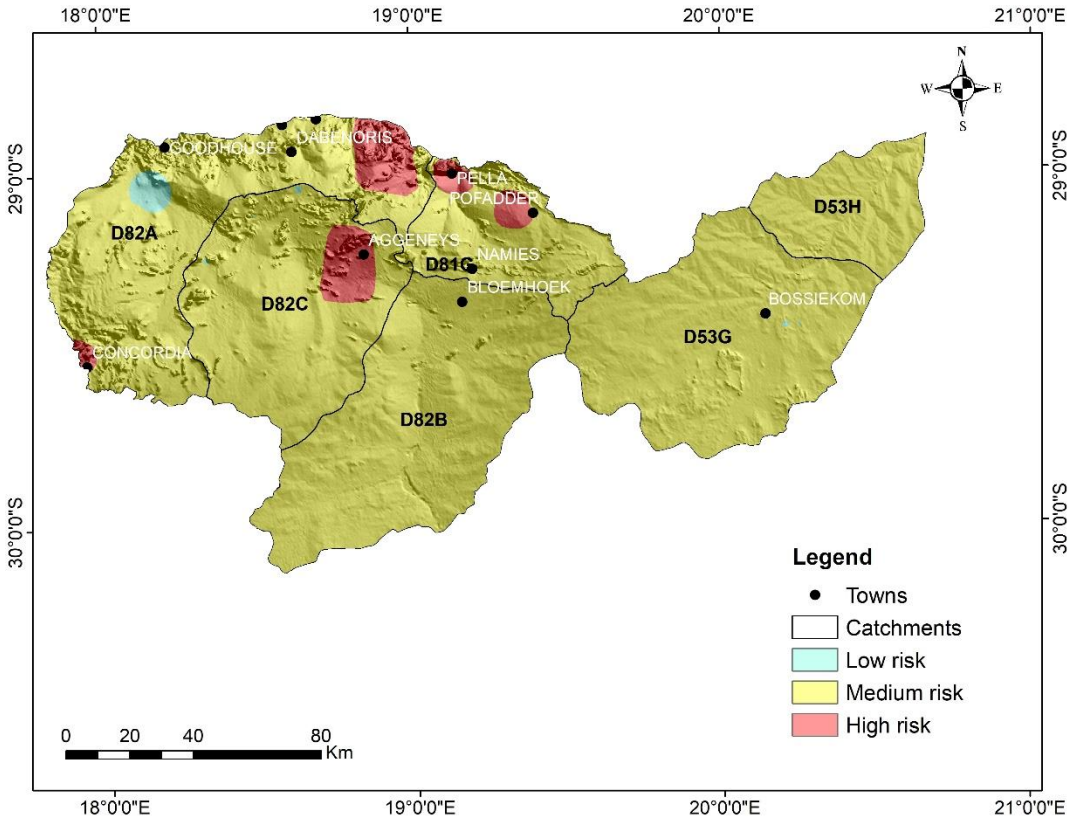

Figure 41: Risk map of uranium concentration to the population of the study area.

6.4 Carnotite

In the Namaqualand region, the main process responsible for carnotite precipitation appears to be changes in the partial pressure of carbon dioxide in the groundwater, supplemented by evapotranspiration. The release of carbon dioxide (exsolving of CO_2 from solution owing to high temperature conditions) destabilises the complexating uranium and vanadium ligands, causing the precipitation of carnotite.

Sulphates, phosphates and fluorides appear to play a major part in the formation of uranium complexation ligands. These ligands are essential in carrying uranium and vanadium in solution along the paleochannels. Based on these ligands, and the dominance of $UO_2(CO_3)_2^{2-}$ and $H_2VO_4^-$ species, the most likely reaction that forms carnotite in the study area may be:

$$\mathbf{2UO_2(CO_3)_2^{2-} + 2H_2VO_4^- + 2K^+ + 3H_2O \leftrightarrow K_2(UO_2)_2V_2O_8.3H_2O + 4H^+ + 4CO_2 + 2O_2}$$

However, other possible reactions are:

$$\mathbf{2UO_2(CO_3)_2^{2-} + 2HVO_4^{2-} + 2K^+ + 3H_2O \leftrightarrow K_2(UO_2)_2V_2O_8.3H_2O + 2H^+ + 4CO_2 + 2O_2}$$

$$\mathbf{2UO_2(CO_3)_3^{4-} + 2H_2VO_4^- + 2K^+ + 3H_2O \leftrightarrow K_2(UO_2)_2V_2O_8.3H_2O + 4H^+ + 6CO_2 + 3O_2}$$

$$\mathbf{2UO_2(CO_3)_3^{4-} + 2HVO_4^{2-} + 2K^+ + 3H_2O \leftrightarrow K_2(UO_2)_2V_2O_8.3H_2O + 2H^+ + 3CO_2 + 6O_2.}$$

The reaction that forms carnotite is reversible; therefore the preservation of the precipitated carnotite is crucial. The influx or recharge of groundwater will result in the carnotite going into solution in the surficial environment. The conditions necessary for the preservation of carnotite are, therefore, high temperatures and low rainfall (arid climate). The higher the temperature and the lower the rainfall, the better the preservation of carnotite.

6.4.1 Sources of uranium, vanadium and potassium

The main sources of uranium and potassium found in the surficial deposits are the underlying granites and gneisses, while the main sources of vanadium are mafic and ultramafic rocks of the Namaqualand Metamorphic Province. Soil geochemical maps of uranium and vanadium highlight the areas that may host possible sources of uranium and vanadium in the surficial uranium deposits. It is interesting to note that there are areas showing high concentrations of uranium in the soil (representing the highly uranium-enriched granitic rocks), but low concentrations of uranium in the proximal groundwater (Figure 43). This is evidenced in the southern and northwestern parts of the catchment D82A, western part of the catchment D82C, northern and southern parts of the catchment D81G, and northwestern part of the catchment D82B. This shows that the presence of highly uranium-enriched rocks is not the only

criterion for a high concentrations of uranium in the groundwater (and hence the possible formation of carnotite). Ideally, the source rocks should contain easily leachable uranium and vanadium. According to Meyer *et al.* (1986), a number of small leucogranites in the Namaqualand Metamorphic Province contain anomalously high concentrations of uranium which are hosted in zircon, apatite, magnetite, biotite and monazite. Uranium contained in zircon and monazite cannot be leached easily in the surficial environment. Unless the uranium- and vanadium-hosting mineral in the rocks is easily leachable, there will be no or very small concentrations of uranium and vanadium in the groundwater within the area. However, vanadium in the soil geochemistry shows a slightly better spatial correlation in respect of vanadium in the groundwater (Figure 44 and 45).

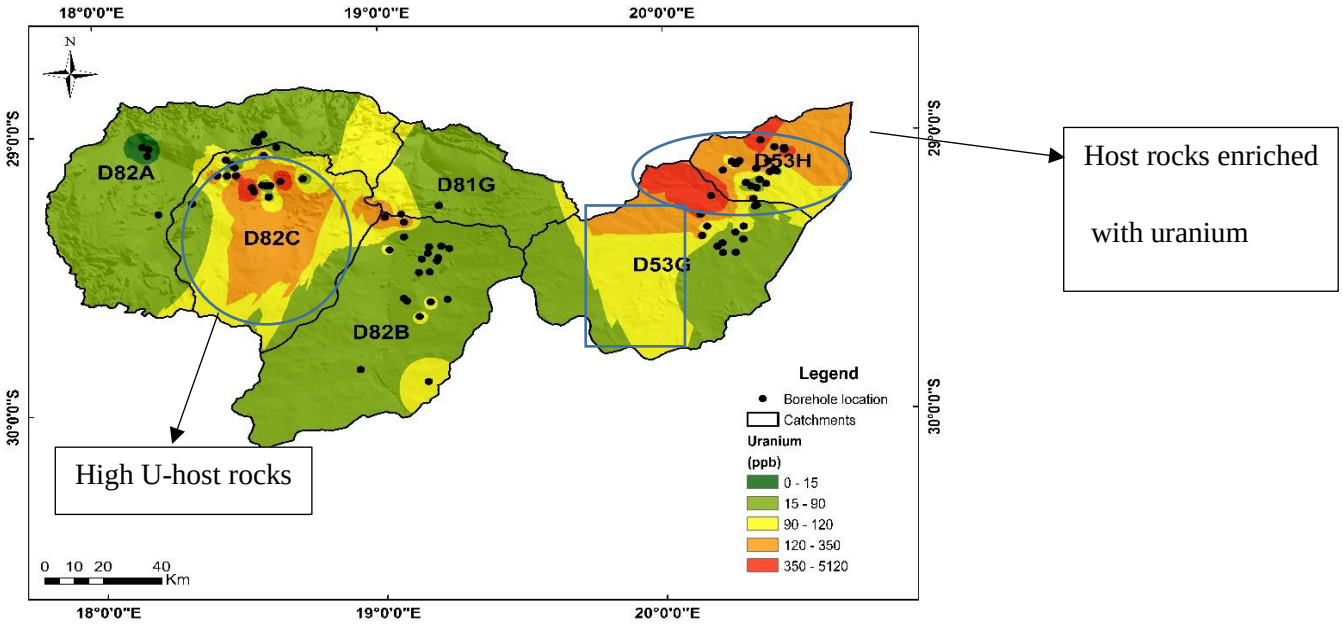

Figure 42: Map showing the groundwater concentrations of uranium in the study area.

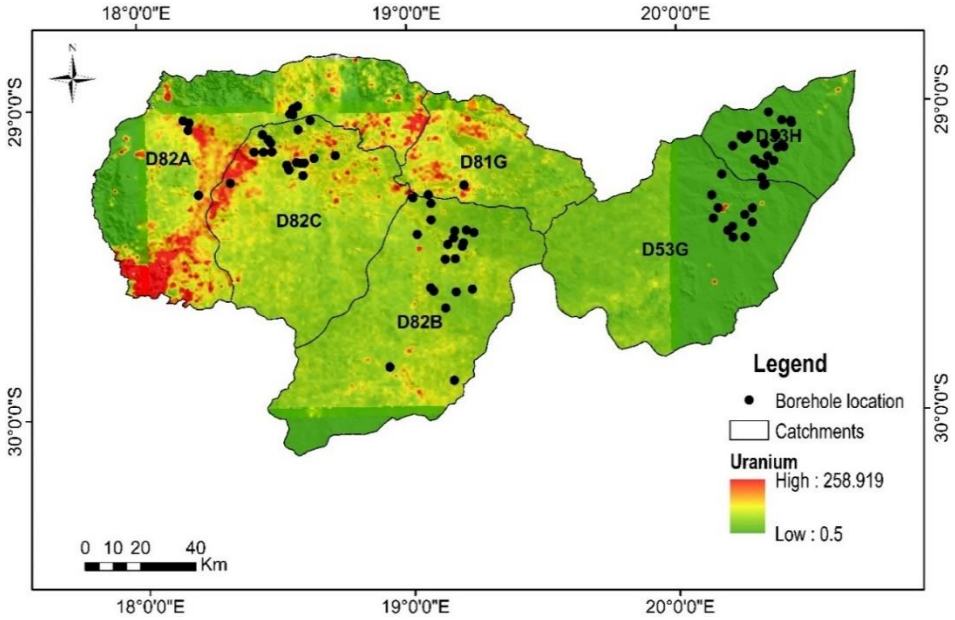

Figure 43: Map showing soil and stream sediment concentrations of uranium (in ppm) in the study area.

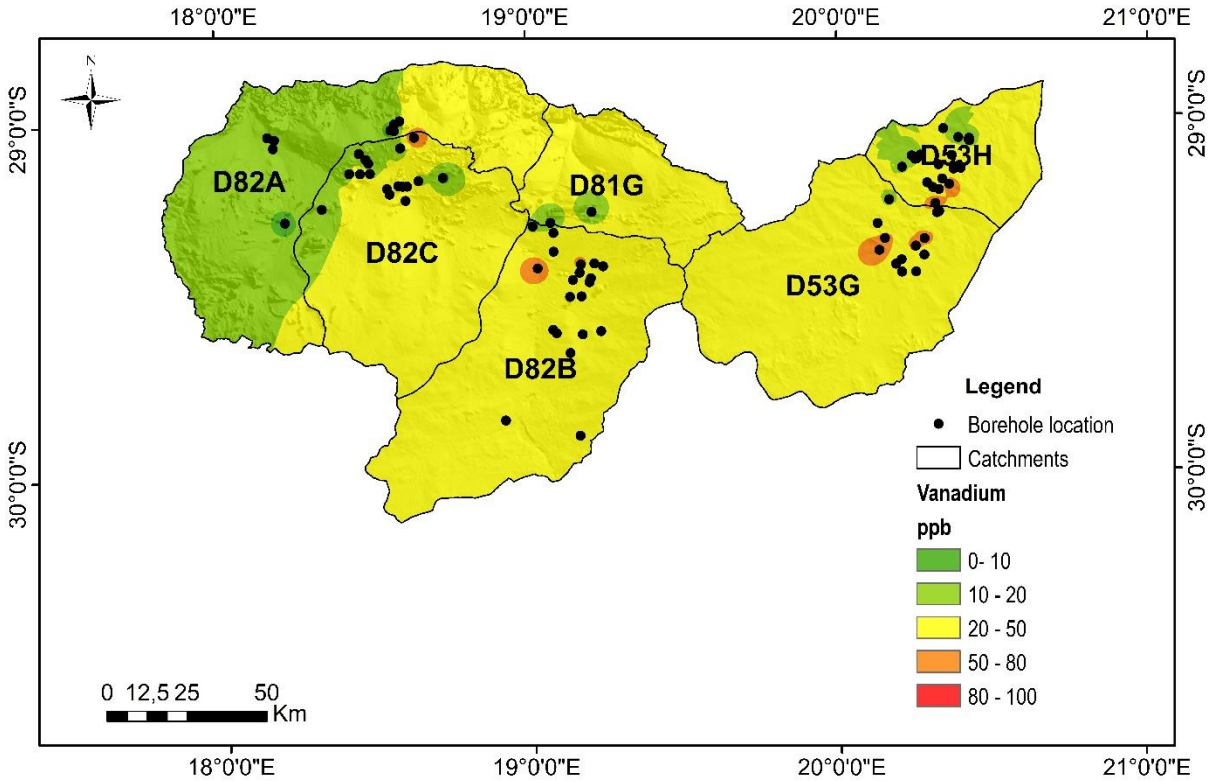

Figure 44: Map showing groundwater concentrations of vanadium in the study area.

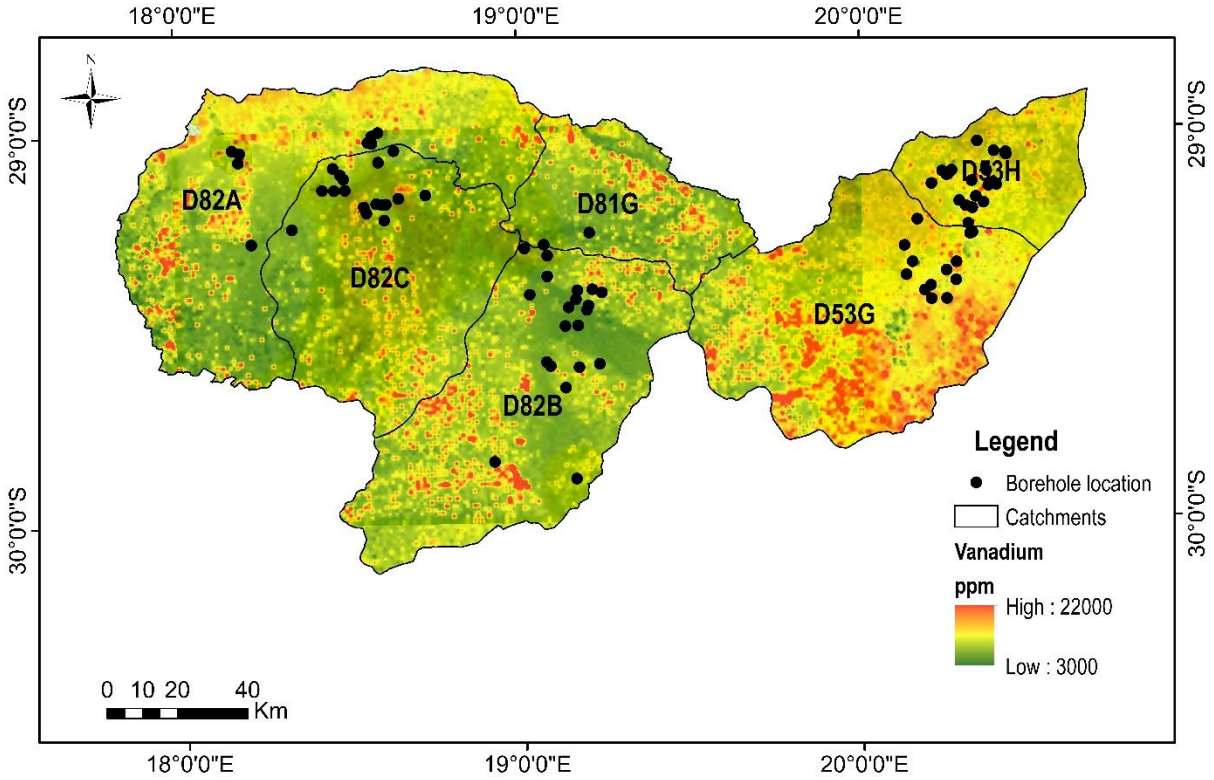

Figure 45: Map showing the soil and stream sediment concentrations of vanadium in the study area.

6.4.2 Carnotite Solubility Index

The Carnotite Saturation Indices obtained based on the modelling of the groundwater geochemistry using PHREEQC was compared with the Carnotite Solubility Indices obtained based on the formula by the Hambleton-Jones and Smith (1986). The results shows that these two methods produce results that are spatially related (Figure 46). Furthermore, the Carnotite Saturation Indices have a very good positive correlation with the Tyuyamunite Saturation Indices as shown in the Figure 47. The high values of carnotite and tyuyamunite saturation indices are restricted within the rocks of the Bushmanland Subprovince (Figure 48Figure 49 and 49). Therefore, only the Carnotite Solubility Index method proposed by Hambleton-Jones and Smith (1986) will be further discussed as a tool for delineation of potential areas for surficial uranium deposits in the study area.

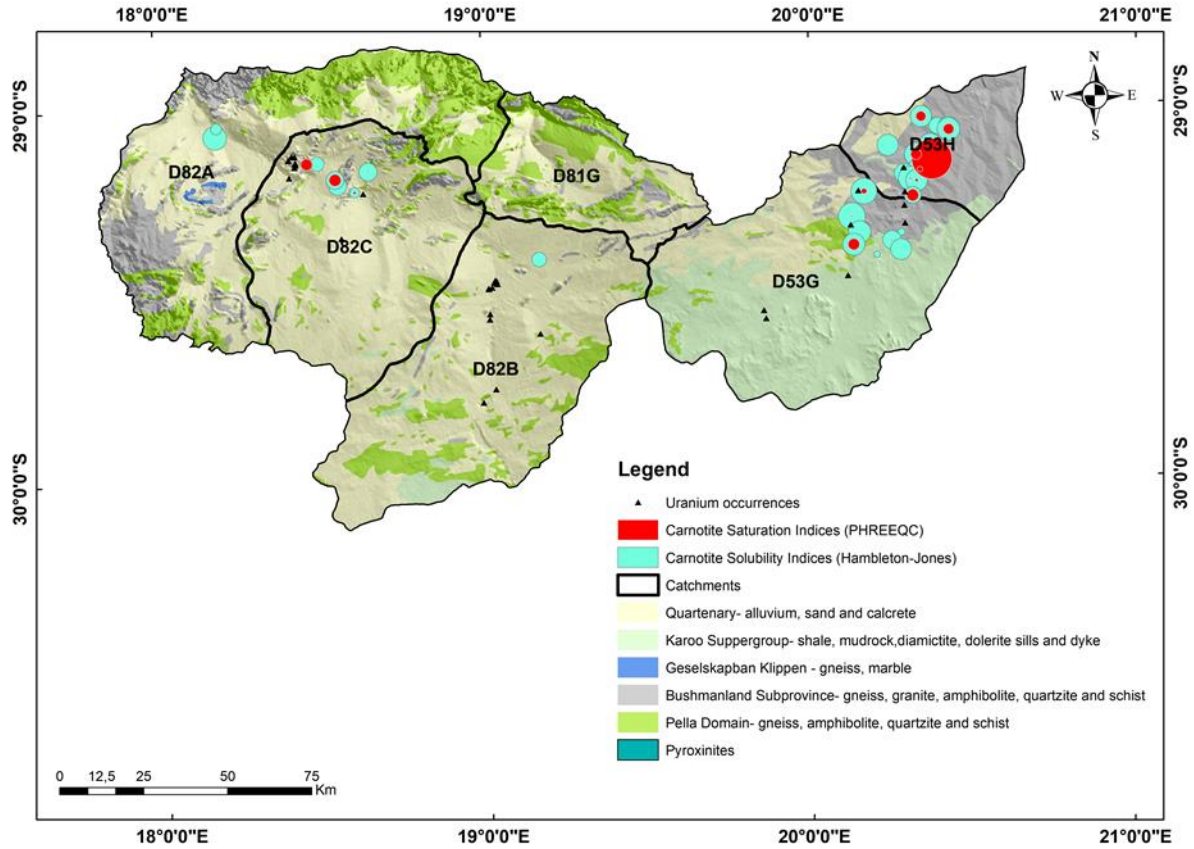

Figure 46: Map of Carnotite Saturation Index using PHREEQC and Carnotite Solubility Index using Hambleton-Jones formula in the groundwater samples of the study area.

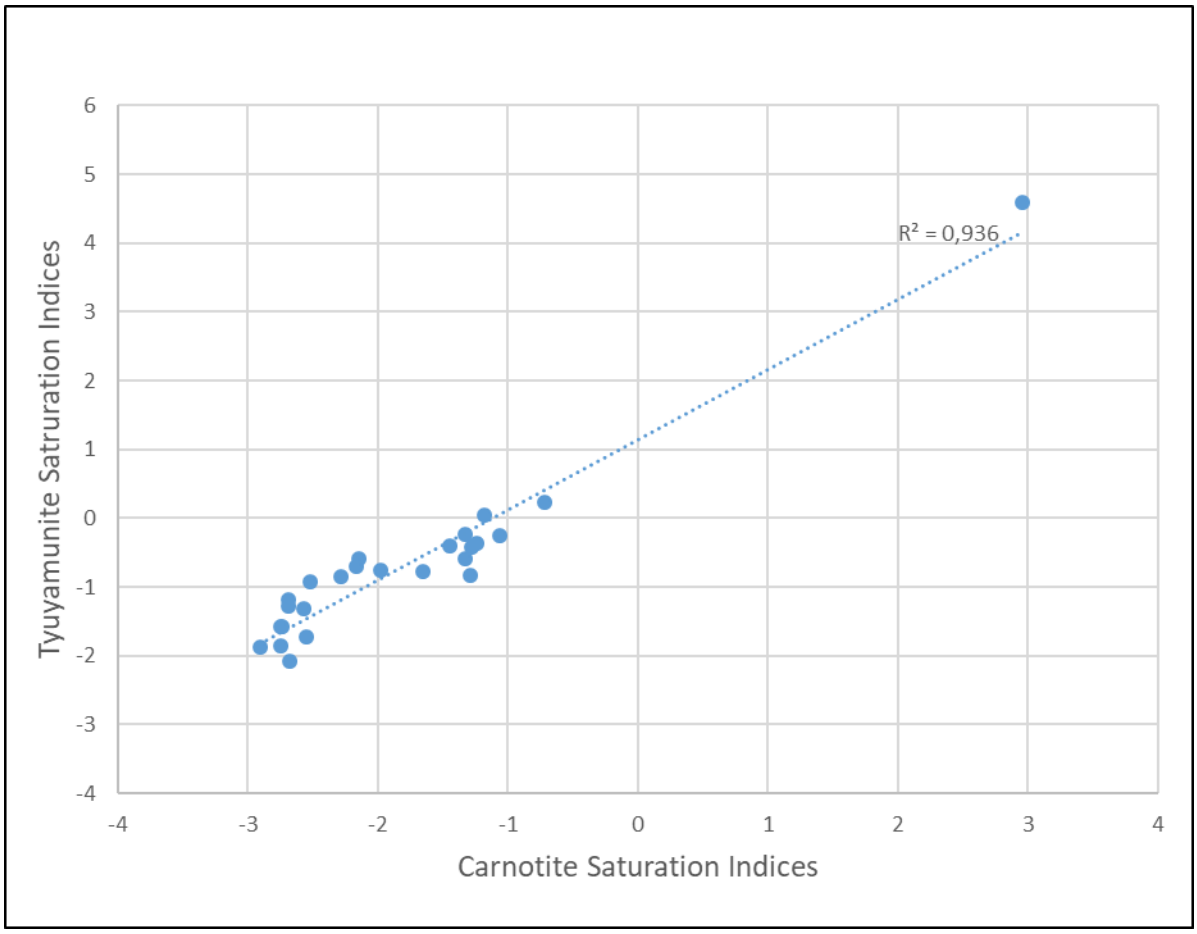

Figure 47: Correlation of carnotite saturation indices and tyuyamunite saturation indices in the study area.

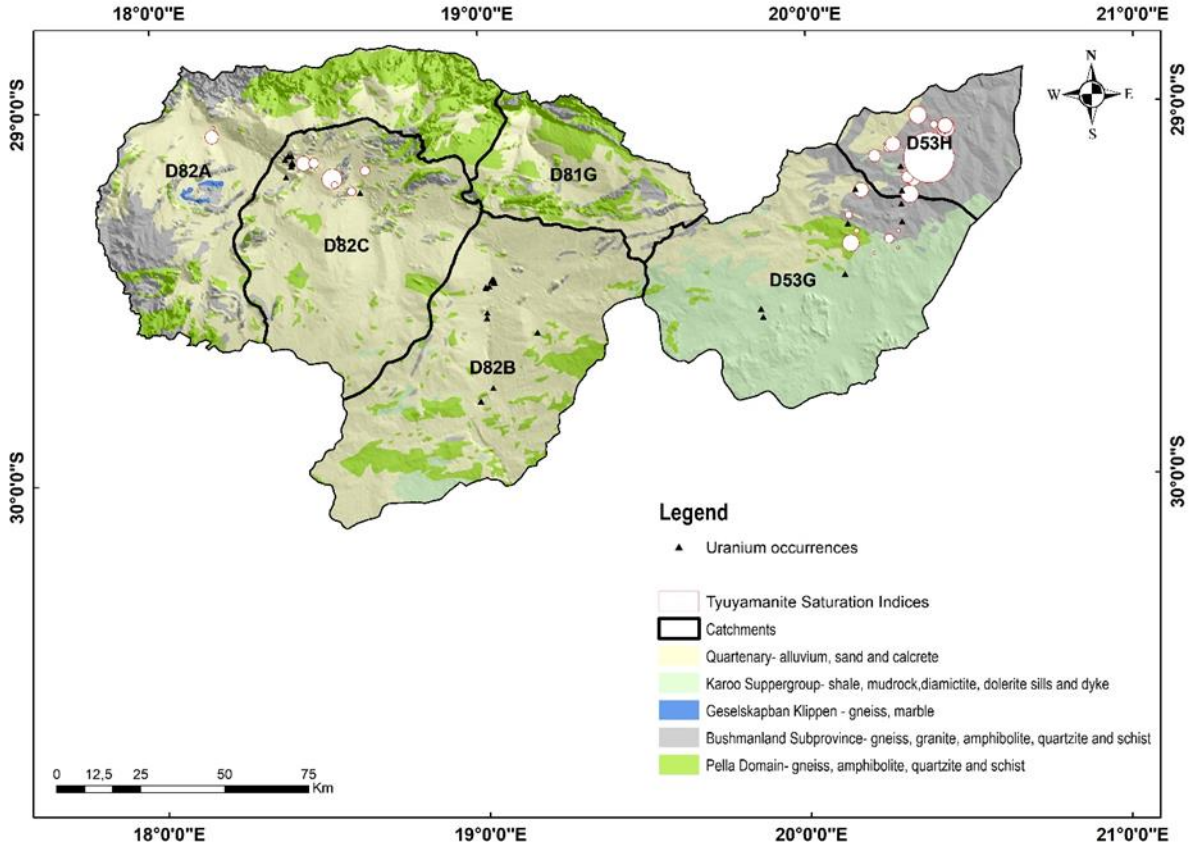

Figure 48: Map showing the tyuyamunite saturation indices (TSI) with the regional geology of the area. Please note that the size of the circles is related to the values of the TSI (the bigger the circle the higher the values of TSI).

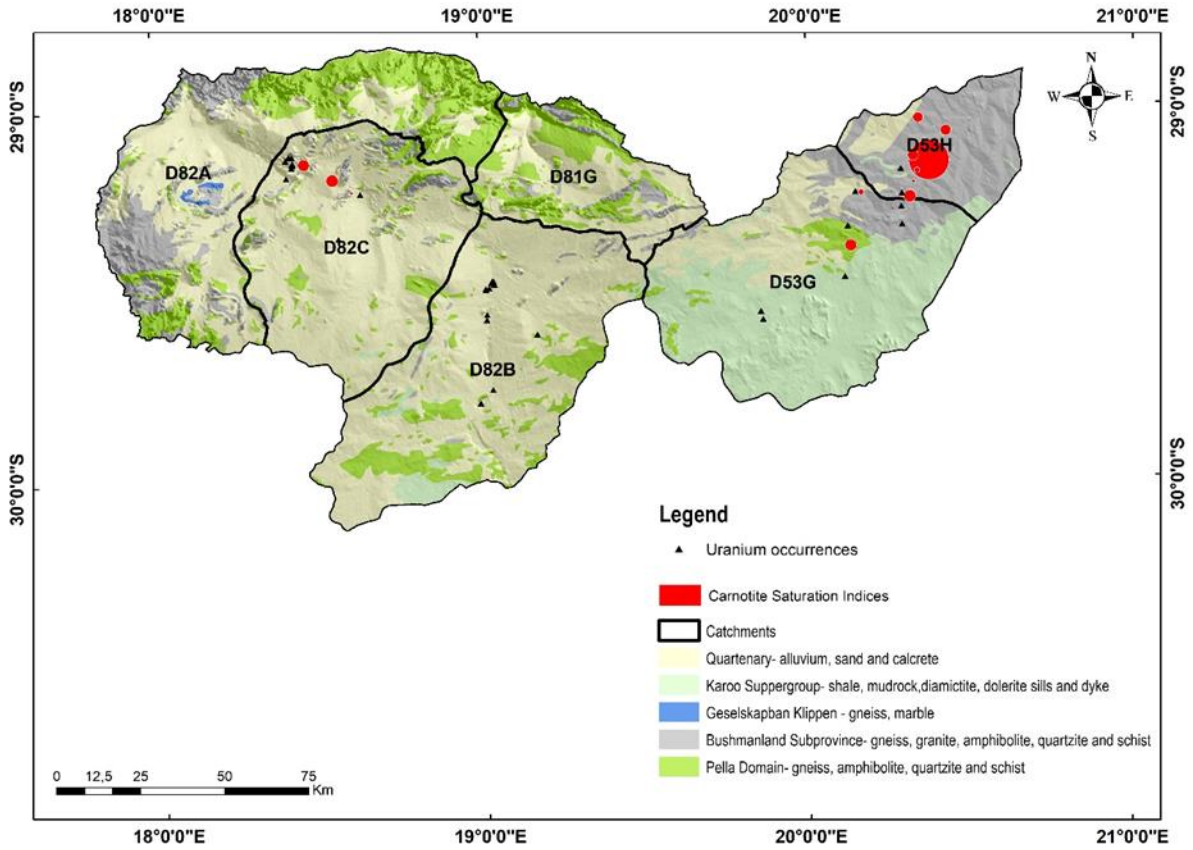

Figure 49: Map showing the carnotite saturation indices (CSI) with the regional geology of the area. Please note that the size of the circles is related to the values of the CSI (the bigger the circle the higher the values of CSI).

Concentrations of uranium, potassium, vanadium and bicarbonates were used to calculate the CSI in order to identify areas which may have potential for carnotite mineralization in the study area (Refer to section 4.5).

The CSI results obtained from the water chemistry data, after using the CSI formula, range from -6.71 to -2.99. The results, however, show that only one sample satisfies the threshold value (-3) proposed by Hambleton-Jones and Smit (1986). There is no CSI value that satisfies the threshold value of 0 under ideal conditions. In addition, Ranalli and Yager (2016) obtained a CSI threshold of about -4 after conducting detailed hydrogeochemical modelling of groundwater at various conditions.

By discriminating CSI values of the study area into anomalous and background CSI populations using statistical analysis (frequency distribution), a threshold value can be obtained for the CSI data. However, this is just a discrimination method of anomalous CSI values that indicates areas that have potential (and not actual precipitation) for carnotite precipitation in the study area. A statistical analysis was done to obtain a threshold CSI value to discriminate between anomalous and background values. The data were grouped into intervals, after which midpoints, frequency and cumulative frequency were

obtained (Table 8). A frequency distribution graph (Figure 50) for the CSI is plotted based on Table 8. In addition, a cumulative frequency distribution graph is plotted to determine the threshold CSI value (Figure 51).

Table 8. Selected class intervals and their resulting midpoints and frequencies for the CSI.

Class intervals (CSI)		Midpoint (CSI)	Frequency	Cumulative frequency
-7.5	-6.5	-7	2	2
-6.5	-5.5	-6	8	10
-5.5	-4.5	-5	32	42
-4.5	-3.5	-4	32	74
-3.5	-2.5	-3	9	83

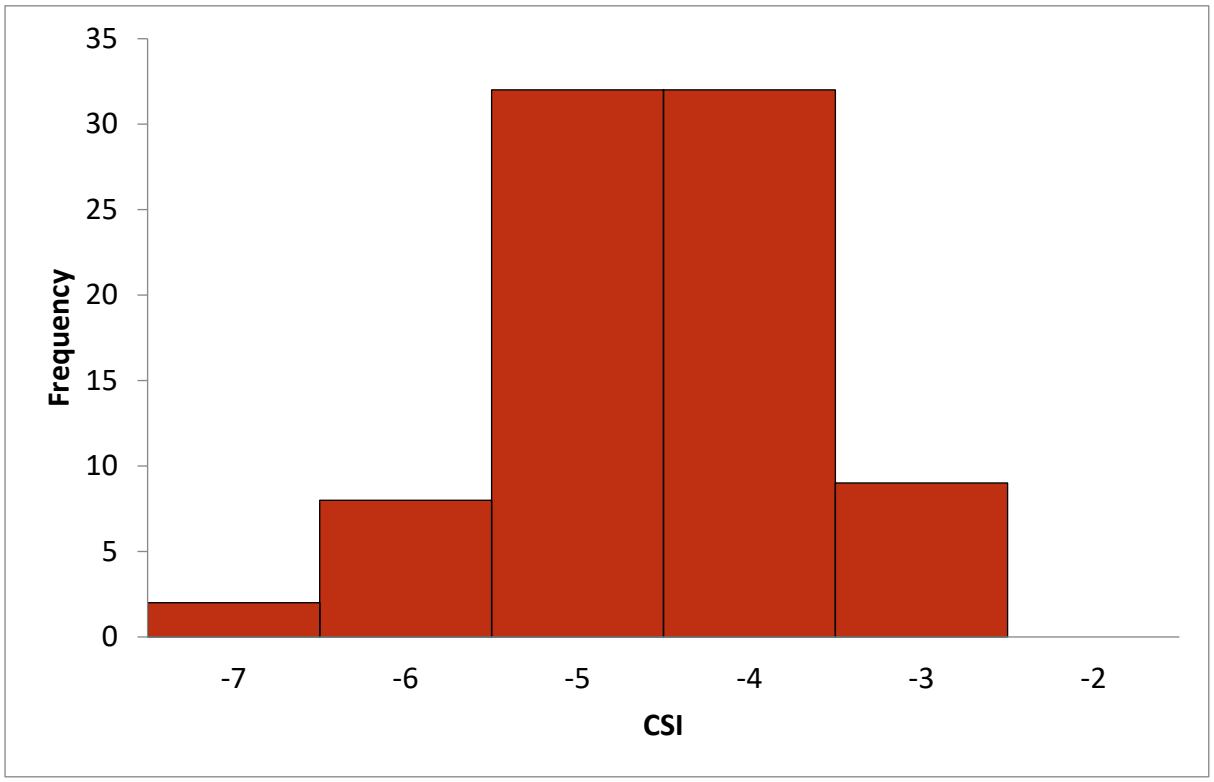

Figure 50: Frequency distribution graph of the CSI values from the groundwater samples.

Therefore, based on Figure 50, a new threshold value of the CSI was estimated. Two methods were used to estimate the threshold — the cumulative frequency distribution of the CSI values (Figure 51) and the box plot (Figure 52).

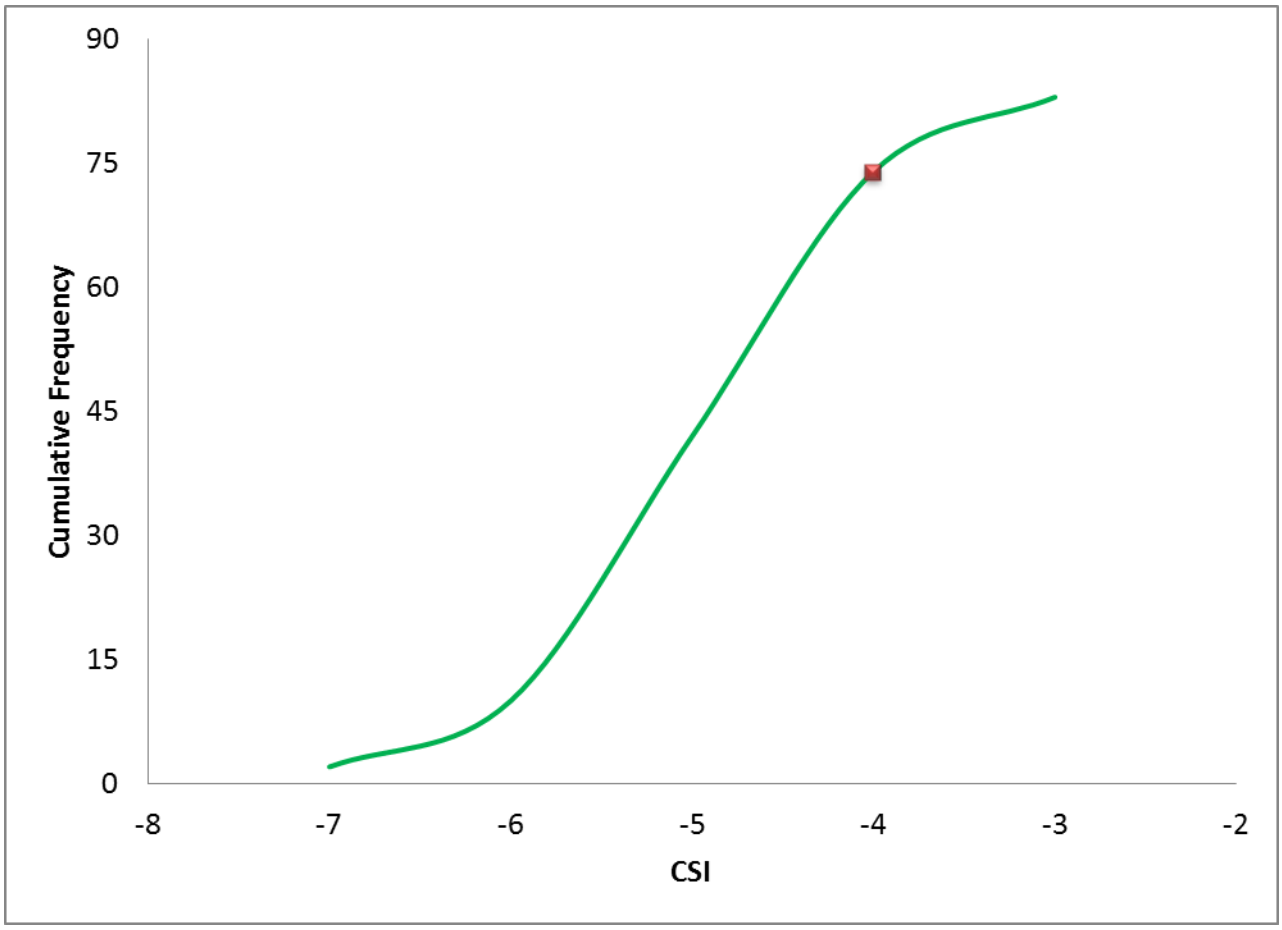

Figure 51: Cumulative frequency distribution graph of the CSI values from groundwater samples.

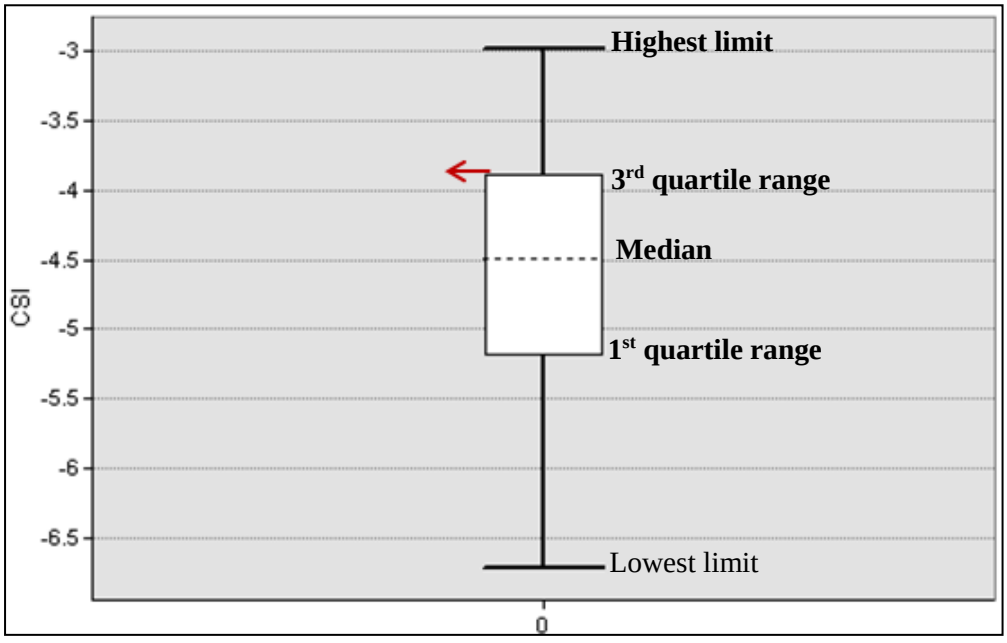

Figure 52: Box and whisker plot of the CSI values.

The cumulative frequency distribution graph of the CSI values (Figure 51) shows a threshold estimate of approximately -4 while the threshold estimate from the box plot (Figure 52) shows a CSI threshold of about -3.8. The average of CSI threshold values from these two methods gives an approximate CSI value of -4. This CSI value was then used as the threshold value for the CSI on the CSI map. About 29% of all the CSI values are at, or above, the threshold value of -4.

6.4.2.1 CSI interpolation

Prior to the interpolation of the CSI data, all the values were converted to positive numbers as an interpolation on negative numbers is impossible. A constant number was added to all the CSI values to ensure that all the values become positive. The lowest CSI value is -6.71, therefore a constant number of seven (7) was added to all the values.

The CSI values were interpolated using IDW and kriging interpolation methods in ArcGIS. The IDW and kriging interpolations were based on the principle of regionalized variables.

According to Sinclair and Blackwell (2002), a regionalized variable is a variable distributed in space, in a partly structured manner, such that there is some degree of spatial autocorrelation. The structured character is called a regionalization and is characterized by the fact that nearby samples are, on average, more similar in value (and hence related) than is the case for distant samples.

The IDW method is generally applied on the basis of distance criteria relative to the point being estimated. The inverse distance method must be done such that weights sum to 1; if not, the method is biased, and therefore unacceptable. Thus, weights are defined as follows (Isaaks and Srivastava, 1989):

$$\mathbf{w_i = (1/d_i^x) / [\sum (1/d_i^x)]}$$

where **w** denotes the weights used for the IDW method; **d** is the distance between the samples, and **x** is an arbitrary power.

According to Sinclair and Blackwell (2002), kriging is an estimation procedure that is globally unbiased (i.e. unbiased, on average, over the entire data range). However, a conditional bias to kriging results can be significant. Kriging is an interpolator that can be exact or smoothed, depending on the measurement error model. The procedure is very flexible and allows investigation of graphs of spatial auto- and cross-correlation. Kriging uses statistical models that allow a variety of output surfaces, including predictions of standard errors, probability and the quantile. The flexibility of kriging may require a great deal of decision making. Kriging assumes that the data result from a stationary stochastic process, and some methods assume normally distributed data. A number of specific methods are included in the general term “kriging”, including simple kriging, ordinary kriging, probability kriging, universal kriging,

indicator kriging and empirical Bayesian kriging, to mention just a few. Only simple kriging, ordinary kriging and empirical Bayesian kriging were used for this study. All these kriging methods depend on the same general principle that the autocorrelation of a regionalized variable can be modelled by a mathematical function inferred from data of the regionalized variable and used to assist in estimation. Simple kriging requires a mean of the field data while ordinary kriging does not require a mean value for interpolation. Empirical Bayesian kriging is an interpolation method that accounts for uncertainty in semivariogram estimation by simulating many semivariograms from the input data.

Kriging interpolation depends on the so-called variogram (or semivariogram) models that are estimated from experimental semivariograms. According to Sinclair and Blackwell (2002), the semivariogram is the principal measure of similarity (i.e., a structural tool) used for geostatistical purposes, although other autocorrelation functions (e.g. the covariogram and the correlogram) that are essentially equivalent may equally well be used for calculation purposes. Autocorrelation studies in geostatistics are often referred to as variography because of the traditional emphasis on the semivariogram. In summary, the semivariogram is half the mean squared difference of values separated by a lag **h**. The formula is as follows (Sinclair and Blackwell, 2002):

$$\gamma^*(\mathbf{h}) = \{ \sum [Z(x_i) - Z(x_i+h)]^2 \} / 2n$$

where $\gamma^*(\mathbf{h})$ is the semivariogram; $Z(x_i)$ is a value of a regionalized variable at location x_i; $Z(x_i+h)$ is a second value at distance **h** from the first; and **n** is the number of samples.

The estimated values of $\gamma^*(\mathbf{h})$ are plotted against the corresponding values of **h**, with the resulting plot defining the experimental semivariogram.

Commonly, $\gamma^*(\mathbf{h})$ is an increasing function as lag increases up to a particular value of h (the range), beyond which the semivariogram is a constant. This relationship means that nearby samples are on average, more similar than is the case with sample pairs, with greater separation. It is this range over which there is similarity that is the average structure of a regionalized variable.

A model is fitted to the experimental semivariogram that approximates the best continuous curve on the individual experimental semivariogram points. The kriging interpolations were based on a spherical semivariogram model (Figure 53). The maximum search distance of 25 km was derived from the semivariogram model, as shown in Figure 53. This is a distance where no relation exists between samples and variabilities of samples remain constant with increasing distances. However, this maximum search distance is inconclusive and, therefore, nearby distances were also used as the maximum search distance with the best search distance being retained. A semivariogram map (Figure 54) was created to show the possible orientations of the semivariogram on the XY plane. There are no discernible preferred

semivariogram orientations that could be deduced from the semivariogram map. Therefore, an omni-semivariogram model was used (where all the orientations are similar).

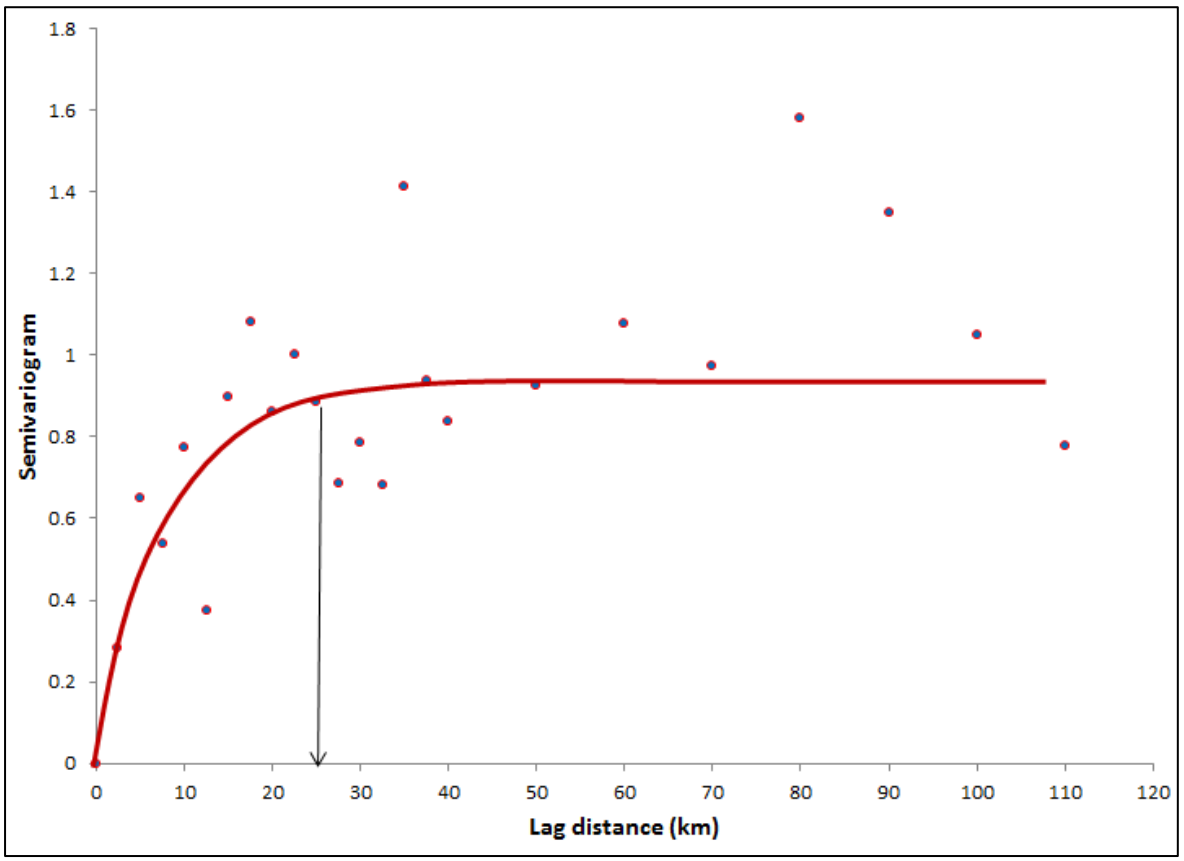

Figure 53: Plot of semivariogram against distance (km) for the CSI values.

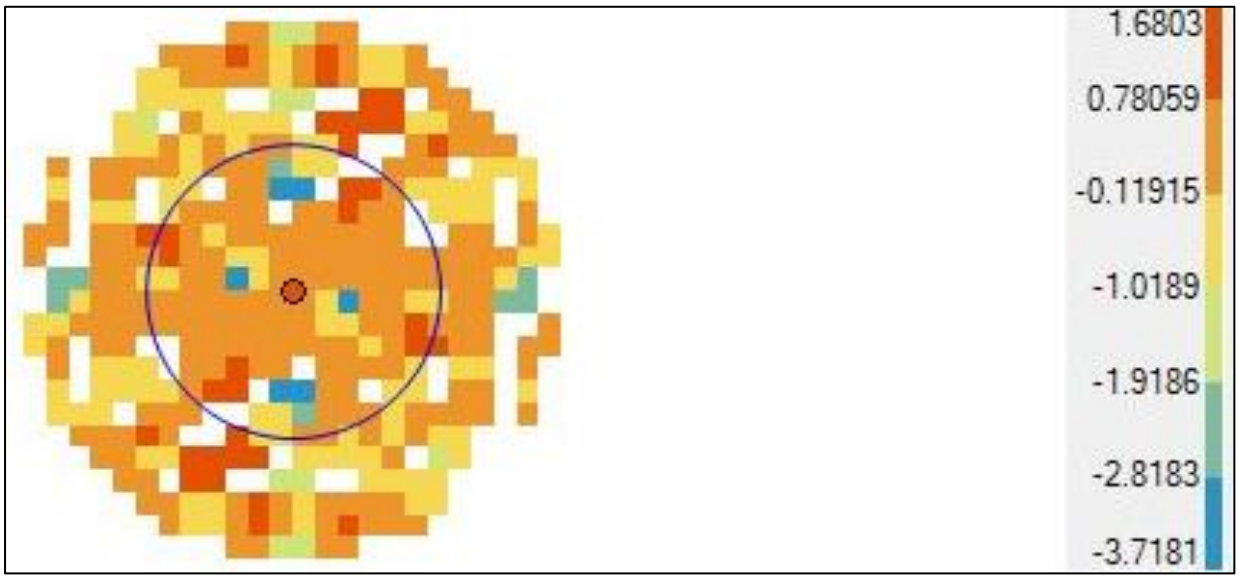

Figure 54: A semivariogram map of the CSI values.

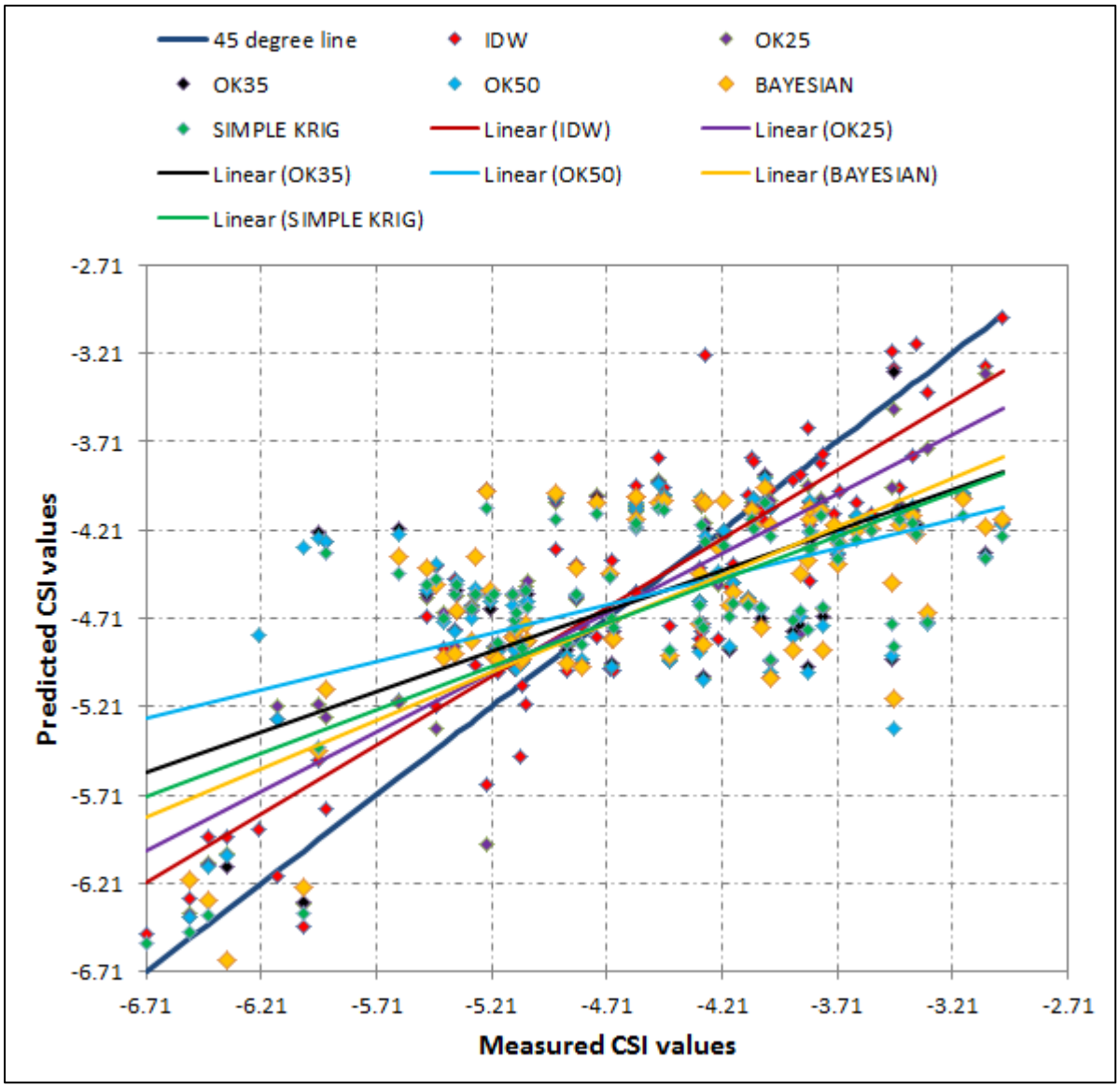

Figure 55: Measured CSI values plotted against the estimated CSI values obtained by IDW, ordinary kriging, simple kriging and empirical Bayesian kriging estimation methods.

6.4.2.2 Cross-validation

Cross-validation is a technique of comparing estimated and measured (true) values using information available in the sample data set. In cross-validation, the estimation method is tested at the locations of the existing samples. The sample value at a particular location is temporarily discarded from the sample data set. The value at the same location is then estimated using the remaining samples. This procedure is an experiment that mimics the estimation process as if sampling at a certain location had never taken place. Once the estimate is calculated, it is compared to the true sample value that was initially removed from the sample data set. This procedure is repeated for all the available samples. In addition to

determining the best estimation method, cross-validation can also be used for determining the best search strategy and testing the semivariogram models ((Isaaks and Srivastava, 1989).

IDW, ordinary kriging, simple kriging and empirical Bayesian kriging methods were used to create a map of the CSI distribution in the study area. In the process of interpolation, estimated CSI values were created from each method. These estimated CSI values were then compared with the original CSI values (measured, or true, values). The IDW and simple kriging used a maximum search distance of 25 km obtained from the semivariogram analysis while, in the ordinary kriging method, three search distances were used (25 km, 35 km and 50 km) (Figure 55). The performance of each estimation method was compared and the best two methods for the CSI data were accepted. The central 45-degree line represents the ideal scenario where the true (measured) CSI values and the estimated CSI values are exactly the same.

As shown in Figure 55, the best CSI estimates were obtained using IDW and ordinary kriging methods at a maximum search distance of 25 km. A conditional bias expectation curve was then created for the two best methods. The conditional expectation curve was drawn through the cloud of the CSI points (Figure 56 and 57). The CSI estimates are deemed conditionally unbiased if their conditional expectation falls on the 45-degree line. The bias of the estimates increases as the conditional expectation curve deviates from the 45-degree line. The IDW method performed better than the ordinary kriging method, as the conditional bias incurred using IDW was less than the conditional bias of the ordinary kriging method.

Other cross-validation methods include the analysis of prediction (estimated) errors. Estimated error is an error obtained by subtracting the measured (true) value from the estimated value. Graphs of the estimated errors for both the IDW and the ordinary kriging methods are shown in Figure 58 and 59. In the ideal case, the cloud of CSI points should be at the zero error line. In addition, the spread of estimation errors around the ideal estimation error, which is zero, is shown in Figure 60.

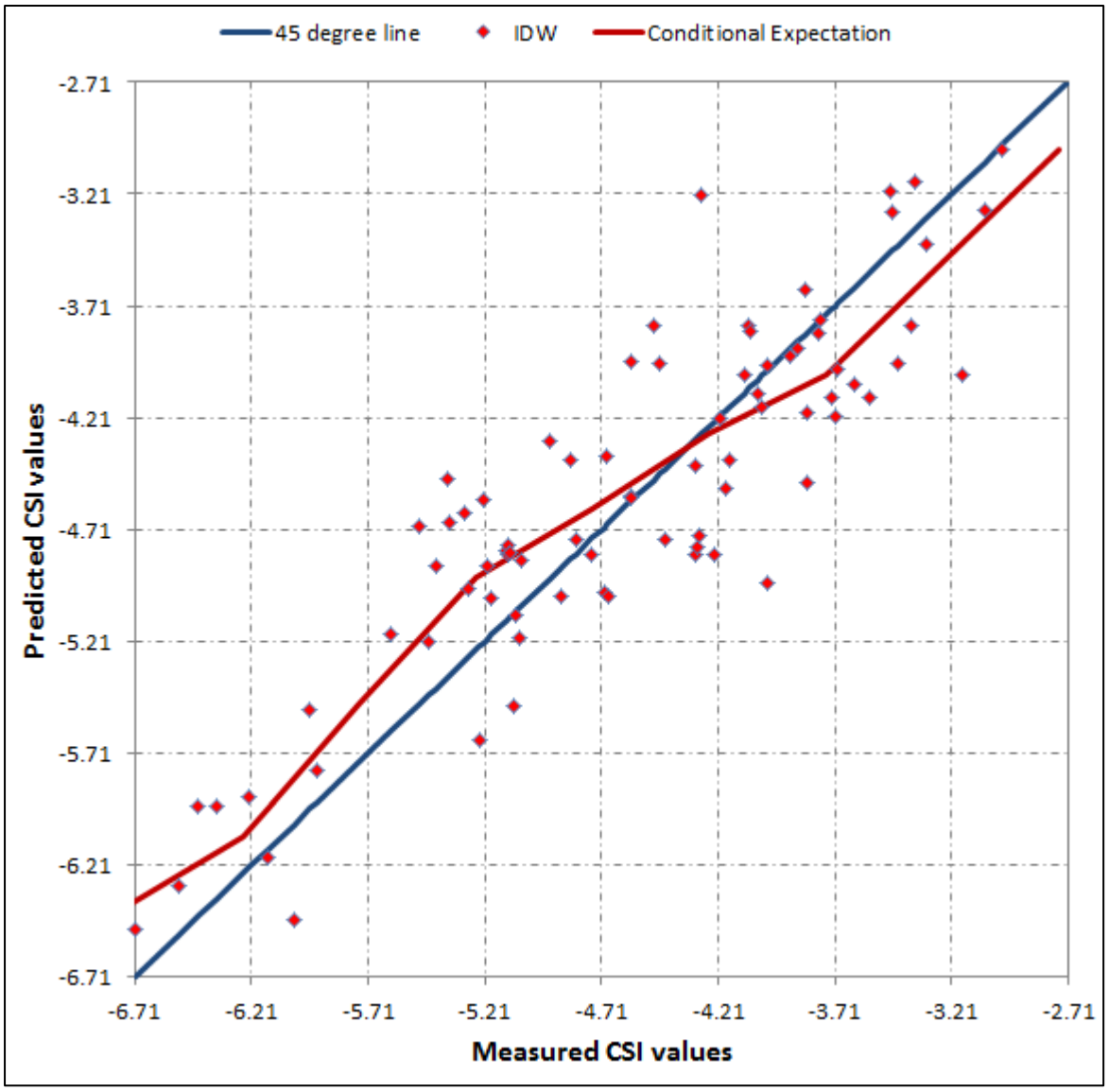

Figure 56: Conditional expectation curve of the CSI original values (measured) against the predicted (estimated) CSI values using the IDW method.

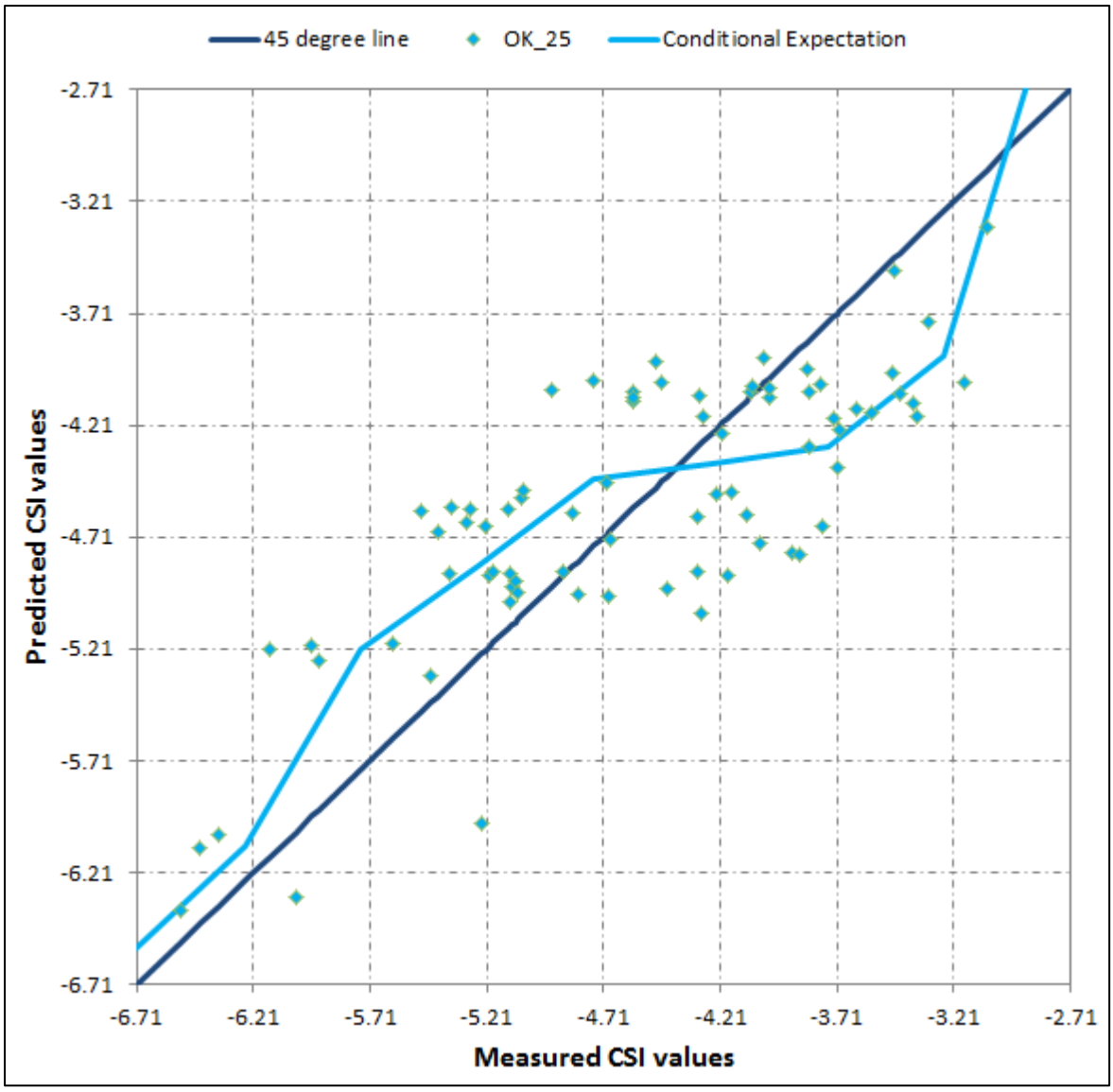

Figure 57: Conditional expectation curve of CSI original values (measured) against the predicted (estimated) CSI values using ordinary kriging method (using 25 km search distance).

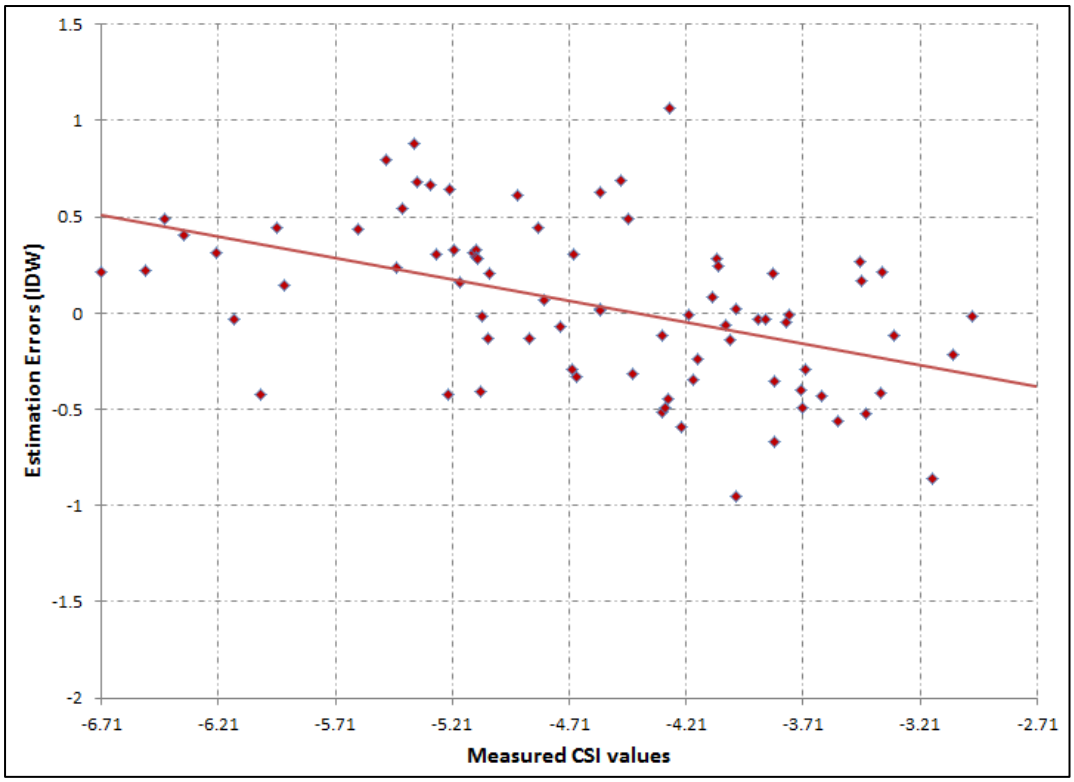

Figure 58: Graph showing the estimation errors of the CSI obtained using the IDW method.

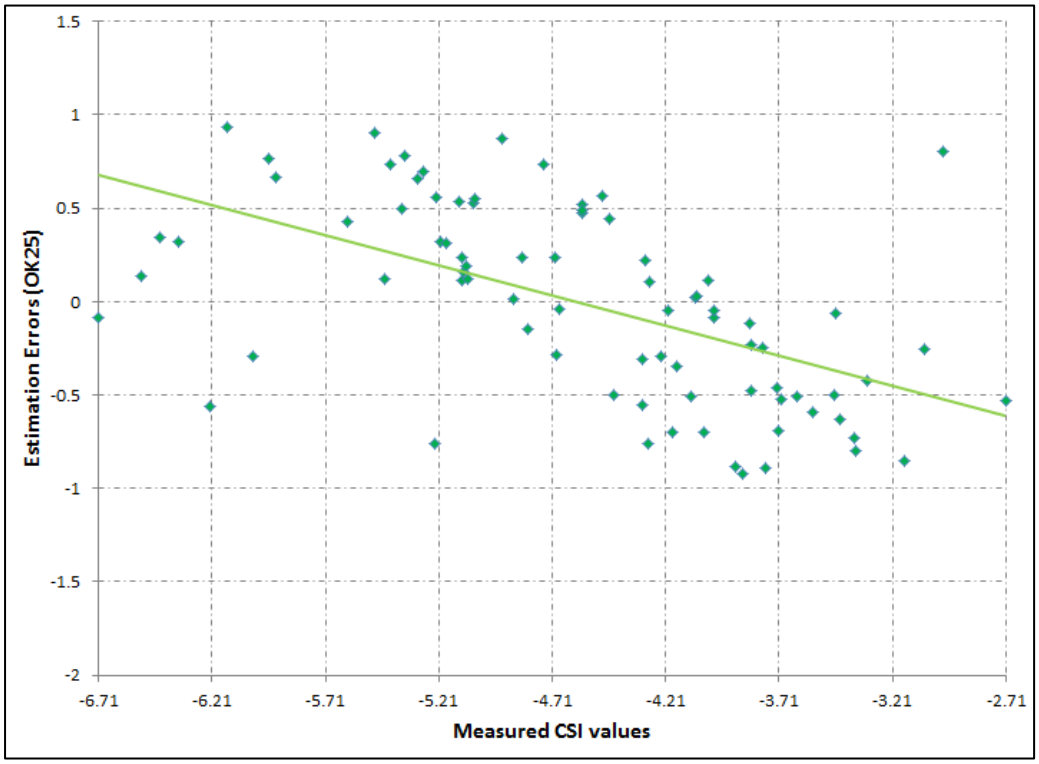

Figure 59: Graph showing the estimation errors of the CSI obtained using the ordinary kriging method.

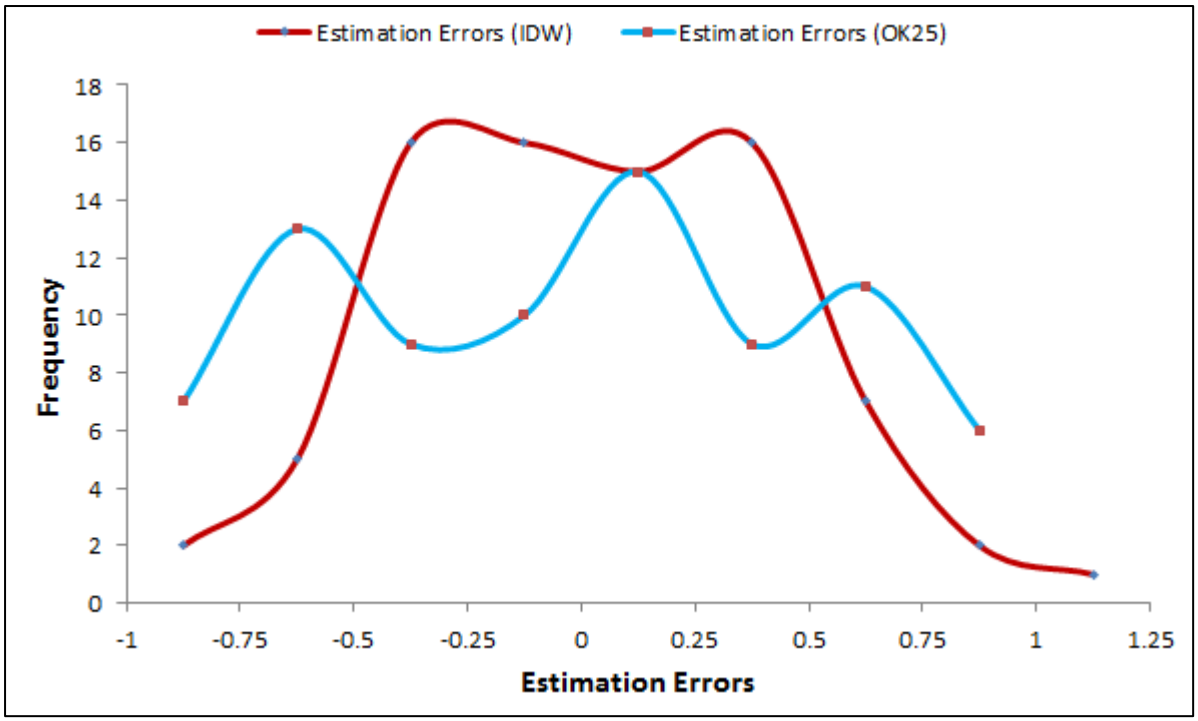

Figure 60: The measure of the spread of the CSI estimation errors obtained using the IDW and the ordinary kriging methods.

The CSI maps obtained by using the IDW and ordinary kriging methods are shown in Figure 61 and 62, using a maximum search radius of 25 km. The IDW map for the CSI distribution was spatially compared against the known surficial uranium occurrences in the study area. Only the relatively larger surficial uranium occurrences were used for this comparison (Figure 61).

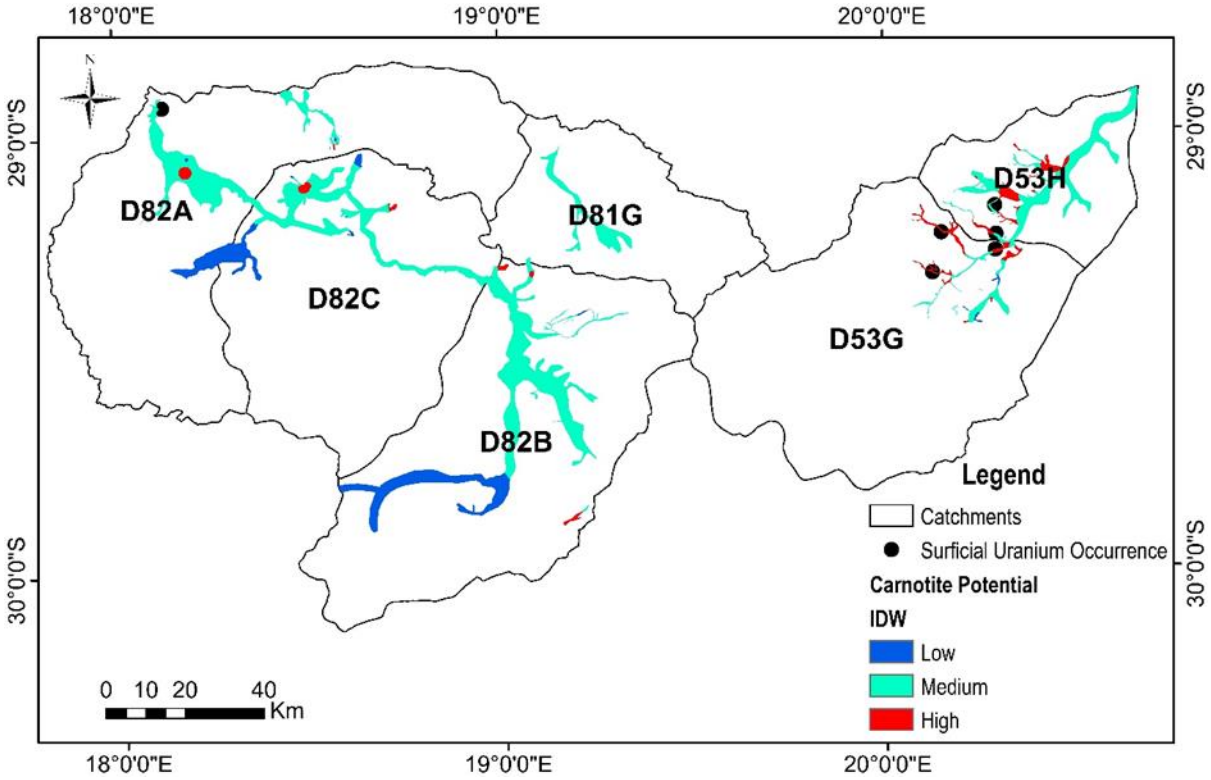

Figure 61: CSI distribution map, interpolated using the IDW method against known surficial uranium occurrences within the palaeochannels in the study area.

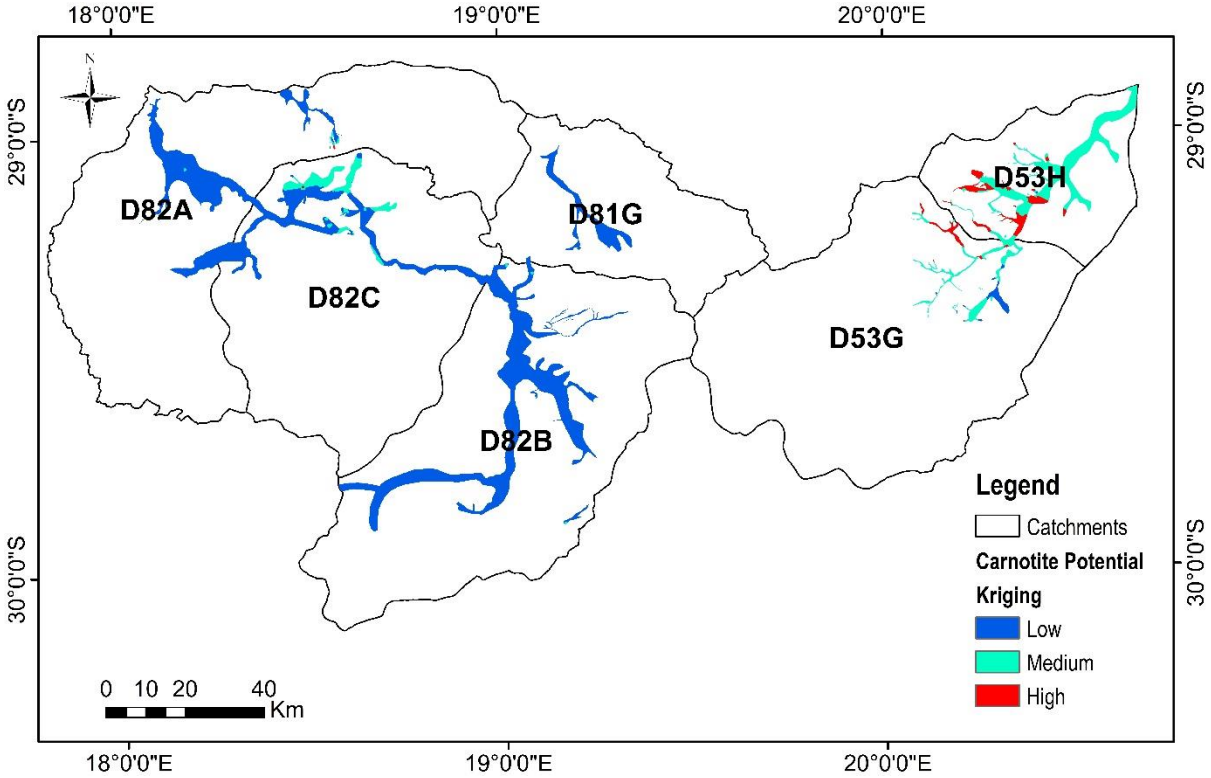

Figure 62: CSI distribution map, interpolated using the kriging method, within the palaeochannels in the study area.

The IDW method overestimates (Figure 58) the lower CSI values by an average of about 4.4% (-6.17) and underestimates the high CSI values by an average of 7.7% (-3.71). The ordinary kriging method overestimates (Figure 59) the lower CSI values by an average of about 5% (-5.3) and, in some cases, overestimates by up to 10% (-5.2). The ordinary kriging method underestimates the high CSI values by an average of 16% (-4.11). The reason for the higher percentage of estimation bias (overestimation of the lower CSI values and underestimation of the higher CSI values) in the ordinary kriging method is the tendency of the kriging method to smooth the estimated values during the estimation process. Ordinary kriging combines many nearby values which increases the smoothing effect, while IDW can use fewer nearby values and hence causes less of a smoothing effect.

The correlation coefficient of the estimated CSI values and measured CSI values in the IDW method is about 79%, while the correlation coefficient in the ordinary kriging method is about 71%. Therefore, in terms of how closely related the estimated values are to the true values, the IDW method shows a better correlation.

The average estimation errors of the CSI values in the IDW method is about 0.04 (1%) and the average estimation errors in the ordinary kriging method is about 0.004 (0.1%). Again, the effect of smoothing in the ordinary kriging method reduces the estimation errors compared to the IDW method. The lower estimation error may not necessarily mean a better estimation method.

The standard deviation of estimation errors of the CSI values in the IDW method is 0.42, while the standard deviation of the estimation errors in the ordinary kriging method is 0.52. Figure 60 shows that the total spread of estimation errors in the IDW is slightly higher than the spread in the ordinary kriging method. However, upon close examination of Figure 58, it can be shown that the majority of estimation errors in the IDW approach zero, and hence the lower standard deviation in the IDW method.

Overall, the IDW method performed better than the ordinary kriging method in estimating CSI values, and therefore the CSI distribution map obtained by IDW was used for spatial correlation with the existing surficial uranium occurrences.

Other estimation methods (simple kriging and empirical Bayesian kriging and ordinary kriging at 35 km and 50 km maximum search distances) did not perform well, and hence were not used for further interpretations (Figure 57). For example, the correlation coefficient of the estimated CSI values and measured CSI values in the simple kriging method is 58% while that of empirical Bayesian kriging is 61%. The correlation coefficients of the estimated CSI values and measured CSI values in the ordinary kriging method at 35 km search distance is 54% while that of the ordinary kriging method at 50 km search distance is 43%. The average estimation errors of the CSI values in the simple kriging method

is 0.081 (2%) and the average estimation errors in the empirical Bayesian kriging method is about 0.082 (2%). The average estimation errors in the ordinary kriging at 35 km and 50 km maximum search distances are 0.018 (0.4%) and 0.003 (0.07%), respectively. The standard deviation of estimation errors of the CSI values in the simple kriging method is 0.66, while the standard deviation of the estimation errors in the empirical Bayesian kriging method is 0.64. The standard deviations of estimation errors of the CSI values in the ordinary kriging method at 35 km and 50 km maximum search distances are 0.69 and 0.76, respectively.

The hydrogeochemical analysis showed good results, with 21 carnotite high-potential areas delineated using the IDW interpolation method, while the kriging method smoothened the distribution of potential carnotite to 14 possible areas (Figure 61 and 62). The CSI showed a good spatial correlation with the existing surficial uranium occurrences (Figure 62).

The existence of source rocks and drainage systems and depositional environments makes the Namaqualand region prospective for calcrete-hosted uranium deposits. It has already been said that the granites are the main source leaching uranium and potassium into the groundwater, whereas vanadium is leached from mafic and ultramafic rocks within the study area. However, there were other factors that played a major role in carnotite formation. These were reduction, sorption, decomplexing of uranyl carbonate complexes, the evaporation of groundwater, variation CO_2 partial pressure, pH, mixing of different groundwaters, reduction/oxidation of groundwater and colloidal precipitation. It is not possible to specify unequivocally which chemical mechanism is most likely to be responsible for carnotite precipitation in, or near, calcrete. In Namaqualand, the sources responsible for higher uranium and the formation mechanism for carnotite cannot be reduced to a single factor. Dissolved uranium, vanadium and potassium concentrations vary widely in the groundwater chemistry in the catchments of the study area. The groundwater of Namaqualand contains concentrations from 5–5120 ppb U, 3–5541 ppb V and 2331–92709 ppm K^+. It is interesting to note that areas that have high concentrations of uranium in the source rocks do not translate into high-potential areas for carnotite. Similarly, areas that have high concentrations of uranium in the groundwater do not have a high potential for carnotite mineralization. The possible explanation for this scenario is that the rocks may have high concentrations of uranium but are locked in minerals (e.g. zircon) that do no leach their uranium easily. Furthermore, in areas where uranium has leached into the groundwater, the other conditions necessary to the formation of carnotite may not exist. The same applies to vanadium in the source rocks and in the groundwater.

The boreholes sampled close to the known surficial occurrences have CSI values that show a potential for carnotite formation. Those CSI values that range from -2.99 to -4 occur within a 5 km radius of the nearest known surficial uranium occurrence.

The method used in this research to calculate and estimate areas that may have a potential for surficial uranium deposits (using the CSI) can be used elsewhere where there are:

- known sources of uranium and vanadium (e.g. granites, gneisses and mafic rocks)
- presence of labile uranium and vanadium (leachability)
- ancient river valley systems and pans
- an arid to semi-arid climate
- occurrences of calcrete and gypcrete.

The CSI method can be applied either by using the existing formula (Hambleton-Jones and Smit, 1986) or by conducting a detailed hydrogeochemical modelling of the groundwater elements to establish the saturation index of carnotite and other minerals of interest.

All the CSI values obtained in the study area range from -6.71 to -2.99 and were not suitable for the threshold value of -3 carnotite saturation. Because the threshold value of -3 was not suitable for the data collected, a statistical analysis was conducted. This was done by discriminating CSI values of the study area into anomalous and background CSI populations. A statistical analysis of carnotite saturation indexes of all groundwater boreholes has the benefit of separating populations of the CSI that are part of the background values, and the population that represents the anomalous CSI. The anomalous CSI represents areas that may have potential for surficial uranium deposits.

Areas of high risk are areas around Dabenoris, Pella, Poffader, Aggeneys and Concordia. The high risk areas covers about 5% of the study area. Human exposure to uranium can result in chemical and radiological toxicities, especially kidney toxicity.

7 CONCLUSION

Groundwater sampling was conducted in Namaqualand to investigate groundwater quality, to establish the distribution of surficial uranium mineralization and to delineate the uranium potential areas for possible future exploration. The groundwater was sampled from 85 boreholes and analysed for its chemical components. The analytical results in respect of the physicochemical properties of the groundwater were compared with the standard guideline values recommended by the WHO (2011) for drinking purpose.

The groundwater chemistry in the six Quaternary catchments ranged from fresh to very saline. Namaqualand is an arid to semi-arid area, having received very little or no rainfall in some years. Salinity is a major problem in the groundwater resources of Namaqualand and is derived from high evaporation, low gradients and the long residence times of the water. Identifying the salinity sources of these aquifers is critical for they are the communities' main water source both for domestic and agricultural purposes. The dissolved solids in the groundwater are derived from rock weathering, marine aerosols and mixing processes.

The solubility of uranium in the groundwater in the study area is controlled by the pH and Eh conditions. The main uranium species are $UO_2(CO_3)_2^{2-}$ and $UO_2(CO_3)_3^{4-}$ which occur at a pH range between 5.5 and 8 and a Eh range between -0.5 and +0.8.

Uranium in the groundwater is high in catchments D82C, D53H and D53G which are located on calcrete, granites, gneisses, amphibolite and schist rock units. The other catchments have low uranium concentrations in the groundwater. These catchments are characterized by the presence of alluvium and calcrete.

There are probably two main sources of uranium in the groundwater within the study area. These two uranium sources are the source rocks (e.g., gneisses and granites) and the dissolution of the existing carnotite and tyuyamunite mineralization.

Uranium may not necessary leach from the granites and gneisses into the groundwater, even if these rocks are enriched with uranium. This is evidenced in the southern and northwestern parts of catchment D82A, the western part of the catchment D82C, the northern and southern parts of catchment D81G, and the northwestern part of catchment D82B. The presence of labile uranium in the source rocks is crucial as some uranium may not be available for leaching, for example uranium in zircon and monazite. Therefore, favourable pH and Eh conditions may not be enough to enable the solubility of uranium in the groundwater.

Areas that have granites and gneisses which are enriched in labile uranium will most likely host groundwater that is enriched in uranium under oxidising conditions. For example, the eastern parts of catchment D82A, the northwestern part of catchment D82C, and the southwestern parts of catchment D81G.

There are areas, mostly in catchment D53H, that have low uranium contents, as shown in the regional soil geochemistry spatial distribution map. However, these areas have existing carnotite and tyuyamunite mineralization. This may be because the existing uranium mineralization is less extensive than the soil geochemistry sample spacing of 1 km, which may therefore easily fail to capture these surficial uranium mineralization. However, the groundwater chemistry shows high amounts of uranium in catchment D53H. The source of the elevated uranium in the groundwater may be the dissolution of the existing carnotite and tyuyamunite mineralization. This is also supported by the carnotite and tyuyamunite saturation indices showing negative values in some parts of the catchment, meaning that the most likely reaction is the dissolution of the carnotite and tyuyamunite mineralization (undersaturated groundwater).

Uranium in the groundwater was compared with other elements/chemicals, based on the statistical relationships using scatter plots. The most interesting relationship was found to be of uranium against salinity and of uranium against TDS. There is a good relationship between uranium and salinity and TDS in the study area (uranium increases in the groundwater as salinity/TDS increases). The increase in salinity and TDS in the groundwater causes an increase in the ionic strength of the groundwater which forces the adsorbed uranium oxide (VI) ion into the groundwater. The fresh groundwater has low ionic strength that may enable the high ionic strength uranium oxide (VI) ion to be adsorbed on other minerals surfaces (i.e., clays). This is not always the case, as the bimodality of the relationship between uranium and salinity/TDS shows that there are areas where there is low saline groundwater (fresh water) and low TDS contents, but high values of uranium.

Surficial uranium prospecting can be done by calculating the CSI in the groundwater to delineate areas that may have potential for carnotite mineralization. The CSI were calculated based on the concentrations of potassium, uranium, vanadium, bicarbonates as well as the pH condition. The CSI obtained ranges from -6.71 to -2.99. CSI distribution maps (gridded maps) were created using geostatistical analysis, i.e. IDW and ordinary, simple and Bayesian kriging. The IDW method performed better overall (showed good correlations with the existing carnotite mineralization) and, hence, was used as a preferred geostatistical method for gridding. Statistical analysis (frequency distribution, cumulative frequency distribution graphs, box and whisker plots) was conducted to find a suitable threshold value of -4 to discriminate between the anomalous and the background CSI.

Approximately 21 potential areas for carnotite mineralization were delineated. The correlation between the delineated potential areas and the existing surficial uranium occurrences was good, i.e. the delineated potential areas included areas of known surficial uranium occurrences. The method used in this research to delineate the areas that may have a potential for surficial uranium mineralization (using the CSI) can be extrapolated to other similar geological environments.

Areas that may pose a risk due to the contamination of uranium in the groundwater were delineated. The risk map was created by combining the probability map with the impact map using multiplication. The probability map represents the likelihood of uranium contamination in the groundwater while the impact map is based on the population density of the study area. The risk matrix of 3 x 3 was used, with 1, 2 and 3 representing low, medium and high risk, respectively. Areas of high risk are located around Dabenoris, Pella, Poffader, Aggeneys and Concordia. The high-risk areas cover about 5% of the study area.

8 RECOMMENDATIONS

The method used in this research to delineate areas that may have potential for surficial uranium mineralization (using the CSI) can be extrapolated to other similar geological environments. Moreover, this study of the uranium content of regional, shallow groundwater shows multiple benefits for exploration, the economy and health.

Given the complexity of the uranium geochemistry in the study area, further investigation is recommended. Fieldwork should include the collection of additional groundwater and rock samples in areas of high uranium content in the granites and gneisses, as well as detailed geological mapping of the study area. Laboratory methods should include ICP-MS, major and trace element XRF analyses and the creation of thin sections for the petrographic description of the rock samples. Furthermore, detailed geochemical modelling of the groundwater should be undertaken to understand not only uranium mineral species and associated saturation indices, but also the saturation indices of each possible mineral species present in the water sample. The modelling may also entail varying the conditions of evaporation, pH and Eh to understand how the various mineral species behave under different conditions. This will enhance our understanding of the groundwater geochemistry. Major and trace elements will assist in identifying the elements that may be present in the rock samples. The petrographic studies should include microscopic studies of the thin sections, scanning electron microscopy and microprobe analysis. These analyses will assist in understanding where the uranium is located in the source rocks, and identify the likely processes for uranium to become soluble in the groundwater.

The shortcomings of this research include the limited groundwater sampling owing to the difficulty in accessing the boreholes and the farms where the boreholes are located. No drilling of boreholes was conducted, and all the sampling was done on the available boreholes from the NGA in the DWS database. It is recommended that new boreholes be drilled for groundwater sampling in areas where there is potential for carnotite mineralization. In addition, follow-up auger drilling should be conducted (soil sampling) in areas that have been delineated as having a high potential for carnotite mineralization.

In the Namaqualand region, there is no communal water supply system and most communities depend on groundwater for drinking water. It was found that, for a large part of the study area, uranium levels in the groundwater exceed the required standard. Therefore, mitigation measures such as water treatment before usage need to be implemented to ensure that communities living in the area are safeguarded against this potential health risk. Medical geology research needs to be conducted to ascertain the impacts of uranium and other harmful elements on people, animals and plants.

9 REFERENCES

Abiye, T.A. and Leshomo, J. 2013. Groundwater flow and radioactivity in Namaqualand, South Africa. *J. Environmental Earth Sciences*. 70:281–293.

Abiye, T., Bybee, G. and Leshomo, J. 2018. "Fluoride Concentrations in the Arid Namaqualand and the Waterberg Groundwater, South Africa: Understanding the controls of mobilization through hydrogeochemical and environmental isotopic approaches. "Groundwater for Sustainable Development 6: 112–120.

Abiye, T.A. and Bhattacharya, P. 2019. Arsenic concentration in groundwater: Archetypal study from South Africa. Groundwater for Sustainable Development, 100246.

Adams, S., Titus, R. and Xu, Y. 2004. Groundwater recharge assessment of the basement aquifers of central Namaqualand. WRC Report No. 1093/1/04.

Adithya, V.S., Chidambaram, S., Tirumalesh, K., Thivya, C., Thilagavathi, R. and Prasanna, M.V. 2016. Assessment of sources for higher uranium concentration in ground waters of the Central Tamilnadu, India. Conf. Series: Materials Science and Engineering 121, 012009.

Albat, H.M. 1984. The Proterozoic granulite facies terrane around Kliprand, Namaqualand Metamorphic Complex. Ph.D. Thesis, Dept. of Geology, University of Cape Town, South Africa. In: Chamber of Mines Precambrian Research Unit. Bulletin 33.

Almond, J. and Pether, J. 2009. Palaeontological heritage of the Northern Cape. Palaeotechnical report, South African Heritage Resource Agency.

Agenbacht, A.L.D. 2007a. The geology of the Pofadder area. Explanation booklet 2918, for 1:250 000.

Agenbacht, A.L.D. 2007b. Geological map, 2918 Pofadder. 1:250 000 series. Council for Geoscience, Pretoria.

Andreoli, M.A.G., Smith, C.B., Watkeys, M., Moore, J.M., Ashwal, L.D. and Hart, R.J. 1994. The geology of the Steenkampskraal monazite deposit, South Africa: Implications for REE-Th-Cu mineralization in charnokite-granulite terranes: Economic Geology, 89:994–1016.

Appelo, C.A.J. and Postma, D. 1996. Geochemistry, groundwater and pollution. Balk, Rotterdam, 536 pp.

Bharti, R., Kalimuthu, R. and Ramakrishnan, D. 2015. Spectral pathways for exploration of secondary uranium: an investigation in the desertic tracts of Rajasthan and Gujarat, India. Advances in Space Research (2015).

Bennet, D.J. and Thomson, J.R. 1989. The Elements of Nuclear Power: Longman Scientific and Technical, Harlow, England, 293 pp.

Blake, C.A., Coleman, C.F., Brown, K.B., Hill, D.G., Lowrie, R.S., Schmitt, J.M. 1956. Studies in the carbonate-uranium system. Journal of American Chemical Society 78 (23): 5978–5983.

Blignault, H.J., Van Aswegen, G., Van Der Merwe, S.W. and Colliston, W.P. 1983. The Namaqualand geotraverse and environs: part of the Proterozoic Namaqua Mobile Belt. Geological Society of South Africa, Special Publication, 10: 1–29.

Bowell, R.J., Barnes, A., Grogan, J., and Dey, M. 2009. Geochemical controls on uranium precipitation in calcrete palaeochannel deposits of Namibia. Proceedings: 24th International Applied Geochemistry Symposium, Fredericton, New Brunswick, 2009, 413–418.

Boyle, D.R. 1982. The formation of basal-type uranium deposits in south central British Columbia, Economic Geology. 77: 1176–1209.

Brindha, K. and Elango, L. 2011. Fluoride in Groundwater: Causes, Implications and Mitigation Measures. *In*: Monroy, S.D. (Ed.), Fluoride Properties, Applications and Environmental Management: 111–136.

Bruneton, P., Cuney, M., Dahlkamp, F. and Zaluski, G. 2014. IAEA geological classification of uranium deposits, International Symposium on Uranium Raw Material for the Nuclear Fuel Cycle (URAM, 2014).

Burns, P.C. and Finch, R. (editors). 1999. Uranium: Mineralogy, Geochemistry and the Environment. Reviews in Mineralogy, 38. Mineralogical Society of America, Washington, D.C.

Campbell, E.E., Parker-Nance, T. and Bate, G.C. 1992. A compilation of the information on the magnitude, nature and importance of coastal aquifers in Southern Africa. WRC Report No 370/1/92.

Carlisle, D. 1980. Possible variations on the calcrete-gypcrete uranium model. U.S. Dept. Energy, GJBX-53 (80), 38 pp.

Carrick, P.J. and Krüger, R. 2007. Restoring degraded landscapes in lowland Namaqualand: lessons from the mining experience and from regional ecological dynamics. Journal of Arid Environments, 70: 767–781.

Chae, G.T., Yun, S.T., Kim, K. and Mayer, B. 2006. Hydrogeochemistry of sodium-bicarbonate type bedrock groundwater in the Pocheon spa area, South Korea: water-rock interaction and hydrologic mixing. Journal of Hydrology 321:326–343.

Chaudhary, V. and Satheeshkumar, S. 2018. Assessment of groundwater quality for drinking and irrigation purposes in arid areas of Rajasthan, India. Applied Water Science 8: 218.

Christie, A.D.M. 1989. Demonstrated coal resources of the Springbok Flats Coalfield. Report 1989-0069. Geological Survey of South Africa, 25 pp.

Cuney, M. 2009. The extreme diversity of uranium deposits: Mineralium Deposita, 44: 3–9.

Cole, D.I. 1998. Uranium: *In*: Wilson, M.G.C., and Anhaeusser, C.R. (editors). The Mineral Resources of South Africa. Sixth edition, Council for Geoscience: 642–658.

Colliston, W.P. and Schoch, A.E. 1996. Proterozoic metavolcanic rocks and associated metasediments along the Orange River in the Pofadder Terrane, Namaqua mobile belt. South African Journal of Geology, 99: 309–325.

Comly, H.H. 1945. "Cyanosis in Infants Caused by Nitrates in Well Water." Journal of the American Medical Association (JAMA) 129: 112–116.

Conrad, J. and Adams, S. 2003. GIS based assessment of groundwater recharge in the fractured rocks of Namaqualand, South Africa. *In* "Groundwater in fractured rocks". Krásný, J. and Sharp, J.M. (editors). International Association of Hydrogeologists Selected Papers. Taylor and Francis: 203–217.

Cornell, D.H., Thomas, R.J., Moen, H.F.G., Reid, D.L., Moore, J.M. and Gibson, R.L. 2006. The Namaqua-Natal Province. *In*: Johnson, M.R., Anhaeusser, C. and Thomas, R.J. (editors). The Geology of South Africa. Council for Geoscience, Pretoria: 325–379.

Cornell, D.H., Pettersson, Å., Whitehouse, M.J. and Scherstén, A. 2009. A new chronostratigraphic paradigm for the age and tectonic history of the Mesoproterozoic Bushmanland ore district, South Africa. Economic Geology, 104: 385–404.

Cortazzo, J.A., Lichtman, A.D. 2014. Methemoglobinemia: a review and recommendations for management. J Cardiothorac Vasc Anesth. 28(4):1043–7.

Council for Geoscience database, 2018. Namaqualand uranium occurrences, South African Mineral Database (SAMINDABA).

Cuney, M. 2009. The extreme diversity of uranium deposits: Mineralium Deposita, 44: 3–9.

Dalziel, I.W.D., Mosher, S., and Gahagan, L.M. 2000. Laurentia-Kalahari collision and the assembly of Rodinia. J. Geol. 108: 499–513.

Davis, C.L., Hoffman, M.T., Roberts, W. 2016. Recent trends in the climate of Namaqualand, a megadiverse arid region of South Africa. South African Journal of Science.

Desmet, P.G. and Cowling, R., 1998. The climate of the Karoo. A Functional Approach. *In*: Dean, W., Milton, S. (editors). The Karoo. Ecological Patterns and Processes. Cambridge University Press, Cambridge: 3–16.

Desmet, P.G. 2007. Namaqualand — A brief overview of the physical and floristic environment. Journal of Arid Environments, 70: 570–587.

De Wit, M.C.J. 1993. Cainozoic evolution of drainage systems in the North-Western Cape. PhD Thesis, University of Cape Town (unpublished).

Dollar, E.S.J. 1998. Palaeofluvial geomorphology in southern Africa: a review. Progress in Physical Geography 22, 3: 325–349.

Driver, A., Desmet, P.G., Rouget, M., Cowling, R.M. and Maze, K.E. 2003. Succulent Karoo Ecosystem Plan Biodiversity Component Technical Report. Cape Conservation Unit, Botanical Society of South Africa Cape Town.

DWAF (Department of Water Affairs and Forestry). 1996. *In*: Holmes S. (editor). South African water quality guidelines (2nd edition) Domestic Use, 1, Pretoria, Department of Water Affairs and Forestry.

DWAF (Department of Water Affairs and Forestry). 2003. Lower Orange Water Management Area: Overview of water resources availability and utilisation. South Africa, Report number P WMA 14000/00/0203.

Eaton, A.D., Clesceri, L.S., Greenberg, A.E. and Franson, M.A.H. 1998. Standard methods for the examination of water and wastewater. 20th edition. Washington, DC, American Public Health Association: 2–24.

Ellis, F. and Lambrechts, J.J.N. 1986. Soils. *In*: Cowling, R.M., Roux, P.M. and Pieterse, A.J. H. (editors). The Karoo biome: a preliminary synthesis Part 1 — physical environment. South African National Scientific Programmes Report No. 124, CSIR, Pretoria:18–38.

Garrels, R.M. and Christ, C.L. 1965. Solutions, minerals and equilibria. Harper and Row, New York, 83.

Gholami, S. and Srikantaswamy, S. 2009. Analysis of agricultural impact on the Cauvery river water around KRS dam. World Appl Sci J 6:1157–1169.

Hambleton-Jones, B.B., Levin, M. and Wagener, G.F. 1986. Uraniferous surficial deposits in southern Africa. *In*: (C.R. Anhaeusser and S. Maske, editors). Mineral Deposits of Southern Africa, II. Geological Society of South Africa, Johannesburg: 2269–2287.

Hambleton-Jones, B.B. and Smit, M.C.B. 1986. Calculation of the Carnotite Solubility Index, Uraniferous surficial deposits in southern Africa. *In*: C.R. Anhaeusser and S. Maske, editors). Mineral Deposits of Southern Africa, II, Geological Society of South Africa, Johannesburg: 81.

Hartnady, C.J.H., Joubert, P. and Stowe, C.W. 1985. Proterozoic crustal evolution in south-western Africa. Episodes 8: 236–244.

Health Canada. 2001. Summary of guidelines for Canadian drinking water quality. Prepared by Federal-Provincial Subcommitee on Drinking Water of the Federal-Provincial Territorial Committee on Environmental and Occupational Health.

Hem, J.D. 1985. Study and interpretation of the chemical characteristics of natural water. USGS, Water Supply (264), 117–120 in India.

Hou, B., Fabris, A.J., Keeling, J.L. and Fairclough, M.C. 2007.Cainozoic palaeochannel-hosted uranium and current exploration methods, South Australia, Mathematics in Engineering, Science and Aerospace Journal 46: 34–39.

International Atomic Energy Agency (IAEA). 2013. Certified reference material IAEA-448: Soil from oil field contaminated with technically enhanced Radium-226, IAEA analytical quality in nuclear applications series, 30 (IAEA/AQ/30), IAEA, Vienna.

International Atomic Energy Agency (IAEA). 2014. Uranium 2014. Resources, Production and Demand. A Joint Report by the OECD Nuclear Energy Agency and the International Atomic Energy Agency: 504.

Isaaks, E.H. and Srivastava, R.M. 1989. An Introduction to applied geostatistics. New York, Oxford University Press, 1989: 561.

Jack, A.M. 1980. The geology of western Namaqualand. Bulletin 29, Precambrian Research Unit. Dept. of Geology, University of Cape Town.

Jacob, R.E., Corner, B. and Brynard, H.J. 1986. The regional geological structural setting of the uraniferous granitic provinces of Southern Africa. *In*: C.R. Anhaeusser and S. Maske (editors). Mineral Deposits of Southern Africa. Geol. Soc. S. Afr.: 1807–1818.

Johnson, C.J., Bonrud, P.A., Dosch, T.L., Kilness, A.W., Senger, K.A., Busch, D.C. and Meyer, M.R. 1987. Fatal Outcome of Methemoglobinemia in an Infant, Journal of the American Medical Association, 257: 2796–2797.

Jordana, S. and Batista, E. 2004. Natural groundwater quality and health. Geologica Acta: An International Earth Science Journal, 2(2): 175–188.

Joubert, P. 1971. Geological survey of Namaqualand and Bushmanaland. Annual Report, Precambrian Research Unit. Dept. of Geology, University of Cape Town.

Joubert, P. 1986. Namaqualand — A model of Proterozoic accretion: Geological Society of South Africa Transactions, 89:79–96.

Jowell, P. and Folb, A. 2004. Into Kokerboom country: Namaqualand's Jewish pioneers. Fernwood Press.

Kenan, A.O. and Chirenje, E. 2016. Uranium in South Africa: Exploration and Supply Capacity. Natural Resources and Conservation 4(2): 25–33.

Kenan, A.O., Magadaza, L., Thomas, A., Zilibokwe, N., Lehong, K. and Pieterse, L. 2017. Namaqualand Surficial Uranium Potential, Report, Council for Geoscience, 2017-0050a.

Khoury, H.N. 2015. Uranium minerals of central Jordan. Review in Applied Earth Science (Trans. Inst. Min. Metall. B), 124(2): 104–128.

Kumar, S.K., Rammohan, V., Sahayam, J.D. and Jeevanandam, M. 2009. Assessment of groundwater quality and hydrogeochemistry of Manimuktha River basin, Tamil Nadu, India. Environ Monit Assess 159: 341–351.

Kumar, A., Rout, S., Narayanan, U., Mishra, M.K., Tripathi, R.M, Singh, J., Kumar, S. and Kushwaha, H.S. 2011. Geochemical modelling of uranium speciation in the subsurface aquatic environment of Punjab State in India. Journal of Geology and Mining Research Vol. 3(5), pp. 137-146.

Kut, K.M.K., Sarswat, A., Srivastava, A., Pittman Jr., C.U. and Mohan, D. 2016. A review of fluoride in African groundwater and local remediation methods. Groundwater for Sustainable Development, 2: 190–212.

Krupka, K.M. and Serne, R.J. 2002. Geochemical factors affecting the behaviour of antimony, cobalt, europium, technetium and uranium in vadose sediments. A report prepared for CH2M HILL Hanford Group, Inc. and the U.S. Department of Energy under contract DE-AC06-76RL01830, USA.

Lee, R.W. and Strickland, D.J. 1988. Geochemistry of groundwater in tertiary and cretaceous sediments of the southeastern coastal plain in eastern Georgia, South Carolina, and southeastern North Carolina. Water Resources Research 24(2): 291–303.

Lehmann, B. 2008. Uranium Ore Deposits. Reviews in Economic Geology, 2:16–26.

Leshomo, J.T. 2011. Investigation of hydrochemistry and uranium radioactivity in the groundwater of Namaqualand, Northern Cape, South Africa. MSc thesis, University of Witwatersrand, Johannesburg.

Levin, M. 1978. Uranium occurrences in the Gordonia and Kuruman Districts: Report, Atomic Energy Corporation of South Africa, PER-37: 24.

Levin, M. 1980. A geological and hydrogeochemical investigation of the uranium potential of an area between the Orange and Kuruman Rivers, northwestern Cape Province: Report, Atomic Energy Corporation of South Africa, PEL-272: 84.

Levin, H. 1983. Geohydrological investigations of the Vaalputs radioactive waste disposal site and environmens. Nuclear Development Corporation of SA (Pty) Ltd. Republic. PER-112 (GEA-404).

Leybourne, M.I. and Cameron, E.M. 2006. Composition of groundwaters associated with porphyry-Cu deposits, Atacama Desert, Chile: Elemental and isotopic constraints on water sources and water-rock interactions. Geochemica et Cosmochemica Acta, 70: 1616–1635.

Lidman, F., Morth, C. M. and Laudon, H. 2012. Landscape control of uranium and thorium in boreal streams – spatiotemporal variability and the role of wetlands, Sweden: Biogeosciences, 9: 4773–4785.

Macey, P.H., Thomas, R.J., Minnaar, H.M., Gresse, P.G., Lambert, C.W., Groenewald, C.A., Miller, J.A., Indongo, J., Angombe, M., Shifotoka, G., Frei, D., Diener, J.F.A., Kisters, A.F.M., Dhansay, T.,

Smith, H., Doggart, S., Le Roux, P., Hartnady, M.I. and Tinguely, C. 2017. Origin and evolution of the 1.9 Ga Richtersveld Magmatic Arc, SW Africa. Precambrian Research 292: 417–451.

Macey, P.H., Bailie, R.H., Miller, J.A., Thomas, R.J., De Beer, C., Frei, D. and Le Roux. P.J. 2018. Implications of the distribution, age and origins of the granites of the Mesoproterozoic Spektakel Suite for the timing of the Namaqua Orogeny in the Bushmanland Subprovince of the Namaqua-Natal Metamorphic Province, South Africa. Precambrian Research: 311.

Makubalo, S.S. and Kenan, A.O. 2018. Carnotite Solubility Index in Namaqualand, Report, Council for Geoscience, 2018-0226a.

Mann, A.W. and Deutscher, R.L. 1978. Genesis principles for the precipitation of carnotite in calcrete drainages in Western Australia. Economic Geology, 73: 1724–1737.

McCarthy, T.S., Moon, B.P. and Levin, M. 1985. Geomorphology of the Western Bushmanland Plateau, Namaqualand, South Africa, South African Geographical Journal, 67(2): 160–178, DOI: 10.1080/03736245.1985.10559713.

Meyer, M., Robb, L.J. and Anhaeusser, C.R. 1986. Uranium and thorium contents of Archaean granitoids from the Barberton Mountain Land, South Africa. Precambrian Research, 33: 303–321.

Midgeley, D.C., Pitman, W.V. and Middleton B.J. 1994. Surface Water Resources of South Africa. Water Research Commission Report, 298/3.1/94.

Miller, W.R. 1979. Application of hydrogeochemistry to the search for base metals. In: Peter J. Hood, (editor). Geophysics and Geochemistry in the Search for Metallic Ores.Geological Survey of Canada, Economic Geology Report, 31: 479–487.

Misra, A., Pande, D., Kumar, K.R., Nanda, L.K., Maithani, P.B. and Chaki, A., 2011. Calcrete-hosted surficial uranium occurrence in playa-lake environment at Lachhri, Nagaur District, Rajasthan, India. Current. Science. 101(1): 84–88.

Mucina, L., Rutherford, M. and Powrie, L. (editors.). 2005. Vegetation map of South Africa, Lesotho and Swaziland, 1:1 000 000 Scale Sheet Maps. South African National Biodiversity Institute, Pretoria.

Murphy, W. M. and Shock, E. L. 1999. Environmental aqueous geochemistry of actinides. *In*: (P.C. Burns and R. Finch, editors). Uranium: mineralogy, geochemistry and the environment, 38: 221–254, USA, Mineralogical Society of America.

Nakwafila, A.N. 2015. Salinisation source(s) and mechanism(s) in shallow alluvial aquifers along the Buffels River, Northern Cape Province, South Africa. MSc thesis. Stellenbosch University, Cape Town.

Nell, J.P. and Van Huyssteen, C.W. 2014. Geology and groundwater regions to quantify primary salinity, sodicity and alkalinity in South African soils. South African Journal of Plant and Soil, 31(3): 127–135

Nencetti, A., Tassi, F., Vaselli, O., Macías, J.L., Magro, G., Capaccioni, B., Minissale, A. and Mora, J.C. 2005. Chemical and isotopic study of thermal springs and gas discharges from Sierra de Chiapas, Mexico. Geofisica International, 44(1): 39–48.

Nriagu, J.O., Bhattacharya, P., Mukherjee, A.B., Bundschuh, J., Zevenhove, R. and Loeppert, R.H. 2007. Arsenic in soil and groundwater: an overview. *In*: Arsenic in Soil and Groundwater Environment: Biogeochemical Interactions, Health Effects and Remediation, Trace Metals and Other Contaminants in the Environment. Elsevier, Amsterdam, 9: 3–60.

Olivier, J., and Van Heerden, J. 1999. The South African fog water collection project. WRC Report, 671/1/99.

Parkhurst, D.L. and Appelo, C.A.J. 2013. Description of input and examples for PHREEQC version 3—a computer program for speciation, batchreaction, one-dimensional transport, and inverse geochemical calculations. US Geological Survey Techniques and Methods, 6, chap. A43:497.

Partridge, T.C. and Maud, R.R. 1987. Geomorphic evolution of Southern Africa since the Mesozoic. South African Journal of Geology, 90: 179–208.

Pietersen, K., Titus, R. and Cobbing, J. 2009. Effective Groundwater Management in Namaqualand: Sustaining Supplies. Report, Water Research Commission, TT 418/09.

Portugal, E., Álvarez, J. and Romero, B.I. 2006. Hydrochemical and isotopical tracers in the lacustrine aquifer of the Cerro Prieto area, Baja Califonia, México. Journal of Geochemical Exploration, 88: 139–143.

Pretorius, D.A. 1976. The nature of the Witwatersrand gold-uranium deposits. *In*: K.H. Wolf (editor). Handbook of Strata-bound and Stratiform Ore Deposits, 7. Elsevier, Amsterdam: 29–88.

Rabemanana, V., Violette, S., De Marsily, G., Robain, H., Deffontaines, B., Andrieux, P., Bensimon, M. and Parriaux, A. 2005. Origin of the high variability of water mineral content in the bedrock aquifer of Southern Madagascar. Journal of Hydrology, 301: 143–156.

Rail, C.D. 1989. Groundwater Contamination: Sources, Control, and Preventive Measures, Technomic, Lancaster, PA:139.

Raith, J.G., Cornell, D.H., Frimmel, H.E. and De Beer, C.H. 2003. New insight into the geology of the Namaqua Tectonic Province, South Africa, from Ion Probe dating of detrital and metamorphic zircon. The Journal of Geology, III(3): 347–366.

Ramesh, K. and Elango, L. 2012. Groundwater quality and its suitability for domestic and agricultural use in Tondiar River basin, Tamil Nadu, India, Environmental monitoring and assessment, 184(6): 3887–3899.

Ranalli, A.J. and Yager, D.B. 2016. Use of mineral/solution equilibrium calculations to assess the potential for carnotite precipitation from groundwater in the Texas Panhandle, USA. Applied Geochemistry, 73(2016): 118–131.

Ribera D., Labrot, F., Tisnerat, G. and Narbonne, J.F. 1996. Uranium in the environment: occurrence, transfer and biological effects. Rev. Environ. Cont. Toxicology, 146: 53–80.

Richards, D.J.1975. Preliminary report on pan mineralization from airborne radiometric surveys, NW Cape Province, South Africa, Department of Mines, Geological Survey Open-File Report, 6.

Robb, L.J., Armstrong, R.A. and Waters, D.J. 1999. The History of Granulite-Facies Metamorphism and Crustal Growth from Single Zircon U–Pb Geochronology: Namaqualand, South Africa. Journal of Petrology, 40: 1747–1770.

Robin, N.S. 2002. Groundwater quality in Scotland: major ion chemistry of the key groundwater bodies. Sci Total Environ 294: 48– 49.

Rutherford, M.C., Westfall, R.H. Leistner, O.A., the Botanical Research Institute (South Africa) and the Dept. of Agriculture and Water Supply. 1986. Biomes of Southern Africa: an objective categorization. Botanical Research Institute, Pretoria, South Africa.

SABS (South African Bureau of Standards). 2016. SABS Water-Check Group, 3, Final report, F5.9-04 Y(3), 26 April 2016: 47.

SABS (South African Bureau of Standards). 2017. SABS Water-Check scheme Group 1, January 2017, Final Report, F5.9-04 Y(1), 22 February 2017: 25.

Stettler, E.H. and Cole, D.I. 1984. Karoo airbone geophysical survey: Report on aerial radiometric anomalies of block 3: Open-file Report, Geological Survey of South Africa, 292: 21.

Slabbert, M.J., Moen, H.F.G. and Boelema, R. 1999. The geology of the Kenhardt area, Explanation of Sheet 2920 scale 1:250 000 Council for Geoscience, Geological Survey, South. Africa.

Sinclair, A.J. and Blackwell, G.H., 2002. Applied mineral inventory estimation. Cambridge, Cambridge University Press: 381.

South African Weather Services, 2017. Namaqualand Annual Rainfall data.

Tankard, A.J., Jackson, M.P., Eriksson, K.A., Hobday, D.K., Hunter, D.R. and Minter, W.E.L. 1982. Crustal Evolution of South Africa: 3.8 Billion Years of Earth History. Springer-Verlag, New York.

Theart, H.F.J. 1980. The geology of the Precambrian terrane in parts of western Namaqualand. Bulletin 30, Precambrian Research Unit. Department of Geology, University of Cape Town.

Titus, R. 2003. Hydrogeochemical characteristics of the basement aquifers in Namaqualand. P.hD. Thesis, University of the Western Cape.

Titus, R., Xu, Y., Adams, S. and Beekman, H. 2009. A tectonic and geomorphic framework for the development of basement aquifers of Namaqualand — A Review. *In*: Titus R., Beekman R., Adams, S. and Strachan, L. (Editors). "The Basement Aquifers of Southern Africa". WRC Report, TT 428/09. ISBN 978-1-77005-898-9.

Toens, P.D. and Hambleton-Jones, B.B. 1984. Surficial Uranium deposits, IAEA, Vienna.

Toens and Partners. 1998. The association of groundwater chemistry and geology with atypical lymphocytes (as a biological indicator) in the Pofadder area, North Western Cape, South Africa. Consultants report to Water Research Commission, South Africa.

Tooth, S. 2000. Process, form and change in dryland rivers: a review of recent research. Earth-Science Reviews, 51: 67–107.

Treasure, P.A. 1977. A ground investigation of some uranium anomalies in the Kenhardt area (20/74). Report, Geological Survey of South Africa, 1977-0035: 6.

Van der Merwe, P.J. 1986. Uranium prospecting in the main Karoo Basin in retrospect. Historical re view, summary of exploration statistics and resource estimates on a company-by-company basis and economic viability of the main Karoo Basin. At. En. Corp. S. Afr., Pretoria, PER-147, 1: 121.

Van der Sommen, J.J., and Geirnaert, W. 1988. On the continuity of aquifer systems on the crystalline basement of Burkina Faso. *In*: I. Simmers (editor). Estimation of Natural Groundwater Recharge: 29–45. D. Reidel Publishing Company.

Visser, D.J.L. (editor). 1989. Explanation of the 1:1.000.000 Geological Map, Fourth Edition. Department of Mineral and Energy Affairs, Government Printer, ISBN 0-621-12516-4.

Weaver, J.M.C., Cave, L. and Talma, A.S. 2007. Groundwater sampling: a comprehensive guide for sampling methods. Second Edition. Water Research Commission, Report, TT 303/07, Republic of South Africa.

Webley, L. 2007. Archaeological evidence for pastoralist land-use and settlement in Namaqualand over the last 2000 years. Journal of Arid Environments, 70: 629–640.

WHO (World Health Organization). 1998. Guidelines for drinking water quality. Addendum to vol. 2: Health criteria and other supporting information. WHO/EOS/98.1, Geneva.

WHO (World Health Organization). 2011. Water and sanitation. Guidelines for drinking-water quality.

Wick, K., Heumesser, C. and Schmid, E. 2012. Groundwater nitrate contamination: Factors and indicators. Journal of Environmental Management. 111(3): 178–186.

10 APPENDICES

The appendices below show data that was used in compiling the thesis. Appendix 1 represents the field measured parameters (Eh, EC, TDS, salinity, temperature and DO). Appendix 2 and 3 represents the major and trace element results analysed by Inductively Coupled Plasma Mass Spectrometry (ICP- MS) at the Council for Geoscience Laboratory. Major ionic species were analysed using a discrete analyser and the results are displayed in Appendix 4. Appendix 5 represents results of calcium carbonate analysed using an Autotitrator Potentiometry. Appendix 1,2,3,4 and 5 helped in understanding the hydrochemistry and the processes driving the evolution of groundwater in the Namaqualand. Appendix 6 represents the CSI results calculated using uranium, vanadium, potassium and bicarbonates values.

10.1 Appendix 1 Field parameters of the groundwater samples in the study area

Samples	Temperature (˚C)	pH	EC (mS/cm)	TDS (mg/L)	Salinity (g/L)	Eh (Volts)	DO (mg/L)
SM001	20.8	7.33	3.7	2520	2.55	0.12	3.5
SM002	19.2	7.43	5.59	3960	3.1	0.17	5.26
SM003	19.5	7.13	9.06	6320	5.09	0.17	2.64
SM004	22.5	7.4	7.5	5310	4.21	0.18	4.71
SM005	13.8	8.42	4.02	2630	2.24	0.18	10.45
SM006	12.8	7.35	4.26	2960	2.31	0.24	8.21
SM007	15.1	7.46	4.05	2830	2.04	0.24	7.9
SM008	19.5	7.53	3.66	2530	1.93	0.06	2.68
SM009	20.7	7.27	2.96	2050	1.55	0.16	4.3
SM010	16.8	7.44	2.57	1760	1.28	0.19	6.26
SM011	26.8	7.57	4.56	3120	2.4	0.11	6.48
SM013	22.8	7.5	3.65	2520	1.91	0.22	4.46
SM014	16.1	8.56	3.04	2090	1.52	0.21	9.78
SM015	22.7	7.29	4.75	3220	2.46	0.22	2.95
SM016	21.7	7.51	5.62	3960	3.06	0.22	7.34
SM017	21.7	7.4	2.45	1740	1.25	0.25	3.5
SM018	16.6	7.46	3.39	2350	1.72	0.22	5.45
SM019	17.7	7.61	1.98	1385	1	0.22	8.81
SM020	19.1	7.18	3.85	2560	1.96	0.21	3.73
SM021	18.4	7.3	3.36	2280	1.81	0.22	3.18
SM022	22.1	7.35	3.46	2400	1.83	0.22	2.02
SM023	17.3	7.58	2.3	1610	1.17	0.24	5.8
SM024	22.2	7.32	3.46	2420	1.84	0.22	5.95
SM025	10.6	8.12	8.39	6020	4.77	0.2	8.61
SM025A	19.2	7.37	9.25	6500	5.14	0.19	4.28
SM026	14.6	7.53	4.02	2800	2.16	0.19	2.81
SM027	16.9	7.27	9.79	1992	1.4	0.19	3.14
SM028	20.2	7.75	3.61	2530	1.92	0.21	5.88
SM029	16.8	7.62	1.21	849	0.61	0.23	8.1
SM030	14.7	8.01	7.49	5250	4.13	0.22	8.06
SM031	18	7.87	0.22	1306	7.83	0.22	7.87
SM032	9.7	7.84	4.84			0.21	8.59
SM033	20.9	7.55	3.52	2480	1.94	0.2	3.61
SM034	13.3	8.08	2.35	4440	3.07	0.21	10.04
SM035	21.9	7.2	14.43	9980	8.28	0.21	14.43
SM036	21.8	7.36	3.46	2460	1.77	0.21	3.12
SM037	22.2	7.34	7.59	5320	4.26	0.22	3.2
SM038	16.1	7.36	4.05	2820	2.13	0.2	4.27
SM039	25.5	7.68	0.75	542	0.375	0.22	4.78
SM040	24.8	7.65	2.09	1450	1.07	0.23	2.9
SM041	22.9	7.94	1.44	1015	0.71	0.23	4.22
SM042	13.6	7.58	4.57	3220	2.5	0.11	2.23
SM043	14.2	8.32	1.37	935	0.68	0.23	3.47
SM044	13.8	8.43	0.48	315	0.22	0.25	3.96
SM045	26	7.22	1.64	1126	0.81	0.24	1.45
SM046	24.9	7.33	3.41	2330	1.62	0.24	1.68
SM047	27.3	7.59	3.13	2280	1.6	0.24	1.84
SM048	25.6	8.31	1.28	917	0.671	0.23	2.19
SM049	27.6	7.98	1.59	1103	0.8	0.24	2.31

Samples	Temperature (˚C)	pH	EC (mS/cm)	TDS (mg/L)	Salinity (g/L)	Eh (Volts)	DO (mg/L)
SM050	9.7	8.38	0.77	538	0.37	0.26	2.63
SM051	8.6	8.31	0.73	500	0.35	0.25	2.1
SM052	7.3	8.91	0.93	649	0.45	0.26	1.26
SM053	19.1	7.72	1.14	800	0.56	0.25	0.61
SM054	17.5	7.75	0.97	642	0.45	0.25	0.88
SM055	11.5	8.26	0.72	532	0.34	0.28	0.9
SM056	15.8	7.91	0.84	592	0.43	0.25	1.2
SM057	18.2	7.76	2.06	1500	1.06	0.21	0.51
SM058	19	7.38	2.62	1750	1.24	0.22	-
SM059	13.9	7.81	0.53	394	0.25	0.19	-
SM060	16.6	7.49	0.53	1127	0.78	0.21	8.3
SM061	18	7.19	2.01	2680	2.68	0.2	0.36
SM062	16.1	8.05	3.72	2700	2.1	0.22	2.06
SM063	25	7.46	3.25	2350	1.68	0.18	1.45
SM064	21.5	7.52	1.02	704	0.5	0.21	1.18
SM065	21	7.27	2.33	1620	1.19	0.19	1.01
SM066	22	7.64	7.17	5010	3.92	0.21	0.96
SM067	16.7	8.72	1.99	1540	1.04	0.21	8.14
SM068	9.1	8.12	3.26	2260	1.69	0.17	0.37
SM069	13.9	7.79	1.41	984	0.71	0.17	6.7
SM070	11.6	8.05	1.39	976	0.7	0.18	3.23
SM071	21.3	7.42	2.52	1800	1.26	0.17	1.43
SM072	17.7	7.36	3.81	2630	2	0.13	1.82
SM073	20.9	7.58	3.19	2230	1.72	0.17	0.6
SM074	19.4	7.78	3.63	2510	1.91	0.15	2.23
SM075	17.5	7.93	3.78	2610	1.83	0.16	2.03
SM076	17.9	7.35	3.15	2240	1.71	0.19	2.35
SM077	17.8	7.51	3.18	2240	1.68	0.18	4.11
SM078	18.5	7.57	3.63	2270	1.73	0.19	1.84
SM079	19.8	7.61	2.77	2060	1.41	0.18	5.44
SM080	20.1	7.52	3.57	2500	1.93	0.18	2.82
SM081	19.5	7.34	6.86	4830	3.83	0.14	1.69
SM082	16.4	7.92	3.79	2560	1.99	0.18	9.99
SM083	9.8	8.73	6.75	4690	3.69	0.18	3.6
SM084	11.6	8.22	4.3	2910	2.29	0.19	3.37
SM085	14.7	7.6	4.93	3510	2.64	0.19	6.44

10.2 Appendix 2: major element results analysed by inductively coupled plasma mass spectrometry (ICP- MS) major ion analyses results (ppb)

Samples	Na	Mg	Al		K	Ca	Fe
SM001	593236	14260	86		7959	136315	672
SM004	556552	14017	85		4900	284168	1328
SM005	761678	71549	89		18679	230027	1939
SM006	1160146	62008	82		15997	514303	1112
SM007	832387	39163	83		13609	358539	1378
SM008	836875	37558	97		13422	341358	11628
SM009	387408	64469	82		17028	177065	781
SM010	332587	75129	627		15286	223891	965
SM011	1449495	57878	83		17955	431881	1734
SM012	1221630	16027	250		5026	86429	399
SM013	1513146	32694	119		15702	326410	1512
SM014	1435683	42984	118		19962	371815	1720
SM015	1062590	28928	136		12853	306008	1465
SM016	620890	111110	118		35167	468456	2334
SM017	393722	51253	119		16783	163886	789
SM018	787339	62084	124		10784	274227	1229
SM019	356216	29221	117		10516	153324	721
SM020	590387	99249	117		25980	381553	1826
SM021	581720	59983	143		10816	261937	1256
SM022	365995	100502	117		14235	329607	1679
SM023	430390	29767	179		11125	191027	979
SM024	666613	40149	97		13298	280070	1409
SM025	2627610	79663	96		25956	602963	2797
SM026	1190720	78022	95		10679	234457	1398
SM027	1318516	43310	199		13359	227827	1265
SM028	564364	135827	94		5936	200481	1239
SM029	125832	33992	94		2331	155942	901
SM030	2214117	49762	99		27764	523749	2664
SM031	944048	84355	100		23678	379576	2169
SM032	12802712	328830	151		92710	926238	5 469
SM033	692109	23540	106		15677	125840	737
SM034	936834	36550	94		22361	186762	1129
SM035	3668061	153856	94		37820	724968	3882
SM036	1286073	124880	93		17697	316652	1900
SM037	1984649	165522	93		24047	501083	3761
SM038	1667487	77181	92		18254	309143	1938

Samples	Na	Mg	Al	K	Ca	Fe
SM039	117134	21397	93	4197	65121	457
SM040	296214	40335	91	7029	116358	994
SM041	179391	25355	100	6408	136123	931
SM042	1420427	95265	94	31740	412601	2727
SM043	180597	28384	91	7326	101661	694
SM044	84375	23570	92	3657	73254	496
SM045	300724	33467	92	14452	71246	538
SM046	1075583	111975	91	25959	461167	2984
SM047	496017	61902	95	11043	220056	1572
SM048	153065	43053	99	9045	117797	797
SM049	318943	21003	94	12110	48544	402
SM050	116262	37817	301	3241	112180	799
SM051	113046	33894	274	3247	104276	691
SM052	151243	49270	92	4739	91658	632
SM053	231600	20120	104	3189	76273	541
SM054	148277	20855	96	2903	86532	632
SM055	200271	15551	16 473	5599	51280	<23.9
SM056	99905	22398	91	4571	68402	621
SM057	315418	54570	91	11092	136179	1011
SM058	983142	124421	92	50849	429267	3174
SM059	109179	21371	91	3689	63523	500
SM060	195008	22888	91	4033	94861	745
SM061	721179	121962	100	32460	352440	2430
SM062	701932	76746	107	23511	223881	1593
SM063	787568	101714	132	27049	281287	2628
SM064	130298	34925	127	5620	98719	821
SM065	316145	71292	125	14682	142997	1209
SM066	1871625	194821	123	77851	352745	2855
SM067	415879	74005	125	21061	57872	527
SM068	1406090	208238	134	38762	401021	3010
SM069	178093	60982	122	18231	123571	1039
SM070	179503	61131	122	18744	125349	1037
SM071	1101818	90065	124	23531	378838	3652
SM072	798589	106294	122	23048	294484	6952
SM073	481917	48737	154	28761	156134	1279
SM074	725602	57848	138	20591	188733	1705
SM075	770002	127859	147	32458	271833	2315
SM076	445056	69756	135	26207	183673	1728
SM077	620044	43134	134	19450	123866	1067
SM078	509233	93892	136	23276	188024	1782
SM079	493888	49843	151	31362	124283	1228
SM080	654372	81018	134	25711	217565	3071
SM081	1459818	242703	136	76209	763415	6131
SM082	621605	70358	135	32366	207730	1721

Samples	Na	Mg	Al	K	Ca	Fe
SM083	535795	89062	138	37817	210593	1977
SM084	488932	81012	134	33024	204041	1910
SM085	653606	82879	131	27566	267543	2330
SM025A	2585446	76168	151	30233	569019	4920
SM002	894594	66819	131	26515	272803	2479
SM003	1573628	70923	131	24138	410952	4031

10.3 Appendix 3: Trace elements analysed by inductively coupled plasma mass spectrometry (ICP-MS)

(All values in ppb)

Samples	Li	Be	B	V	Cr	Mn	Co	Ni	Cu	Zn	Ga	As	Se	Rb	Sr	Mo	Ag	Cd	Te	Ba	Tl	Pb	Bi	U
SM001	122,1	48,3	820,3	14,0	6,4	3,7	2,8	8,6	6,4	25,5	2,4	22,57	48,97	4,25	1917,19	74,85	5,29	2,06	1,63	10,90	0,64	<0.06	0,72	162,52
SM004	94,8	48,3	687,0	11,7	2,7	3,2	3,0	14,5	5,7	37,3	2,3	22,99	48,88	3,71	3412,99	21,96	4,72	1,87	1,49	5,33	0,64	<0.06	0,72	40,45
SM005	212,5	48,3	1417,0	22,1	4,1	4,5	3,2	19,9	9,6	30,5	2,5	28,59	90,84	6,41	5408,72	42,63	5,11	1,98	1,94	16,57	0,64	<0.06	0,72	174,54
SM006	176,2	48,3	1274,0	19,4	4,4	6,0	3,0	12,1	7,9	64,2	2,5	25,33	84,58	20,52	3285,32	47,85	4,41	1,98	4,39	18,95	0,64	<0.06	0,72	337,13
SM007	161,3	48,3	1100,0	19,7	4,4	3,8	3,0	15,1	8,7	43,4	2,5	25,51	72,40	10,93	3744,48	39,88	4,33	1,94	2,01	17,18	0,64	<0.06	0,72	106,25
SM008	150,6	48,3	843,0	15,8	3,5	158,4	3,2	15,2	18,2	324,1	2,4	24,36	75,87	10,31	3535,97	46,62	4,25	1,97	2,36	12,75	0,63	<0.06	0,72	75,33
SM009	85,1	48,5	884,2	13,8	4,9	4,3	2,8	9,7	5,3	59,1	2,8	22,40	63,12	4,53	2267,63	13,88	4,01	1,84	1,80	32,26	0,64	<0.06	0,72	87,80
SM010	67,9	48,3	762,6	20,0	5,1	6,2	2,9	12,0	4,4	158,1	2,9	23,31	70,68	13,14	2449,47	18,93	4,03	1,87	1,65	36,80	0,64	<0.06	0,71	267,09
SM011	229,2	49,3	1551,6	38,1	4,4	10,8	3,2	20,5	12,7	137,0	2,6	31,93	111,42	64,70	5358,99	47,08	4,54	2,06	2,08	21,17	0,64	<0.06	0,72	73,15
SM012	40,5	48,3	628,8	11,5	8,1	4,0	2,6	6,1	4,1	567,0	3,2	21,37	36,55	2,86	1022,86	39,24	3,94	1,97	1,54	53,17	0,64	<0.06	0,72	119,58
SM013	322,6	23,3	1444,0	23,4	3,4	2,6	2,0	17,1	10,4	61,0	1,8	28,56	95,23	82,27	4445,03	51,03	6,32	1,57	2,35	12,81	1,47	<0.06	1,50	59,25
SM014	415,4	23,2	1722,7	28,4	4,2	2,2	2,1	18,4	13,6	59,1	1,8	30,93	116,01	108,63	5418,98	66,68	5,44	1,62	2,94	12,20	1,47	<0.06	1,49	81,82
SM015	288,7	23,2	1237,3	24,0	3,0	2,0	2,0	15,8	9,8	62,5	1,7	28,01	83,81	52,60	4148,06	41,50	4,76	1,54	2,24	8,16	1,45	<0.06	1,49	56,34
SM016	259,9	23,2	2084,8	34,5	4,0	26,9	2,6	25,6	14,7	1900,7	1,8	35,03	140,91	60,44	6455,71	40,52	5,04	1,69	2,57	9,76	1,48	<0.06	1,49	93,42
SM017	138,5	23,3	1224,3	14,3	7,4	5,6	1,7	9,8	4,7	851,8	2,0	22,10	54,32	2,90	2058,39	37,92	4,34	1,52	2,68	20,48	1,45	<0.06	1,49	148,93
SM018	167,1	23,3	2023,1	18,1	6,7	2,1	1,9	14,3	6,8	45,4	1,9	23,98	74,40	5,78	3127,97	82,93	4,36	1,79	2,82	19,89	1,45	<0.06	1,49	100,32
SM019	132,7	23,2	796,4	11,4	5,4	2,2	1,7	8,8	4,2	79,6	1,9	21,83	51,45	6,09	1774,92	68,89	4,33	1,67	2,08	20,67	1,44	<0.06	1,49	56,06
SM020	240,2	23,2	2915,3	30,1	9,4	10,2	2,2	21,4	13,8	49,6	2,1	28,48	101,31	3,32	5051,71	46,92	4,48	2,25	3,57	29,26	1,45	0,12	1,49	261,76
SM021	162,7	23,3	2010,1	18,7	5,3	2,5	1,9	14,4	6,6	43,1	1,9	24,31	72,93	5,82	2979,84	81,22	4,39	1,78	2,86	20,03	1,45	<0.06	1,49	99,11
SM022	115,5	23,4	953,7	16,5	5,1	3,9	2,1	18,6	4,2	670,0	2,1	25,75	87,85	8,98	3635,23	20,69	4,43	1,47	2,11	30,59	1,45	<0.06	1,49	169,67
SM023	244,5	23,0	939,2	15,6	3,5	2,4	2,1	13,2	9,9	1138,5	2,4	20,50	48,34	5,09	3362,65	59,18	4,40	2,64	3,01	21,89	1,45	1,04	1,41	257,31

Samples	Li	Be	B	V	Cr	Mn	Co	Ni	Cu	Zn	Ga	As	Se	Rb	Sr	Mo	Ag	Cd	Te	Ba	Tl	Pb	Bi	U
SM024	329,9	23,0	1237,2	18,1	3,8	2,8	2,3	16,3	6,9	50,3	2,4	22,53	67,53	2,82	4731,68	57,82	4,39	1,82	2,73	25,16	1,45	0,22	1,41	298,96
SM025	616,0	23,0	2419,0	58,6	4,9	4,0	2,8	31,3	25,7	39,3	2,3	49,27	166,00	40,05	8964,62	53,11	4,64	1,82	5,16	16,13	1,46	0,17	1,42	160,16
SM026	253,2	23,0	1430,1	32,9	4,7	5,8	2,3	15,5	17,4	42,9	2,3	31,96	82,61	46,70	3888,75	17,75	4,44	1,69	2,86	17,45	1,45	0,13	1,41	35,50
SM027	291,5	23,0	1561,6	32,2	5,4	10,8	2,2	15,9	13,2	198,6	2,1	31,07	83,49	47,17	3351,58	26,98	4,42	1,72	2,68	6,10	1,47	0,11	1,41	61,17
SM028	110,2	22,9	1697,7	20,6	6,0	18,2	2,4	14,8	22,4	171,2	2,2	24,89	86,78	8,60	3204,20	6,92	4,40	1,66	2,70	16,21	1,46	0,11	1,41	14,04
SM029	47,8	22,9	363,7	44,7	7,2	2,5	2,1	17,9	11,4	327,2	2,9	20,60	33,24	2,82	1270,07	3,35	4,37	2,21	1,90	48,43	1,46	0,52	1,41	6,64
SM030	660,8	23,1	1942,6	54,5	5,3	4,5	2,8	29,3	23,0	68,2	2,3	48,06	155,78	52,33	7088,15	62,34	4,58	2,03	3,68	19,34	1,47	0,11	1,41	99,35
SM031	252,3	23,0	1522,4	30,3	5,6	2,1	2,5	24,3	23,4	46,8	2,3	31,95	121,77	13,17	5405,99	24,10	4,50	1,73	3,23	18,33	1,45	0,77	1,41	177,20
SM032	3096,6	23,1	5035,4	210,7	14,9	15,2	4,3	63,9	123,1	23,8	3,0	169,96	536,50	100,06	21628,55	32,92	5,73	1,79	9,77	52,88	1,47	0,12	1,43	98,42
SM033	178,8	15,4	926,0	30,7	6,4	1,9	1,6	9,9	11,0	64,7	1,6	26,54	51,66	3,55	1540,15	24,29	5,57	1,58	1,98	12,10	1,39	0,36	1,28	50,61
SM034	253,8	15,5	1118,1	26,7	4,0	2,1	1,7	13,7	10,6	442,8	1,5	29,31	68,37	5,47	2637,58	22,34	5,66	1,47	2,58	4,09	1,38	<0.06	1,28	75,69
SM035	906,3	15,7	3280,1	96,7	8,0	2,2	2,9	44,9	43,6	25,1	1,8	73,36	254,85	82,80	12090,99	48,06	7,05	1,61	7,64	24,87	1,49	<0.06	1,28	181,27
SM036	225,6	15,5	2096,1	36,6	6,0	13,2	2,1	21,6	18,0	886,4	1,8	34,38	130,00	13,05	4780,44	21,06	5,28	1,49	4,77	18,01	1,38	<0.06	1,28	73,53
SM037	406,3	15,6	2218,0	58,3	6,2	19,1	2,7	35,7	23,3	238,3	1,8	50,69	159,62	56,80	7816,62	20,70	5,45	1,54	3,59	23,31	1,47	<0.06	1,28	93,14
SM038	329,2	15,5	2282,4	56,3	5,7	4,4	2,0	22,8	19,6	177,4	1,8	39,06	121,86	5,35	4410,52	54,47	5,31	1,61	3,72	20,10	1,38	<0.06	1,28	108,00
SM039	9,8	15,4	155,5	9,4	2,5	11,0	1,4	7,2	2,2	159,1	2,6	19,79	29,46	3,10	507,27	2,84	5,11	1,40	1,76	61,00	1,38	<0.06	1,28	5,11
SM040	25,7	15,5	306,1	15,2	3,0	13,1	1,6	10,1	3,7	146,5	2,6	23,23	48,72	4,89	1073,35	3,33	5,14	1,39	1,89	62,17	1,38	<0.06	1,28	10,13
SM041	17,1	15,4	191,8	11,1	2,3	15,9	1,7	11,1	2,5	52,7	3,4	21,05	39,20	4,16	1367,73	4,30	5,15	1,38	1,74	108,14	1,38	<0.06	1,28	8,59
SM042	292,3	15,5	1322,0	51,9	6,8	13,1	2,8	30,3	14,2	37,1	1,9	44,79	155,14	48,61	5573,65	21,00	5,39	1,46	2,74	27,40	1,38	<0.06	1,28	39,96
SM043	77,0	15,5	318,7	7,2	2,4	1,5	1,5	8,4	3,0	26,0	1,8	19,83	37,70	20,21	661,63	7,45	5,11	1,40	1,82	19,31	1,38	<0.06	1,28	85,49
SM044	41,9	15,4	207,3	13,9	2,9	1,6	1,4	6,5	2,0	99,8	2,3	18,83	52,77	4,85	444,20	2,91	5,11	1,42	1,70	49,36	1,38	<0.06	1,28	100,75
SM045	253,2	15,4	349,6	5,7	2,3	209,7	1,4	6,6	3,6	35,5	1,6	19,22	31,64	66,50	313,29	2,71	5,12	1,45	1,75	10,42	1,38	<0.06	1,28	1,82
SM046	173,3	15,6	1238,7	35,1	5,3	2,5	2,4	34,2	10,3	23,2	1,7	37,67	143,01	25,55	4809,47	50,57	5,29	1,62	3,29	19,55	1,38	<0.06	1,28	346,54

Samples	Li	Be	B	V	Cr	Mn	Co	Ni	Cu	Zn	Ga	As	Se	Rb	Sr	Mo	Ag	Cd	Te	Ba	Tl	Pb	Bi	U
SM047	122,5	15,5	764,7	14,9	3,8	8,5	1,8	19,2	6,5	27,0	1,5	24,06	64,09	20,60	1444,33	34,29	5,14	1,71	2,70	3,98	1,38	<0.06	1,28	236,07
SM048	67,7	15,4	247,6	9,5	3,5	4,6	1,6	15,1	4,3	307,6	2,4	19,94	32,17	8,44	470,41	31,13	5,12	1,62	1,82	51,84	1,38	<0.06	1,28	150,89
SM049	49,7	15,4	601,4	13,2	3,5	3,7	1,4	5,3	3,3	21,9	2,2	21,19	45,65	7,80	818,35	10,01	5,13	1,41	2,15	42,72	1,38	<0.06	1,28	13,92
SM050	70,0	15,4	346,5	3,8	3,0	6,1	1,5	10,7	2,1	28,9	1,5	18,42	28,19	6,95	465,83	5,68	5,11	1,38	1,92	4,82	1,51	<0.06	1,28	46,81
SM051	65,1	15,4	271,5	5,3	3,7	2,1	1,5	9,2	3,3	53,8	1,6	18,52	28,61	4,58	434,44	13,47	5,11	1,42	1,79	11,51	1,43	<0.06	1,28	49,96
SM052	93,2	15,4	351,4	7,1	3,6	2,4	1,5	8,3	3,8	10,2	1,8	19,49	33,28	6,01	531,50	15,48	5,12	1,43	1,70	21,20	1,43	<0.06	1,28	65,13
SM053	78,8	15,0	625,3	24,3	4,5	1,3	1,6	7,8	3,1	25,8	1,6	19,85	30,89	1,71	626,62	16,38	5,66	1,36	2,12	17,37	1,22	<0.06	1,27	69,01
SM054	84,5	15,1	291,6	7,1	2,0	10,8	1,7	9,0	2,3	240,8	1,2	19,49	28,13	2,83	361,36	24,78	5,36	1,41	1,40	<0.31	1,22	<0.06	1,26	175,97
SM055	<0.22	53,5	15,0	55403,5	7,3	3,0	389,1	1,5	5,9	<3.6	8,8	1,83	19,21	25,69	6,31	370,66	19,15	5,11	<0.04	1,55	<0.06	1,22	<0.01	1,27
SM056	63,5	14,9	340,8	6,4	3,7	4,2	1,7	8,6	2,0	163,1	1,3	19,56	29,07	2,17	536,91	11,76	5,08	1,36	1,52	2,39	1,22	<0.06	1,26	68,38
SM057	128,6	15,0	830,4	12,6	3,8	2,3	1,8	12,8	3,4	73,6	1,7	22,85	61,03	18,51	1082,03	64,10	5,43	2,00	1,89	23,04	1,29	<0.06	1,27	5123,36
SM058	194,5	15,0	2017,6	44,1	5,6	3,0	2,7	37,0	9,3	53,2	2,1	40,67	141,44	8,27	4795,89	15,04	6,38	1,37	2,91	47,16	1,22	<0.06	1,27	68,42
SM059	40,3	15,0	333,9	7,8	2,8	1,9	1,6	7,0	2,6	86,6	1,3	19,95	28,21	1,74	457,54	16,04	4,77	1,37	1,56	3,60	1,22	<0.06	1,27	17,79
SM060	24,1	15,0	242,4	10,7	3,8	10,5	1,8	12,3	3,7	686,1	2,5	20,94	34,76	1,86	581,20	8,30	4,80	1,38	1,51	61,76	1,22	<0.06	1,27	48,45
SM061	105,2	15,0	1397,5	32,7	6,3	2,0	2,5	31,7	6,9	12,4	1,7	32,72	117,56	9,75	3631,29	7,36	5,22	1,33	2,15	23,83	1,22	<0.06	1,27	46,91
SM062	108,8	14,9	1480,3	24,3	4,6	1,6	2,0	19,1	6,7	340,0	1,6	29,07	105,90	9,52	2594,09	21,31	4,97	1,40	2,60	14,28	1,22	<0.06	1,27	47,60
SM063	133,5	22,9	1979,8	29,0	5,0	81,1	3,4	33,5	10,3	1241,4	2,3	32,47	136,72	8,58	3535,12	18,16	6,02	1,74	3,51	17,04	1,58	0,39	1,67	31,11
SM064	68,0	23,0	490,7	8,6	4,8	4,3	2,3	12,0	2,9	88,6	2,2	22,14	38,43	1,80	755,19	14,01	4,78	1,69	2,20	10,69	1,58	<0.06	1,66	81,16
SM065	86,9	23,1	943,4	22,7	4,8	2,3	2,3	16,7	5,4	17,6	2,5	25,58	75,22	10,23	1558,06	16,88	4,94	1,79	2,64	29,05	1,58	<0.06	1,66	175,75
SM066	203,1	23,0	3598,9	80,5	15,0	3,7	3,1	38,6	22,7	15,8	2,6	59,28	271,86	26,83	6617,33	21,76	6,60	1,72	4,54	34,70	1,58	0,17	1,67	95,30
SM067	162,8	23,0	1380,5	18,4	6,9	2,5	2,1	10,0	7,0	9,9	2,1	26,16	60,96	27,26	1077,55	34,41	4,79	1,77	2,98	5,67	1,58	<0.06	1,66	182,30
SM068	297,5	22,9	1611,3	61,9	6,9	42,4	3,4	37,4	15,5	568,4	2,7	54,70	189,35	20,65	5345,21	12,84	5,43	2,18	3,87	41,07	1,58	<0.06	1,67	54,50
SM069	111,5	23,0	443,0	12,8	3,7	4,4	2,2	16,3	3,1	1430,9	2,3	24,53	41,38	23,87	482,37	4,63	4,71	1,69	2,96	17,46	1,59	<0.06	1,67	32,22

Samples	Li	Be	B	V	Cr	Mn	Co	Ni	Cu	Zn	Ga	As	Se	Rb	Sr	Mo	Ag	Cd	Te	Ba	Tl	Pb	Bi	U
SM070	114,1	23,0	439,1	11,3	3,7	60,9	2,5	16,7	3,4	1497,7	2,3	23,63	40,51	23,90	467,83	4,52	4,70	1,67	2,68	17,38	1,59	<0.06	1,66	31,55
SM071	191,9	23,1	1203,9	42,1	5,8	20,3	3,4	34,4	11,5	1310,0	2,5	40,75	151,30	37,62	4519,42	46,09	4,93	1,88	7,30	25,99	1,58	<0.06	1,67	196,86
SM072	171,1	23,0	1077,4	38,7	5,1	133,8	4,0	28,0	9,0	296,6	2,5	35,28	122,25	23,98	3207,23	15,90	4,85	1,79	3,96	27,63	1,59	<0.06	1,66	62,85
SM073	92,8	19,6	1705,0	18,3	4,1	7,3	2,2	15,1	6,1	131,3	1,4	23,29	87,00	7,61	2005,49	19,23	6,72	1,56	2,93	2,91	1,15	<0.06	1,13	29,88
SM074	143,1	19,6	1678,6	26,4	4,2	6,0	2,3	19,0	8,1	82,0	1,7	26,92	112,80	12,89	2365,13	20,05	5,98	1,55	3,22	17,77	1,14	<0.06	1,13	31,90
SM075	78,9	19,6	1420,6	35,0	4,8	9,2	2,6	26,8	8,1	121,6	1,8	33,08	152,64	12,95	3964,59	9,43	5,83	1,51	2,67	22,29	1,14	<0.06	1,13	69,43
SM076	173,7	19,7	1056,6	24,9	4,5	5,1	2,2	18,5	5,4	200,7	1,5	26,47	91,39	8,24	2166,52	12,50	5,03	1,53	2,33	9,71	1,14	<0.06	1,13	101,65
SM077	160,7	19,7	1429,3	23,2	5,7	1,6	2,0	12,8	6,6	183,0	1,4	25,79	85,39	7,37	1445,73	24,81	4,96	1,82	2,68	1,18	1,14	<0.06	1,13	95,55
SM078	48,4	19,6	1046,1	24,4	4,2	13,3	2,3	17,4	6,1	352,4	1,7	26,16	102,37	10,45	2357,42	5,17	4,95	1,52	2,21	19,03	1,14	<0.06	1,13	31,51
SM079	81,8	19,6	1173,3	21,6	4,2	8,6	2,1	12,6	6,0	193,1	1,6	23,81	76,80	9,91	1722,99	14,89	4,83	1,54	2,28	12,58	1,14	<0.06	1,13	30,87
SM080	112,3	19,7	1700,4	26,4	4,5	48,8	2,6	22,2	7,6	2872,9	1,7	27,17	114,15	11,15	2600,66	18,42	4,92	1,59	7,40	16,01	1,14	<0.06	1,14	37,30
SM081	255,1	19,6	2808,1	76,2	7,6	63,8	4,8	70,6	17,7	859,6	2,1	65,02	352,56	19,22	10878,61	8,47	5,74	1,53	7,99	43,61	1,14	<0.06	1,13	36,36
SM082	169,9	19,6	1393,8	32,7	5,4	2,4	2,3	19,9	7,4	73,1	1,6	29,64	112,97	12,28	2575,07	19,30	4,80	1,66	3,19	10,57	1,14	<0.06	1,13	53,63
SM083	212,9	19,2	2074,2	42,3	5,7	4,2	2,4	22,7	12,4	56,2	2,0	34,76	155,17	22,47	3455,56	22,38	3926,62	1,74	3,15	18,83	1,60	0,28	1,45	75,66
SM084	167,1	19,2	1174,5	28,7	5,1	11,4	2,4	22,0	6,5	414,7	1,9	29,00	104,66	8,39	2593,46	9047,98	4,98	1,69	2,56	10,75	1,60	0,44	1,45	80,49
SM085	172,6	19,2	1608,7	33,1	5,0	2,8	2,6	26,8	8,3	132,8	1,8	30,79	108,04	6,78	2792,47	6431,65	4,94	1,71	3,06	5,93	1,60	<0.06	1,45	111,21
SM025A	498,0	19,3	3303,0	95,5	8,2	9,2	3,6	53,4	30,9	276,2	2,1	63,19	229,39	40,72	8548,73	32400,41	5,90	1,85	4,47	20,95	1,60	<0.06	1,45	134,49
SM002	186,3	19,1	1758,2	36,7	5,3	1,9	2,6	27,8	10,6	15,8	2,1	31,15	141,51	10,92	4070,26	49,05	5,01	1,85	3,07	19,98	1,60	<0.06	1,45	139,00
SM003	391,2	19,2	2299,0	59,3	5,9	23,9	3,1	41,9	19,6	236,8	2,2	43,03	197,15	4,99	6220,67	37,77	5,00	1,81	3,72	25,89	1,60	<0.06	1,45	116,69

10.4 Appendix 4: Ionic species analysed using the discrete analyser (DA) (mg/L)

Samples	Cl^-	Cr^{6+}	Fl^-	NO_2^-	NO_3^-	PO_4^{3-}	SO_4^{2-}
SM001	648.1	0.0055	<0.06	<0.008	11.30	0.06	619.07
SM002	918.6	0.0083	2.08	<0.008	13.96	0.03	517.81
SM003	2127.7	0.0126	2.16	<0.008	26.38	0.03	1109.77
SM004	1868.9	0.0136	2.44	<0.008	14.82	0.03	953.27
SM005	1108.4	0.0089	<0.06	0.978	16.04	0.12	680.96
SM006	1486.0	0.0125	<0.06	<0.008	12.64	0.03	1177.01
SM007	1646.8	<0.0008	2.31	<0.008	16.23	0.03	829.08
SM008	1023.3	0.0023	3.98	<0.008	<0.01	0.03	808.75
SM009	1289.9	0.0082	2.58	<0.008	65.23	0.10	452.08
SM010	676.9	0.0063	1.58	<0.008	73.75	0.04	384.65
SM011	1920.4	0.0117	1.39	0.148	74.80	0.03	873.74
SM012	262.5	0.0049	2.27	0.016	16.48	0.11	149.13
SM013	1912.0	0.0101	2.05	<0.008	86.39	0.03	807.63
SM014	1842.9	0.0026	2.70	0.061	36.38	0.03	927.96
SM015	1907.9	0.0102	1.85	<0.008	57.47	<0.02	789.99
SM016	2268.1	0.0138	2.15	<0.008	111.60	<0.02	1093.50
SM017	435.6	0.0076	2.84	<0.008	42.61	0.02	464.38
SM018	669.1	0.0150	3.45	<0.008	36.71	<0.02	760.70
SM019	388.3	0.0051	2.86	<0.008	33.81	<0.02	337.31
SM020	1093.6	0.0148	2.97	0.015	18.17	<0.02	915.39
SM021	676.2	0.0129	3.42	<0.008	46.49	<0.02	755.12
SM022	776.6	0.0056	1.91	0.028	203.59	<0.02	498.04
SM023	321.5	0.0032	3.01	<0.008	93.57	<0.02	692.11
SM024	650.6	0.0083	2.75	<0.008	130.29	<0.02	914.73
SM025	3669.9	0.0122	2.32	0.323	22.49	<0.02	1635.61
SM026	1543.6	0.0079	1.66	<0.008	122.98	<0.02	714.11
SM027	1535.3	0.0083	1.64	0.016	103.98	<0.02	722.01
SM028	689.5	0.0081	0.88	<0.008	113.87	<0.02	888.66
SM029	219.2	0.0033	0.80	<0.008	98.59	0.05	131.17
SM030	3399.9	0.0152	2.70	0.308	34.74	0.08	970.49
SM031	1454.9	0.0162	1.99	0.014	176.66	0.06	760.84
SM032	16509.8	0.0047	2.33	<0.008	<0.01	<0.02	3801.71
SM033	846.5	0.0077	2.81	<0.008	21.93	0.02	398.76
SM034	1317.3	0.0030	2.98	0.015	3.71	0.05	511.75
SM035	5080.4	0.0154	2.39	<0.008	13.16	0.06	1918.10
SM036	1851.3	0.0142	1.63	0.027	299.35	<0.02	943.50
SM037	2753.5	0.0135	1.83	0.033	125.83	<0.02	1166.04
SM038	1769.3	0.0131	3.84	<0.008	57.61	<0.02	989.73
SM039	226.5	0.0026	0.49	<0.008	13.42	0.38	65.55
SM040	583.3	0.0013	0.74	<0.008	12.59	<0.02	161.89
SM041	381.9	0.0031	0.67	<0.008	15.02	<0.02	153.05

Samples	Cl^-	Cr^{6+}	Fl^-	NO_2^-	NO_3^-	PO_4^{3-}	SO_4^{2-}
SM042	2368.6	0.0109	3.04	0.016	14.62	0.02	644.26
SM043	251.9	0.0008	1.84	<0.008	14.48	<0.02	241.47
SM044	113.6	0.0053	1.16	<0.008	40.89	0.10	86.35
SM045	242.2	0.0083	1.23	0.057	<0.01	0.04	530.40
SM046	1655.0	0.0089	1.83	<0.008	19.46	<0.02	769.67
SM047	677.1	0.0050	2.55	<0.008	65.87	<0.02	558.67
SM048	266.5	0.0037	1.83	<0.008	50.72	<0.02	148.08
SM049	379.9	0.0035	1.39	<0.008	22.16	<0.02	156.39
SM050	140.3	0.0029	3.04	<0.008	12.85	<0.02	227.59
SM051	172.1	0.0018	2.69	<0.008	14.67	0.09	138.12
SM052	247.5	0.0063	3.54	0.050	7.77	<0.02	185.94
SM053	143.1	0.0099	5.63	0.018	81.31	<0.02	131.49
SM054	173.8	0.0027	4.05	<0.008	12.56	0.04	165.19
SM055	128.7	0.0026	4.36	<0.008	3.71	<0.02	145.90
SM056	159.2	0.0022	2.90	<0.008	21.53	<0.02	90.83
SM057	470.4	0.0018	2.73	<0.008	8.69	<0.02	278.72
SM058	1410.7	0.0105	1.84	<0.008	104.87	<0.02	648.18
SM059	120.2	0.0033	2.89	<0.008	13.74	<0.02	92.90
SM060	265.7	0.0070	1.82	0.175	13.92	<0.02	154.28
SM061	1180.1	0.0086	1.71	0.013	145.56	<0.02	587.84
SM062	990.1	0.0119	2.72	0.016	34.03	<0.02	546.18
SM063	1161.3	0.0061	2.65	0.048	61.87	0.07	675.36
SM064	183.2	0.0026	2.43	<0.008	29.47	0.02	100.26
SM065	463.5	0.0057	2.09	<0.008	86.81	<0.02	322.70
SM066	2834.6	0.0308	2.11	<0.008	43.94	0.03	923.15
SM067	445.7	0.0046	5.87	0.076	7.38	0.07	10.62
SM068	2120.0	0.0066	2.84	0.015	1.72	<0.02	658.83
SM069	288.2	0.0023	2.00	0.022	6.88	<0.02	322.84
SM070	290.7	0.0015	1.48	0.044	6.67	0.04	322.94
SM071	1695.5	0.0077	2.52	0.331	13.17	0.04	813.22
SM072	1384.7	0.0022	1.85	0.056	0.64	<0.02	561.17
SM073	751.7	0.0095	3.13	0.020	40.74	0.07	434.26
SM074	943.0	0.0133	2.32	<0.008	104.83	<0.02	507.75
SM075	1374.4	0.0087	1.91	<0.008	64.05	<0.02	674.69
SM076	881.9	0.0168	3.30	0.014	25.98	<0.02	261.20
SM077	777.5	0.0120	3.15	<0.008	52.95	<0.02	272.76
SM078	819.9	0.0118	1.95	0.015	32.08	<0.02	445.42
SM079	621.5	0.0013	1.78	0.010	128.65	<0.02	319.34
SM080	951.2	0.0046	2.86	0.442	27.00	<0.02	547.04
SM081	2739.0	0.0100	2.57	0.115	66.82	<0.02	879.58
SM082	1002.3	0.0107	2.87	<0.008	58.18	<0.02	361.74
SM083	1650.7	0.0120	3.17	1.225	121.01	<0.02	598.30
SM084	963.3	0.0112	2.81	0.916	106.04	<0.02	346.46

Samples	Cl^-	Cr^{6+}	Fl^-	NO_2^-	NO_3^-	PO_4^{3-}	SO_4^{2-}
SM085	1106.7	0.0130	2.12	<0.008	72.93	<0.02	494.23
SM0025A	3381.0	0.0161	2.91	0.021	32.56	0.02	1445.05

10.5 Appendix 5: Metrohm autotitrator potentiometry results

Sample Identity	pH	Temperature	Phenolphthalein Alkalinity mg/L CaCO3	Methyl orange Alkalinity mg/L CaCO3	Total alkalinity mgl CaCO3
SM001	7.46	19.29	0.00	175.61	175.61
SM002	7.47	18.92	0.00	169.96	169.96
SM003	7.29	18.92	0.00	153.26	153.26
SM004	7.50	18.74	0.00	152.64	152.64
SM005	7.89	18.69	0.00	149.28	149.28
SM006	7.33	18.76	0.00	162.53	162.53
SM007	7.43	18.74	0.00	130.48	130.48
SM008	6.95	18.93	0.00	105.63	105.63
SM009	7.43	19.14	0.00	217.06	217.06
SM010	7.49	18.94	0.00	180.41	180.41
SM011	7.59	18.75	0.00	134.04	134.04
SM012	8.02	18.79	0.00	184.81	184.81
SM013	7.57	18.84	0.00	121.28	121.28
SM014	7.62	18.84	0.00	87.45	87.45
SM015	7.46	18.76	0.00	111.85	111.85
SM016	7.58	18.87	0.00	125.53	125.53
SM017	7.96	18.90	0.00	272.10	272.10
SM018	7.50	19.37	0.00	209.85	209.85
SM019	7.75	19.33	0.00	184.49	184.49
SM020	7.34	19.33	0.00	287.17	287.17
SM021	7.48	19.32	0.00	213.42	213.42
SM022	7.50	19.32	0.00	185.56	185.56
SM023	7.76	19.31	0.00	205.66	205.66
SM024	7.75	19.38	0.00	212.02	212.02
SM025	7.71	19.42	0.00	145.36	145.36
SM026	7.62	19.46	0.00	184.27	184.27
SM027	7.43	12.14	0.00	281.21	281.21
SM028	7.68	12.13	0.00	315.96	315.96
SM029	7.53	12.63	0.00	369.53	369.53
SM030	7.76	13.10	0.00	162.77	162.77
SM031	7.77	13.60	0.00	194.90	194.90
SM032	7.62	14.14	0.00	338.02	338.02
SM033	7.54	14.33	0.00	286.40	286.40
SM034	7.84	14.70	0.00	225.20	225.20
SM035	7.30	15.06	0.00	215.96	215.96
SM036	7.48	15.27	0.00	297.12	297.12
SM037	7.37	15.56	0.00	239.35	239.35
SM038	7.57	15.63	0.00	333.59	333.59
SM039	7.51	15.86	0.00	101.20	101.20
SM040	7.50	16.20	0.00	100.81	100.81

Sample Identity	pH	Temperature	Phenolphthalein Alkalinity mg/L CaCO3	Methyl orange Alkalinity mg/L CaCO3	Total alkalinity mgl CaCO3
SM041	7.67	16.31	0.00	92.04	92.04
SM042	7.40	16.55	0.00	106.35	106.35
SM043	7.95	16.66	0.00	210.00	210.00
SM044	8.11	17.28	0.00	174.55	174.55
SM045	7.48	17.47	0.00	50.03	50.03
SM046	7.69	17.56	0.00	197.41	197.41
SM047	7.67	17.64	0.00	218.11	218.11
SM048	8.04	17.83	0.00	230.77	230.77
SM049	7.76	17.94	0.00	129.91	129.91
SM050	7.95	18.04	0.00	278.24	278.24
SM051	8.02	18.18	0.00	216.46	216.46
SM052	8.22	18.34	0.00	230.58	230.58
SM053	7.76	16.16	0.00	0.00	0.00
SM054	7.66	16.08	0.00	463.08	463.08
SM055	8.13	16.05	0.00	580.11	580.11
SM056	7.87	15.98	0.00	568.94	568.94
SM057	7.66	15.98	0.00	540.29	540.29
SM058	7.47	15.86	0.00	433.04	433.04
SM059	7.79	15.83	0.00	395.71	395.71
SM060	7.49	15.79	0.00	413.69	413.69
SM061	7.42	15.76	0.00	572.61	572.61
SM062	8.03	15.72	0.00	442.28	442.28
SM063	7.56	15.68	0.00	422.54	422.54
SM064	7.73	15.65	0.00	624.32	624.32
SM065	7.58	15.61	0.00	630.99	630.99
SM066	7.72	15.57	0.00	528.55	528.55
SM067	8.45	15.56	43.95	695.82	739.77
SM068	7.83	15.57	0.00	214.58	214.58
SM069	7.89	15.57	0.00	292.65	292.65
SM070	7.88	15.81	0.00	300.3	300.3
SM071	7.53	15.78	0.00	356.65	356.65
SM072	7.22	15.77	0.00	223.22	223.22
SM073	7.65	15.81	0.00	535.81	535.81
SM074	7.74	15.85	0.00	454.87	454.87
SM075	7.81	15.89	0.00	359.42	359.42
SM076	7.49	15.92	0.00	549.62	549.62
SM077	7.67	15.94	0.00	572.59	572.59
SM078	7.74	15.97	0.00	365.56	365.56
SM079	7.61	16.46	0.00	574.75	574.75
SM080	7.46	16.50	0.00	478.61	478.61
SM081	7.37	16.41	0.00	355.21	355.21
SM082	7.69	16.33	0.00	470.78	470.78

Sample Identity	pH	Temperature	Phenolphthalein Alkalinity mg/L CaCO3	Methyl orange Alkalinity mg/L CaCO3	Total alkalinity mgl CaCO3
SM083	8.16	16.12	0.00	374.51	374.51
SM084	7.94	15.91	0.00	471.1	471.1
SM085	7.57	16.14	0.00	539.21	539.21
SM025A	7.48	16.00	0.00	343.87	343.87

10.6 Appendix 6: CSI values of the groundwater samples in the study area

SampleID	CSI	SampleID	CSI	Sample	CSI
SM001	-4,46	**SM041**	-5,37	**SM081**	-4
SM002	-3,56	**SM042**	-3,46	**SM082**	-4,82
SM003	-3,38	**SM043**	-5,22	**SM083**	-4,29
SM004	-5,23	**SM044**	-4,1	**SM084**	-4,69
SM005	-3,72	**SM045**	-5,45	**SM085**	-4,68
SM006	-3,63	**SM046**	-3,32		
SM007	-4	**SM047**	-4,31		
SM008	-4,07	**SM048**	-4,84		
SM009	-4,58	**SM049**	-5,11		
SM010	-3,83	**SM050**	-6,36		
SM011	-3,78	**SM051**	-5,96		
SM013	-4,06	**SM052**	-5,61		
SM014	-3,44	**SM053**	-		
SM015	-4,08	**SM054**	-5,1		
SM016	-3,37	**SM055**	-4,16		
SM017	-4,54	**SM056**	-6,44		
SM018	-4,58	**SM057**	-3,84		
SM019	-4,93	**SM058**	-4,31		
SM020	-3,83	**SM059**	-6,71		
SM021	-4,58	**SM060**	-6,14		
SM022	-4,3	**SM061**	-5,05		
SM023	-4,2	**SM062**	-5,08		
SM024	-4,02	**SM063**	-5,09		
SM025	-3,16	**SM064**	-6,22		
SM0025A	-3,71	**SM065**	-5,06		
SM026	-4,66	**SM066**	-3,9		
SM027	-4,7	**SM067**	-5,12		
SM028	-6,03	**SM068**	-3,77		
SM029	-6,52	**SM069**	-5,28		
SM030	-3,47	**SM070**	-5,36		
SM031	-3,7	**SM071**	-4,04		
SM032	-2,99	**SM072**	-4,18		
SM033	-4,75	**SM073**	-5,49		
SM034	-4,28	**SM074**	-5,3		
SM035	-3,07	**SM075**	-4,44		
SM036	-4,49	**SM076**	-4,88		
SM037	-3,87	**SM077**	-5,11		
SM038	-4,23	**SM078**	-5,1		
SM039	-5,93	**SM079**	-5,42		

SampleID	CSI	SampleID	CSI
SM040	-5,2	**SM080**	-5,18